

**Lehrstuhl für Leichtbau
Technische Universität München**

Ground Dynamics of Flexible Aircraft in Consideration of Aerodynamic Effects

Martin Spieck

Vollständiger Abdruck der von der Fakultät Maschinenwesen
der Technischen Universität München
zur Erlangung des akademischen Grades eines

Doktor-Ingenieurs

genehmigten Dissertation.

Vorsitzender: Univ.-Prof. Dr.-Ing. Gottfried Sachs

Prüfer der Dissertation: 1. Univ.-Prof. Dr.-Ing. Horst Baier
2. Hon.-Prof. Dr.-Ing. Dieter Schmitt

Die Dissertation wurde am 11.12.2003 bei der Technischen Universität München
eingereicht und durch die Fakultät für Maschinenwesen
am 21.07.2004 angenommen.

Acknowledgements

The author wishes to express his appreciation to Prof. W. Kortüm, who, as a principal advisor, had strongly supported this work, and had a major impact on orientation and structure of this work. His tragic and untimely death was a severe loss, not only in respect of this work, but to everyone who had the privilege to know him. An equal debt of gratitude is owed to Prof. H. Hönlinger, who not only stood in to offer his support and advice, but also carefully reviewed and triggered valuable notions to many parts of this thesis.

I would further like to thank Prof. H. Baier and Prof. D. Schmitt of the Technical University of Munich, who have shown a profound interest in this work, and who have made it possible for me to conduct the thesis at the TU Munich.

The department of Vehicle System Dynamics of the German Aerospace Center in Oberpfaffenhofen has provided a unique working environment. My thanks go to all my colleagues who were always willing to lend me an open ear; without their information and assistance, this work would not have been possible in this form. Knowing I will not be able to give everyone the credit he or she deserves, I would nevertheless like to thank especially Dr. W.-R. Krüger, Dr. W. Rulka, Dr. A. Jaschinski, Dr. F. Kiessling, M. Rippl, and the late Dr. R. Schwertassek.

Finally, but not least, my thanks go to those friendly individuals who were talked into reviewing this thesis. The scientific fraction, with their probing questions, forced me to provide a (hopefully) clear-cut structure and illustrating explanations - every undetected flaw will dampen my ultimate gratitude. As a side effect, my wife Sabine, who sacrificially reread this work several times for expression, formatting and orthography, may now be regarded as a specialist on modal aerodynamics in multibody systems.

Contents

1	Introduction	9
1.1	Overview	9
1.2	Scope	10
1.3	Contents	11
2	Background and Previous Work	13
2.1	Concurrent Engineering in Modern Aircraft Design	13
2.2	Aircraft Ground Dynamics Analysis and Simulation	16
2.2.1	Techniques	16
2.2.2	Actual Dynamic Problems in Aircraft Ground Operation	17
2.3	Multibody Simulation	19
2.3.1	Overview	19
2.3.2	Fundamentals of Multibody Simulation	20
2.3.3	Multibody System Coordinates	23
2.3.4	Multibody Systems Formalisms	23
2.3.5	Numerical Integration	24
2.3.6	Multibody Simulation in Aircraft Ground Dynamics	25
2.3.7	Methods of Modelling Aeroelastic Effects in Multibody Systems	26
2.4	Computational Fluid Dynamics	30
2.4.1	Overview	30
2.4.2	Fundamentals of Computational Fluid Dynamics	31
2.4.3	Computational High-Lift Aerodynamics	33
2.5	Fluid-Structure Interaction	34
3	Solution Strategy	37
3.1	The Problem of Aeroelastic Effects in Aircraft Ground Analysis	37
3.1.1	Shortcomings of Conventional Simulation Capabilities	37
3.1.2	Importance of Simulation of Aerodynamic / Aeroelastic Effects	38
3.1.3	Requirements on an Aeroelastic Enhancement to MBS	39
3.2	Aerodynamic Preprocessing as a Possible Solution	40
4	Deformable Bodies in Multibody Simulation Systems	43
4.1	Classification of Multibody Systems	43
4.2	Equations of Motion of Hybrid Multibody Systems	44
4.3	Deformable Bodies	45
4.4	Presumptions of Deformable Bodies in MBS	46
4.5	Representation of Deformable Bodies	46
4.6	Kinematics of the Deformable Body	47
4.7	Nonlinear Equations of Motion of the Single Deformable Body	48
4.8	Linearisation of the Elastic Deformation	50
5	The Approach of Aeroelastic Preprocessing	55
5.1	The Principle of Superposition	55
5.1.1	Prerequisites and Assumptions of Superposed Aerodynamics	56
5.1.2	Superposition of Aerodynamic Effects	57

5.2	The Principle of Modal Aerodynamics for Multibody Systems	59
5.3	Representation of Aerodynamics in the Equations of Motion	60
5.3.1	Multibody System Aerodynamics in Descriptor Form	60
5.3.2	Multibody System Aerodynamics in State-Space Representation	61
5.4	Modal Representation of Rigid Body Aerodynamics	62
5.4.1	Aerodynamics of the Reference Configuration	63
5.4.2	State-dependent Aerodynamics of the Rigid Body	64
5.4.3	Load Distribution on the Elastic Airframe	65
5.5	Aerodynamic Effects of Control Surface Deflections	66
5.5.1	Effects of Control Surface Deflections on Rigid Body Motion	67
5.5.2	Distribution of Control Loads on the Elastic Airframe	68
5.6	Aerodynamic Effects of Structural Deformations	69
5.6.1	Aerodynamic Force Increments of Elastic Aircraft Deformation	69
5.6.2	Aerodynamic Effects Due to Aerodynamic Damping / Excitation	70
5.6.3	Effects of Structural Deformation on Overall Body Motion	75
5.6.4	Distribution of Loads Caused by Elastic Airframe Deformations	76
5.7	The Enhanced Equations of Motion of the Deformable Body	77
6	Realisation Aspects of Aeroelastic Preprocessing	79
6.1	Basic Workflow of Aeroelastic Preprocessing	79
6.2	Software Tools for Aeroelastic Preprocessing	81
6.2.1	Computational Structural Mechanics	82
6.2.2	Computational Fluid Dynamics	83
6.3	Coupling of CFD Model and Modally Reduced CSM Model	84
6.3.1	Coupling With Rigid Connexions	86
6.3.2	Cubic Spline Interpolation	87
6.3.3	Finite Interpolation Elements	88
6.3.4	Scattered Data Interpolation	90
6.3.5	Automated CFD - mCSM Interpolation	91
7	Applications	93
7.1	Reference Aircraft Models	93
7.1.1	Reference Model 1: Aerobatic Glider	93
7.1.2	Reference Scenarios and Simulation Models	94
7.1.3	Reference Model 2: Large Transport Aircraft	96
7.1.4	Reference Scenarios and Simulation Models	96
7.2	Aerodynamics in Aircraft Ground Dynamics Simulation	99
7.2.1	Dynamic Behaviour of the Aircraft	99
7.2.2	Impact of Aeroelastic Effects on Dynamic Landing Gear Loads	101
7.2.3	Relevance of Aeroelastic Effects in Aircraft Ground Dynamics	103
7.3	Computational Performance of Aeroelastic Preprocessing	104
7.3.1	Computational Performance of Reference Aircraft Model 1	104
7.3.2	Computational Performance of Reference Aircraft Model 2	106
8	Conclusion	109
8.1	Summary	109
8.2	Contributions	110
8.3	Future Work	111

Appendix A	Aircraft Coordinate Systems	113
Appendix B	Acronyms and Abbreviations	115
Appendix C	List of Symbols	117
Appendix D	List of Figures	121
Appendix E	List of Tables	123
References		125

1 Introduction

1.1 Overview

Aircraft serve simply one purpose: they are built to fly.

But despite this apparent fact, ground related issues play an important part in modern aircraft design, such as:

- strength: ground loads are usually responsible for dimensioning load cases on major parts of the airframe such as rear fuselage, wing root and centre section,
- weight saving: the landing gear is responsible for about 8% of the overall aircraft weight,¹
- safety: more than 50% of accidents² occur when the aircraft is on the ground (including take-off and landing),
- costs: ground loads related problems are often detected very late in the development process, thus causing disproportionate costs, jeopardising the time schedule and leaving little freedom for design improvements.

Accordingly, aircraft ground operability is one of the (many) key factors of a successful aircraft design. It has to be treated with the same diligence as disciplines whose significance in aircraft design is perhaps more obvious, like aerodynamics, flight mechanics or propulsion. The research reported here deals with an important part of aircraft ground operation: aircraft ground dynamics.

In the world of computer aided engineering (CAE), multibody simulation (MBS) is the favoured tool for analysis of the dynamics of ground-based vehicles. In research programmes and industrial applications, MBS has proven to be an efficient tool for analysis and evaluation of the ground dynamics of large, flexible aircraft structures as well. For the applications performed so far, aerodynamic effects could only be included by relatively simple means. In future, nevertheless, MBS will have to provide more sophisticated capabilities. Increasing structural flexibility of the next generation of aircraft designs will further raise the demands on the analysis of ground dynamics. This will apply for touch-down sequences as well as for ground run and take-off simulations, e.g. to prevent unpredicted load peaks or poor performance, to save weight by optimising landing gear and airframe to real-world scenarios³ and to avoid resonance phenomena when travelling over uneven runways.

-
1. Quantity given with respect to OWE (Operational Weight Empty) of civil transport aircraft
 2. Accidents of U.S. carriers over 5-year period (1994-1998) reported to NTSB (U.S. National Transport Safety Board)
 3. In this report, the expression "scenario" is used for a given motion sequence of the aircraft; ranging from a simulation of the next few instants after a defined initial state to a sequence of state-dependent or pre-defined manoeuvres, e.g. a landing sequence from final approach to stand-still.

To meet future requirements, MBS will have to provide the user with an efficient tool to realistically distribute aerodynamic lift on the elastic airframe, it will have to account for fluid-structure interaction when the airframe flexes under flight and ground loads, but also allow for rapid simulation of the free-flying, manoeuvring aircraft.

This report introduces a method to enhance the capabilities of MBS to meet these requirements: an approach is presented to include aerodynamic / aeroelastic effects into multibody simulation of elastic bodies with lift-generating surfaces. In particular, this work describes the approach itself, its embedding into an MBS environment and outlines the technical realisation as an aeroelastic MBS preprocessing tool.

The emphasis is put on the practical applicability in aircraft development programmes. The concept targets the specific needs of aircraft ground dynamics analysis, providing an adjusted compromise between accuracy of the simulation and operating expense. It combines fast and efficient computation of the task as well as low additional user effort for model set-up, dynamic analysis and evaluation of the simulation. Close concurrence with other CAE tools ensures smooth and effective working.

1.2 Scope

With increasing performance of the established CAE tools, the importance of “interdisciplinarity” has become more and more apparent. In aeronautics, fluid-structure interaction is one of the major research fields of multidisciplinary aircraft analysis. The majority of these studies and applications concentrate on the interaction of aerodynamic loads and structural deflection of the aircraft at its major design point(s), at cruise configuration and conditions. These solutions, however, do not suit the specific needs of aircraft ground dynamics applications. This report presents a new approach to rapid and robust simulation of the free-flying, elastic aircraft for that particular area.

In the field of MBS-based aircraft ground analysis, the key applications are

- dynamic behaviour of the aircraft on touch-down and ground run,
- dynamic loads on airframe and landing gear,
- optimisation of the landing gear lay-out,
- airframe / landing gear interaction.

The simulation scenarios thus include touch-down impact, take-off and landing sequences, high-speed ground run and low-speed taxiing and turning. They are characterised by

- nonlinear dynamics and complex kinematics,
- large body motion (translations and rotations),
- aircraft in high-lift configuration at comparatively low speeds,
- wide range of flow conditions (angle of attack, velocity),
- aerodynamic loading conditions dependent on elastic deformations and deformation velocities,
- pilot control inputs / deployment of lift dumping devices,
- feedback controlled (sub-)systems, i.e. mechatronic components (anti-skid system, actuators, ...).

Although MBS-based aerodynamics are likely to be applicable in other areas of aerospace engineering as well, e.g. flight mechanics, flight control system (FCS) design, gust or manoeuvre loads alleviation systems or adaptive control, the work presented here focuses on the specific questions of aircraft ground dynamics. Applying a widely accepted definition of aeroelasticity which describes it as “a science which studies the mutual interaction between aerodynamic forces and elastic forces, and the influence of this interaction on aeroplane design”, [1], this work proposes an approach to establish an “aeroelastic tool” optimised for MBS-based aircraft simulation.⁴

1.3 Contents

This work consists of eight main chapters, not counting annex and references.

Chapter 1 shall provide an introduction into the thematic area of this dissertation and a brief explanation of the work which is presented.

Chapter 2 is intended to highlight fundamentals and background of the main themes covered as well as previous work which is connected to these topics. It outlines environment and “boundary conditions” the proposed approach will have to live up to, and introduces the key subject of this work, aircraft ground dynamics analysis, and its most important engineering disciplines.

Chapter 3 specifies the problem which shall be overcome and reveals a possible solution strategy. To elucidate the objective of this work more extensively, the shortcomings of conventional analysis and simulation practices are discussed and requirements for an improved technique are derived.

Chapter 4 recapitulates the approach to represent deformable bodies in multibody systems which will be applied in this work. After a brief depiction of the modelling strategy, the equations of motion of the single, deformable body will be set up - the starting point for the introduction of aeroelastic effects.

Chapter 5 describes the modelling approach for the free-flying, manoeuvring, elastic aircraft by superposition of section-wise linearised aerodynamics and the principle of modal aerodynamics. This leads to the approach of aeroelastic preprocessing, which includes aeroelastic effects on a deformable multibody system structure in state-space representation: the equations of motion of the body are enhanced by additional terms which are required to represent aerodynamic and aeroelastic effects.

Chapter 6 discusses aspects of the practical realisation of the presented approach of aeroelastic preprocessing, such as the preprocessing workflow, software

4. The work presented here has been performed using the MBS software tool SIMPACK; the desired aeroelastic functionality shall consequently fit to this tool. Although the underlying method to account for aerodynamic and aeroelastic effects in MBS is independent from the favoured approach of multibody modelling, differences will appear - mainly regarding questions of practical realisation.

tools which may be employed and some information on fluid-structure interpolation for this specific task.

Chapter 7 contains two application examples: the model of a large transport aircraft in selected landing scenarios to point out the impact of aerodynamic and aeroelastic effects on dynamic behaviour and applied dynamic loads; and a model of an aerobatic glider performing reference manoeuvres to demonstrate the computational advantage of the proposed approach.

Chapter 8 subsumes the contents of this work and highlights the contributions to the field of aircraft ground dynamic analysis. Suggestions for further activities in this field conclude the main section.

2 Background and Previous Work

In the last two decades, strategies and methods used in aircraft design have undergone significant changes, and the development continues. The main driver of this development is without question the rapid progress in computer- and software technology. The impact is ubiquitous in aerospace industry: in engineering, manufacturing, project management, logistics, to name but a few examples. Concentrating on the engineering point of view, the main progress has been the development of a multitude of software tools for aircraft analysis and design. In the last years, these applications have developed from “stand-alone” tools to solve specific, usually monodisciplinary problems in the development of an aircraft to an environment in which most of the development process itself is being embedded. A vast amount of activities in research and software development has therefore been devoted to create interdisciplinary links and multidisciplinary analysis and optimisation capabilities. Basically, this work is a contribution to this area as well.

This section shall provide an introduction into the main themes of this work. After some basic information about the aspects of computational aircraft design in general, a brief state-of-the-art of aircraft ground dynamics analysis will highlight the main topic itself. An overview over multibody simulation as the major tool of system dynamics analysis and the area of aerodynamic analysis and fluid/structure interaction will provide additional background information.

2.1 Concurrent Engineering in Modern Aircraft Design

Concurrent engineering (CE), sometimes denominated (almost synonymously) as simultaneous engineering or integrated product development (IPD), can be defined as a systematic approach to the integrated, concurrent design of products and their related processes, including manufacture and support, [2]. In simple words, the main objective is to develop better products at reduced costs and in less time. Stalk and Webber, [3], have shown that these three tasks are closely connected: shortening development lead time and, consequently, costs is not a goal in itself, it has to be combined with competitive advantages. This demand requires a thorough, detailed understanding of the product very early in the design process, thus offering great freedom of design, but calling for very high standards of analysis capability.⁵

The concept of CE was made possible by the progress in computational engineering. CAE tools like CAD (computer aided design), FEA (finite element analysis) or CFD (computational fluid dynamics) are well known examples for engineering software which provides the necessary analysis power in the specific engineering discipline. For most of these tools, the underlying principles have been developed in the 1960ies.

5. To conform with the objectives of this work, the following passages on concurrent engineering will focus on CE design rather than on CE manufacturing and support.

Their “triumphant march” in engineering, however, began when massive but cheap computer power became available about 15-20 years ago.

The ability to analyse a system thoroughly is only one step towards efficient and successful concurrent engineering. One major characteristic of true CE is that tasks are being carried out in an integrated approach in both “dimensions” - over the timeline, respectively the various phases of a product development process (vertical integration), as well as across disciplines (horizontal integration), Figure 2.1, [4]. Parallelising the development process in a vertical integration measure requires a thorough understanding of the design as early as possible and a sophisticated project management, [5], whereas horizontal integration poses strong demands on handling and updating of product data and the ability of both, specialists and their (software) tools, to work in an interdisciplinary environment.

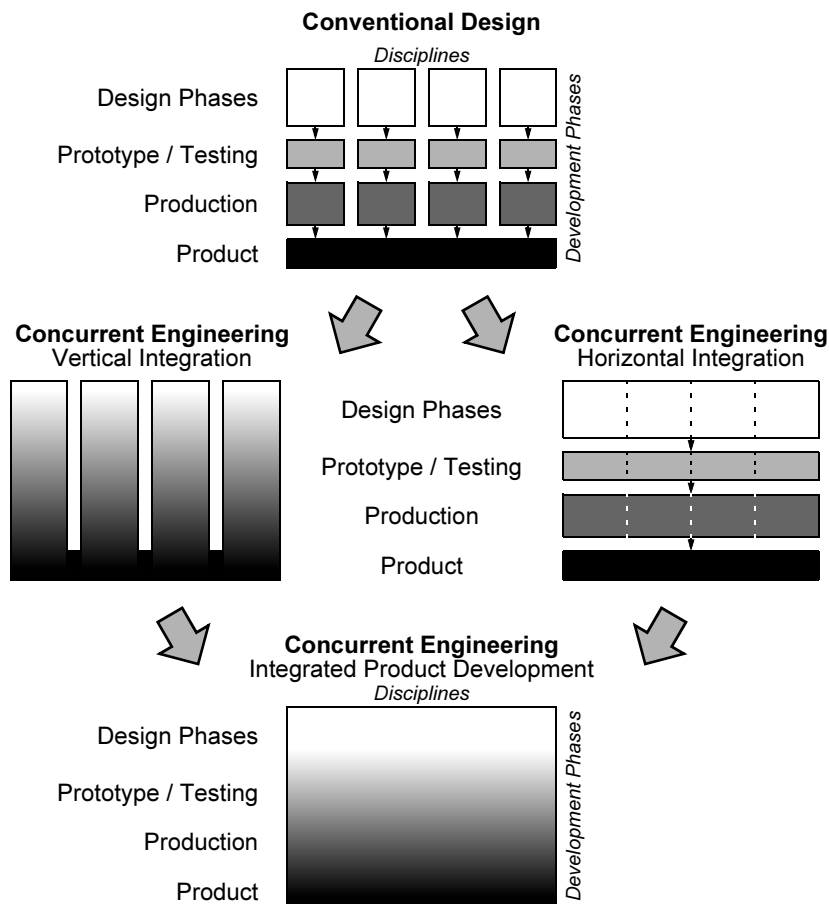


Figure 2.1 The Concept of Concurrent Engineering

Contrary to a parallelised development process, interdisciplinary design does not directly cut down costs or lead time. It is nevertheless essential for the development of advanced products to link the various engineering disciplines in order to achieve reliable knowledge about the product and to advance it straight towards the final design, avoiding re-design loops or last-minute fixes.

Thus, modern CAE tools must be able to communicate with other CAE applications of a different discipline, e.g. to exchange results or to share model data, [6]. With growing perfection of commercial CAE software tools, the research interest in this field has moved towards efficient coupling and interfacing of different engineering disciplines. New developments have to fit into the CAE environment prevailing in today's world of engineering.

For CAE applications, the approach of concurrent engineering can be characterised by two catchwords: interdisciplinarity and efficiency. It is not sufficient to provide means to account for interdisciplinary effects in a CAE domain; the approach has to be quick, simple to use and robust.

The specific CAE software tools apply different modelling strategies. Each discipline focuses on some aspects of the system. Models of different disciplines may have a certain redundancy, which can be used for coupling; e.g. CAD can provide other tools like FEA or MBS with geometric and mass data, material properties and visual representations of parts. For consistent, not-redundant data management, a common product data management (PDM) database system providing the necessary data for all tools, [7], would be highly desirable. In practice, however, this approach is difficult to realise for multidisciplinary design tasks: the high number of different applications to be connected and the rapid development progress of CAE tools, combined with the problem that many tools require very specific data which have to be automatically provided or updated, lead to complex system which offers little flexibility. Furthermore, physical coupling of disciplines (multi-physics) requires more effort than to solely access a common database - often, an in-depth analysis of a multidisciplinary problem is not possible without specialised connexions.

Aviation has always been a driver towards more sophisticated analysis methods and design strategies. The concept of concurrent engineering was quickly adopted, if not co-developed, in major aircraft development programmes. Examples of programmes where CE has been consequently applied are the McDonnell Douglas (now Boeing) F/A-18 E/F, [8], or the Boeing 777, [9]. The latter is being considered, and also marketed, as the first aircraft which was completely designed in the computer, earning honorary titles like "21st Century Jet", [10]. The main focus in both programmes was to streamline the CAD/CAM-process (Computer Aided Design/Computer Aided Manufacturing). The economic effects were encouraging; e.g. for the Boeing 777, nonconformance events, a problem which seriously affected Boeing's production quality and efficiency, were reduced by approximately 75%. From the engineering point of view, however, the design process was not as "concurrent" as desirable. The concept of integrated design, i.e. the coupling of the design processes of different engineering disciplines, still proved to be problematic. As a consequence, both programmes mentioned above were troubled with technical difficulties because of interdisciplinary interactions, [11], [12].

More recent approaches consider a multidisciplinary CE design environment rather as a network of different tools connected by flexible, tailor-made interfaces and pre-/post-processors to build a coupled software system. Examples for this approach are research programmes like ENHANCE⁶ and AMANDA⁷, software environments created in industrial projects like ACE (Airbus concurrent engineering), [13], or additional

tools like front-ends for efficient, standardised modelling in a multidisciplinary environment, e.g. Pad3D, [14]. The highly interconnected design environments should enable every user to work in an interdisciplinary way, from his own workplace and without the necessity to become a specialist in a multitude of engineering disciplines.

The concurrent engineering strategies and environments which are being developed will form the basis for future aircraft design analysis. "Virtual design teams" will work on "virtual prototypes" in "virtual reality" environments. The well-known quote which says that "...when the weight of the paper equals the weight of the airplane, only then you can go flying..."⁸ will probably be still valid for the next generations of airliners because of the paperwork necessary for proposals, supplier contracts and legal disclaimers, but for the future in engineering disciplines, it appears that the first metal will not be cut before the number of analyses performed are equal to the projected development costs.

2.2 Aircraft Ground Dynamics Analysis and Simulation

It is widely presumed that the landing gear is subjected to highest loads during landing impact. In reality, landing conditions are critical for only about 20% of the landing gear structure - ground handling conditions are critical for the rest of the structure, [15]. Accordingly, numerous, often conflicting factors influence functionality, performance, comfort and safety. Most requirements demand extensive analysis and evaluation capabilities, [16], [17]. Aircraft ground dynamics is involved in most of these applications.

2.2.1 Techniques

Analysis of the dynamic behaviour of an aircraft returning to or running on the ground has been performed for a long time. In the early days of aviation, the governing equations of motion have been written down by hand, [18]. Generic modelling strategies enabled engineers to perform linear system analyses efficiently with slide rule or, later, with the help of analog, hybrid or digital computers. The achieved results provided a good outline for the lay-out of landing gear and affected airframe components; the fine-tuning, nevertheless, had to be done in the field.

Further developments in computer simulation techniques have lead to different approaches, [19]:

- Custom-made simulation software solves specific problems of aircraft ground dynamics. In most cases, it is in-house software of aircraft manufacturers or landing

6. ENHANCE (Enhanced Aeronautical Concurrent Engineering): European RTD project in the 5th Framework Programme; timeframe: 1999-2002.
7. AMANDA (A Multidisciplinary High Performance Numerical Development System for Aircraft); Research programme funded by Helmholtz-Gesellschaft (HGF); timeframe: 1999-2001.
8. Quote is attributed to Donald W. Douglas Sr. (1892-1981), founder of Douglas Aircraft Company.

gear suppliers. Some of these applications are in modular form (e.g. airframe structure, landing gear model, numerical treatment, solution analysis) and can be assembled to different solution sequences. Examples of custom-made codes are GRAP and SD-Approach (BAe Systems, Stirling Dynamics Ltd.), [20], [21].

- Commercial engineering software tools usually offer improved handling qualities, more detailed documentation and a high degree of continuity. In general, they represent the latest state-of-the-art in their specific discipline:
 - General simulation environments are widely used in industry for various applications. These tools, e.g. MATLAB Simulink, [22], [23], MATRIX_x Systembuild, [24], offer easy-to-use possibilities for conventional (linear) system analysis.
 - Engineering software packages specialised on system dynamics analysis provide at least the same functionality than that offered by custom-made applications. The most common tool in this respect is multibody simulation software, e.g. SIMPACK, [25], DADS, [26], or MSC.ADAMS, [27], which can be used for very detailed, nonlinear simulation of complex scenarios.

With increasing importance of an aircraft's dynamic behaviour on the ground and growing complexity and interdisciplinarity of the problems to be solved, the use of specialised commercial simulation tools is clearly favoured in industry and research. Today, almost all major aircraft and landing gear manufacturers use one of the major MBS software packages for their ground dynamic analyses.

One, if not the major application of MBS simulation in this area is landing gear (and airframe) design and rating according to certification cases. Additionally, the ability of MBS to provide a virtual testbed for realistic, in-depth simulation of an aircraft's dynamic behaviour is used to investigate new or improved concepts or to tackle prevalent problems and develop fundamental solutions. In most cases, these applications require sophisticated analysis and evaluation methods and often are the design drivers towards improved and enhanced simulation capabilities.⁹ Examples are the evaluations of the ground dynamics of very large aircraft, [28], or the investigation about the benefits of semi-active landing gear shock absorbers to damp resonance effects during ground run, [29], [30].

2.2.2 Actual Dynamic Problems in Aircraft Ground Operation

History of aviation provides numerous examples of problems with landing gear dynamics, from the very beginning to the latest developments. Troubles of modern transport aircraft due to unforeseen or underestimated dynamic effects span from sub-standard ground handling qualities in crosswind conditions (e.g. Boeing 767) over landing gear shimmy (e.g. Fokker 100, Boeing C 17 Globemaster) and brake chatter (e.g. Fairchild Dornier 328JET) to vibrational problems due to airframe/landing gear interaction.

9. Additional information on the employment of MBS in aircraft ground dynamics can be found in Section 2.3.6, page 25.

The last problem is not new either, but appears to become more severe in recent development programmes. Since the emergence of jet fighter aircraft with its increased take-off- and landing speeds, this type of aircraft has been troubled by coupled (rigid body) heave-pitch oscillations on uneven surfaces. Because of larger wheel bases, high momentum of inertia and usually lower landing speeds, transport aircraft were less critical in this respect. Progress in performance and lightweight design, however, has revealed an additional phenomenon: ground induced oscillations of the deformable, elastic airframe causing increased dynamic loads and partially violent local accelerations.

One of the first civil transport aircraft which was seriously troubled by this effect is the Aérospaciale/BAC Concorde, [31]. Several factors contributed to this sensitivity; among them the slender fuselage with pilots and the first passenger rows situated way in front of the nose gear leg, Concorde's "sporting" take-off speeds (up to 215 kts in hot-and-high conditions) and high tyre and oleo stiffness. The problem was eventually solved with a two-stage nose gear oleo with reduced stiffness at the MTOW working point, [32]. It was considered, at that time, to be a problem of this particular configuration. In the 1980ies, conventional transport aircraft designs turned out to become affected as well, e.g. McDonnell Douglas (now Boeing) MD-90-30 and Airbus A340-300. It is to be expected that further progress in lightweight construction will increase the sensitivity of aircraft to this kind of vibrational problem as well as probably introduce new forms of dynamic interactions.¹⁰ It will be important for the economic success of future aircraft developments to detect and predict possible problems as early in the design process as possible - vibrational interactions will hardly be "show-stoppers" of a new design, but they are very expensive to overcome and usually lead to suboptimal solutions, as they are often discovered as late as in flight tests or even after entry-into-service of a new type, as it was the case for the A340.

Several research programmes were initiated on this behalf, both on national and European level. Airframe/landing gear interactions were, respectively are treated in the German programmes "Flexible Aircraft I", [33], to "Flexible Aircraft III". Examples for programmes funded by the European Commission are LAGER (Landing Gear Research Technologies For Future Design), [34], and ELGAR (European Landing Gear Advanced Research), [28].

10. Looking at new Airbus developments, the A340-600, with its stretched fuselage, is predetermined to be sensitively in this respect. The A380, nevertheless, might be prone to airframe/ground load interactions as well. Due to its compact fuselage, it is likely that the "classical" fuselage bending flexibility will be less important in this respect than combined airframe deformations, e.g. warping or shifting modes.

2.3 Multibody Simulation

2.3.1 Overview

Multibody simulation codes are efficient CAE tools to simulate the linear and nonlinear dynamic behaviour of mechanical and mechatronic systems. An important part of this wide area is the system dynamics of vehicles, [35]. In practical applications, MBS can be regarded as a “virtual testbench” for these systems. Behaviour and performance of the entire system, or of its major components, are being evaluated in a virtual environment often long before the first prototype of the system is ready for field tests. In this respect, it represents some kind of central tool in a virtual design environment. Figure 2.2 shows how MBS is being embedded into the world of CE by interfaces to other CAE tools, thus forming a specific part of a CE network.

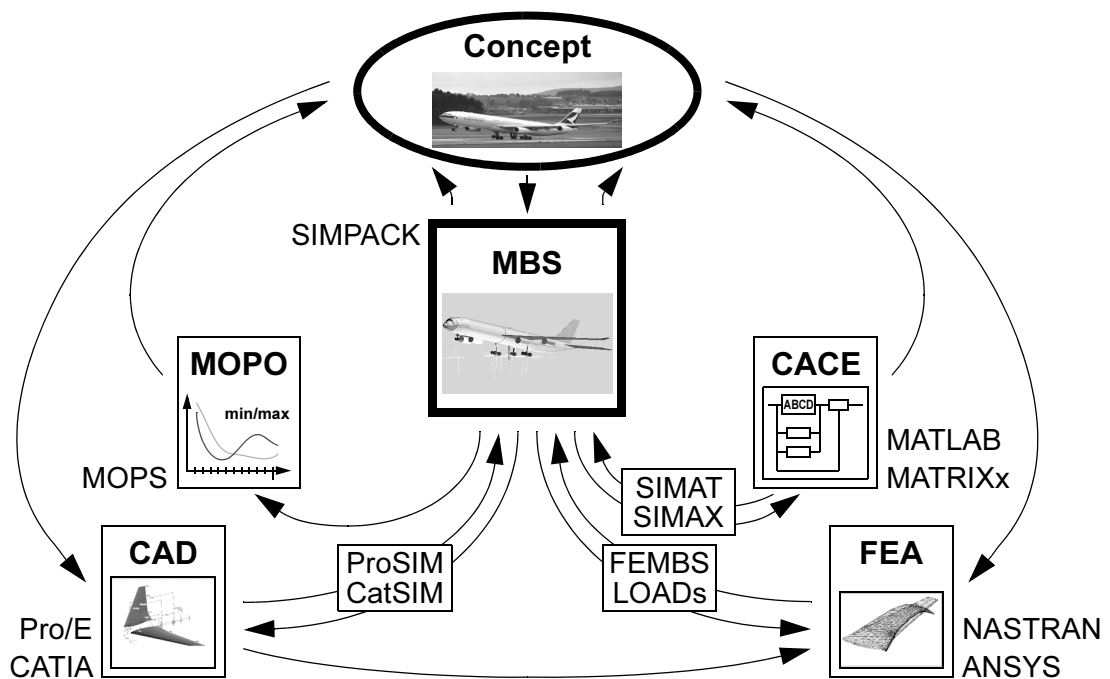


Figure 2.2 Multibody Simulation in a Concurrent Engineering Environment

MBS systems usually consist of a multitude of distinctive bodies which undergo large translational and rotational motions relative to their surrounding area as well as to each other. Similar to the components of a real mechanical system, connexions to other parts of the system and applied forces influence the motion of an MBS body. The bodies of the MBS system are usually assumed to be rigid. In hybrid multibody systems, MBS bodies may additionally be subjected to relatively small, elastic deformations. Accordingly, multibody system dynamics may be defined as “the dynamic analysis of systems of interconnected bodies undergoing general translation and rotation”, [36].

The discipline of multibody simulation descends from the classical mechanical problem of translational and rotational motions of rigid bodies. *Newton*, *d’Alambert*, *Euler* and *Lagrange* created the basis for deriving the equations of motion of multibody systems. The rise of mechanical mechanisms and machinery in the 19th century stimulated interest in kinematics and, to a lower extent, system dynamics of these mechanisms, but in general analysis capabilities remained limited to linear (or linearised) systems undergoing small or planar motions or vibrations.

In the 1960ies, the situation changed. The need for more capable analysis of dynamic systems, e.g. for the nonlinear motion of high speed mechanisms or of spacecraft, boosted the activities in this area - supported by the fact that with the rise of computational abilities, efficient analysis of complex systems became feasible. The first “general purpose” multibody programs were constructed, [37], [38]. Its multibody formalisms already allowed generating and integrating the equations of motion automatically from an input data set defining the geometrical and mechanical properties of the bodies, their interconnexions and the system state at initial time, [36].

The 1980ies saw the first commercial products established on the general engineering market. From then on, new multibody formalisms, e.g. $O(N)$ -algorithms, [39], [40], generating the equations of motion in explicit or in residual form, [41], drastically cut down the computational effort. Various numerical integration algorithms were developed or incorporated, [42], to ensure stable and problem-adequate numerical computation. Besides time integration, MBS codes offer a variety of special numerical analysis methods, in particular for linear system analysis (linearisation, eigenvalues, root locii, frequency response, stochastic analysis in frequency and time domain), stationary solutions (equilibria, nominal forces) and kinematic analysis. Graphical user interfaces (GUI) for model setup and evaluation simplified the use of dynamic analysis and reduced the sources of error in model set-up and interpretation of results. An overview of multibody codes can be found in [35], [43] - [45].

Once being considered as a tool for rough, quick evaluations early in the development process, MBS now serves in almost all design phases: from system evaluations in conceptual and preliminary design over accompanying analysis in detail and final design to virtual field tests and certification. The range of application is wide: besides the “classical” fields of application such as aerospace, automotive, wheel/rail and robotics, MBS can be found in real-time simulation models for simulators and hardware-in-the-loop (HIL) applications, adaptive control and biomechanics.

2.3.2 Fundamentals of Multibody Simulation

The method of multibody simulation supports primarily the analysis of the motion, i.e. kinematics, kinetics and dynamics, of mechanical and mechatronic systems.

After input of the describing model data (e.g. system topology, mechanical properties of bodies and joints, applied external forces and moments, initial values), MBS codes automatically generate the equations of motion of the model as a nonlinear set of equations, generally in the form of a system of ordinary differential equations (ODE) or

differential-algebraic equations (DAE). A variety of optimised solvers is available to generate solutions numerically.

Basically, a multibody simulation system consists of two types of elements: *bodies* and *connexions*. Bodies may be rigid or deformable, whereas connexions may be kinematic (joints) or kinetic (force elements).

Bodies

Rigid bodies have a simple structure: they are characterised by a reference frame, their mass and inertia tensor, and usually additional frames (markers) as attachments for force elements or joints to other bodies. Although bodies may boast a detailed, perhaps CAD-generated graphical representation for the visualisation of model set-up and results, this rudimentary data set is sufficient to represent the respective (rigid) body in MBS analysis.

In principle, the set-up of an MBS system containing deformable bodies does not differ from a purely rigid MBS system. For a deformable body, the MBS system receives an additional time dependency - the elastic deformation of the body. In general, elastic bodies are modelled under the assumption of small, elastic and reversible deformations which usually derive from the linear superposition of pre-calculated mode shapes.

Joints

Joints are assumed as ideal, backlash-free and weightless connexions between bodies (or frames). They reduce the number of degrees of freedom, forcing the bodies of an MBS system to motion sequences which would not occur without them. Thus, joints have to apply reaction (or constraint) forces acting orthogonal to the motion planes defined by the constraints. The reaction forces restrict the motion envelope of the system so it conforms with the geometric boundary conditions (manoeuvrability) of the system.

Two different types of joints can be distinguished: “normal” joints are connecting links in MBS systems with tree-like topology, respectively are those links in a system which connect the “from-body” to a body of higher topology level (so this system would have a tree-like structure if only this type of joints were present), whereas links which close a kinematic loop are, obviously, called loop-closing joints, see Figure 2.3.

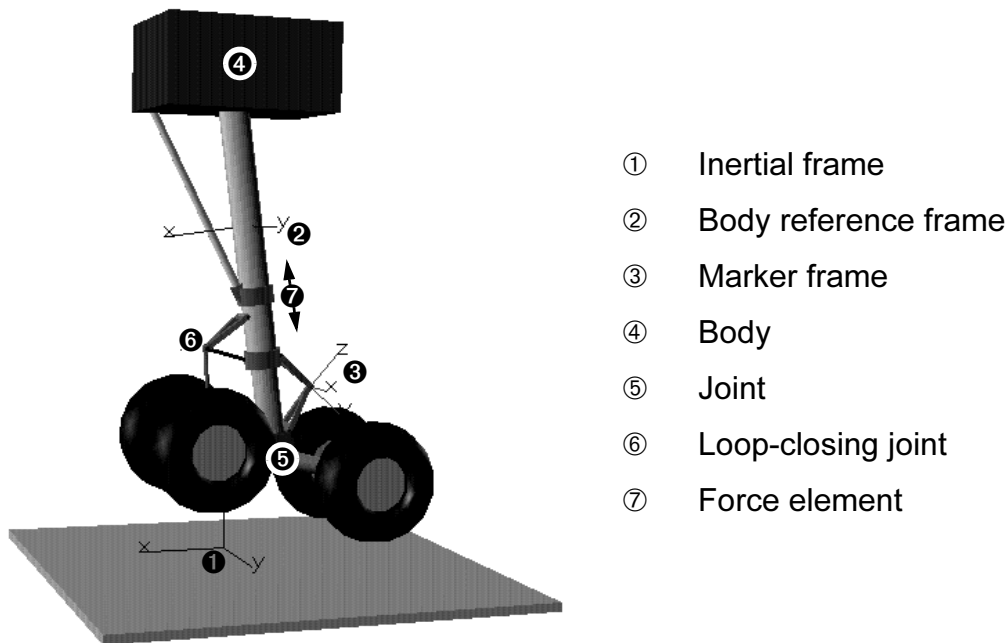
Force Elements

Force elements apply external or internal forces and torques in the system. They may depend upon the state of the system, e.g. the distance between two points, and upon time. Force elements do not affect the degrees of freedom of the system, but may introduce additional states, or boundary conditions, to the differential equation system of the MBS model.

Analytical Techniques

Modern MBS tools offer a multitude of methods to analyse and simulate the generated MBS system. An overview of analysis features can be found in [46]; the most important are:

- **Static analysis** includes the computation of quantities of interest, e.g. positions, applied or constrained forces or other measurements, in static equilibrium or quasi-static states.
- **Kinematic analysis** serves for system assembly, e.g. computation of consistent initial conditions of closed-loop systems on position, velocity and acceleration level, and simulation of the kinematic behaviour (forward and inverse kinematics) of a model.
- **Linear system analysis** linearises the equations of motion numerically, which opens up the entire range of linear system analysis methods, such as covariance analysis, computation of eigenvalues and eigenvectors or root locii analysis.
- **Nonlinear dynamic analysis** delivers a numerical solution of the equations of motion at distinct time steps. A variety of integrators are available to efficiently treat the problem in question, e.g. with respect to numerical stiffness and state or time discontinuities.



- ① Inertial frame
- ② Body reference frame
- ③ Marker frame
- ④ Body
- ⑤ Joint
- ⑥ Loop-closing joint
- ⑦ Force element

Figure 2.3 Elements of MBS Models; here: Drop Test of A340 - Main Landing Gear Leg

2.3.3 Multibody System Coordinates

In general, two basic approaches to define the multibody system exist, [47]:

- In the first approach, the configuration of the system is identified by using a set of Cartesian coordinates that describe the locations and orientations of the bodies, resulting in six coordinates for each body to account for the six degrees of freedom of rigid body motion. The connexions between bodies are introduced by an additional set of nonlinear algebraic constraint equations, thus forming a set of DAEs. This approach is often referred to as using *absolute coordinates*.
- The second approach, with its *relative coordinates*, accounts for the reduction of degrees of freedom because of joint connexions between bodies from the outset: it describes the location and orientation of a body in reference to the “from-body”, i.e. the neighbouring body which has a lower level in the system’s kinematic topology. Thus, only the actual degrees of freedom of the connecting joint, and consequently of the body in question, are added to the system.¹¹

Depending on the application, the relative coordinates approach will generate a significantly smaller set of equations. This advantage is at least partially impaired by the comparatively increased complexity of the equations of motion and more complex generation of the Jacobian matrix. Both approaches are realised in commercially available MBS software packages; advanced methods are employed to accelerate the MBS analysis, e.g. sparse-matrix algorithms for efficient handling of the large system matrices (esp. the Jacobian matrix) generated with absolute coordinates, or scanned-Jacobian techniques to accelerate the evaluation of the Jacobian in relative coordinates. A detailed comparison between both approaches can be found in [48].

2.3.4 Multibody Systems Formalisms

The motion of a multibody system with the mass matrix \mathbf{M} can be described by its generalised coordinates \mathbf{q} , velocities $\dot{\mathbf{q}}$ and accelerations $\ddot{\mathbf{q}}$

$$\mathbf{M}(\mathbf{q})\ddot{\mathbf{q}}(t) = \mathbf{f}(\mathbf{q}, \dot{\mathbf{q}}, \boldsymbol{\lambda}, t) - \mathbf{G}^T(\mathbf{q}, t)\boldsymbol{\lambda}. \quad (1)$$

\mathbf{f} is the vector of applied and gyroscopic forces and $\mathbf{G}^T\boldsymbol{\lambda}$ represents the constraint forces. The constraint matrix \mathbf{G} defines the restrictions which enforce a system motion consistent with the kinematic constraints, and the vector of Lagrangian multipliers $\boldsymbol{\lambda}$ contains the magnitude of constraint forces.

The equations of motion can be (numerically) solved by two different approaches, [48]:

11. Each body of a multibody system has a connecting joint. The body may have additional constraints created by one or more loop-closing joints. Multibody systems in state-space representation have a set of minimal coordinates which automatically account for these constraints, the more common multibody systems in descriptor form use additional algebraic constraints to account for them. For more details on the representation of MBS, please refer to Section 4.2.

- Classical formalisms reduce the equations of motion by mechanic principles, e.g. the principle of virtual work. With the additional information that constraint forces act orthogonal to the unconstrained motions of the system, they separately compute mass matrix, constraint matrix and the applied forces. The computational effort increases at least with the power of two in respect to the degrees of freedom of the system.
- O(n)-formalisms account for the orthogonality of constraint forces and unconstrained coordinates at a local joint rather than for that of the entire system. Additionally, they exploit the kinematic structure of the system. As a result, the equations of motion can be generated explicitly in the form

$$\ddot{\mathbf{q}} = \mathbf{M}^{-1}(\mathbf{f}(\mathbf{q}, \dot{\mathbf{q}}, \boldsymbol{\lambda}, t) - \mathbf{G}^T(\mathbf{q}, t)\boldsymbol{\lambda}) = \mathbf{h}(\mathbf{q}, \dot{\mathbf{q}}, \boldsymbol{\lambda}, t). \quad (2)$$

For O(n)-algorithms, the computational effort increases only linear with the degrees of freedom. Further reduction can be achieved by residuum formalisms, which generate the equations of motion for implicit integration algorithms, using information about the characteristics of the terms which are exerted by the integrator.

2.3.5 Numerical Integration

In the equations of motion, all unknown variables (absolute acceleration, Lagrangian multipliers, ...) appear in linear form. The transformation of the kinematic state variables \mathbf{z}

$$\mathbf{x} = (\mathbf{z}^T, \dot{\mathbf{z}}^T)^T \quad (3)$$

delivers a set of first order differential equations of the form

$$\dot{\mathbf{x}} = \mathbf{f}(\mathbf{x}, t). \quad (4)$$

As we know the state \mathbf{x} , the first derivative of \mathbf{x} in respect to time, $\dot{\mathbf{x}}$, and consequently all other unknowns, can be computed. Choosing an initial condition

$$\mathbf{x}_0 = \mathbf{x}(t = t_0) \quad (5)$$

allows to execute a numerical time integration of the equations of motion, delivering the system's behaviour over time. The choice of the employed integration algorithm is mainly influenced by the required precision as well as stiffness and stability aspects of the system. The precision is defined by the user's (and the job's) requirements. Stiffness and stability are influenced by the physical properties of the system, the modeling approach and the characteristics of the integration method.¹² Additional factors such like state-dependent discontinuities may further limit the range of applicable integrators. Table 2.1 gives an overview of MBS integration methods, [49].

12. Although some consideration prior to the time integration may exclude some integration methods from the possible choices, it is often difficult to select an appropriate integrator for the job right from the start, not to speak of the best integrator settings. Trial-and-error is not uncommon to determine an acceptable (fast, stable and adequately precise) integration method and its optimal parameters.

Integrator	Method	Area of Application
DOPR156	Runge-Kutta method	non-stiff, smooth models
RK Bettis	Runge-Kutta method	non-stiff models with splined model parameters
LSODE	multistep method	stiff systems, systems with elastic components
LSODA	multistep method	systems with state-dependent stiffness
LSODAR	multistep method	systems with state-dependent stiffness
SODASRT	multistep method for DAEs	systems with closed loops, with or without discontinuities
RADAU 5	backward Euler method	systems with closed loops, systems with highly oscillating components
EXPEUL	forward Euler method	for test and comparison
IMPEUL	backward Euler method	for test and comparison

Table 2.1 Numerical Integration Methods for MBS Equations of Motion

2.3.6 Multibody Simulation in Aircraft Ground Dynamics

The technology of multibody simulation with its associated software tools has been developed to analyse complex, arbitrary mechanical and mechatronic systems. The dynamic motion of a free-flying aircraft is apparently dominated by the movement of one body with its six rigid body degrees of freedom - a system which does not necessarily require the particular capabilities of sophisticated multibody codes.

It has to be observed that the emphasis of aircraft ground dynamics analysis lies on the correct representation of the dynamics of this particular vehicle, not on the flight mechanics.¹³ Aircraft ground dynamics has been dealt with by using multibody simulation for a long time and with excellent results. This is not astonishing as the dynamics of aircraft landing gears and their interaction with the airframe represent a somewhat “classical” application of multibody simulation, see Figure 2.4, quite similar to those in other areas of vehicle dynamics such as automotive or wheel/rail, [50]. In fact, MBS represents a major tool for aircraft ground dynamics analysis and evaluation, ground loads analysis and airframe and landing gear certification.

Thus, multibody simulation serves in a wide range of application fields in aircraft ground dynamics analysis - throughout the aircraft’s design process. Among them are:

- *overall dynamic behaviour*, e.g. landing impact, high-speed rolling;
- *ground loads* on airframe and landing gear;
- *handling qualities* on/near the ground;

13. Nevertheless, the use of multibody simulation as a tool for aircraft flight mechanics is growing as well, e.g. in the research programmes AMANDA (A Multidisciplinary High Performance Numerical Development System for Aircraft) or AeroSUM (Aerodynamic Simulation of Unsteady Manoeuvres).

- *ground handling*, e.g. push-back, sharp low-speed turns;
- *rough or unpaved runway* performance;
- *shimmy* analysis;
- *safety issues* and other cases which are difficult or hazardous to examine in field tests;
- *certification* analyses and
- analysis of *unconventional configurations* where no data is available to serve as a reference for heuristic approaches.

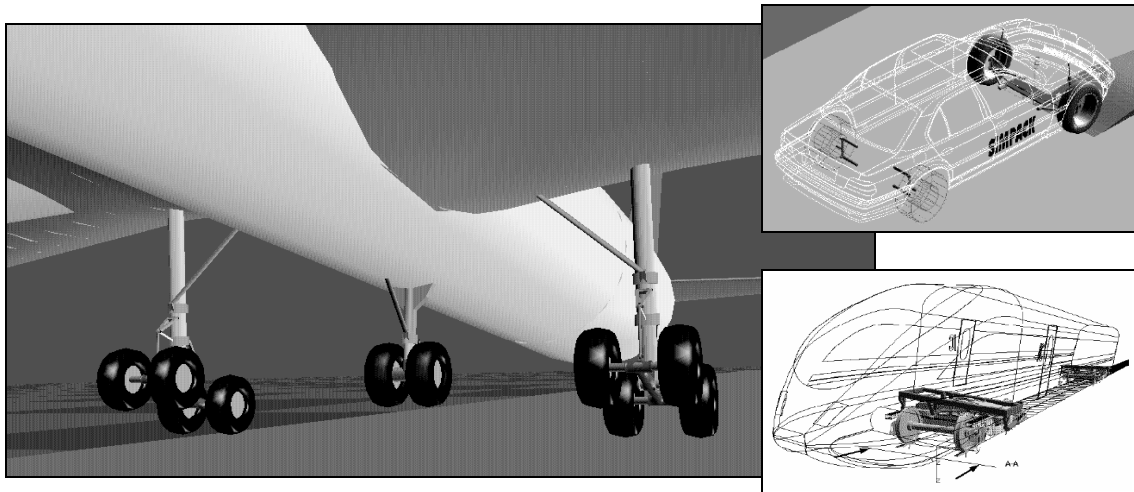


Figure 2.4 Typical MBS Applications: Automotive (upper right), Wheel / Rail (lower right) and Aerospace - Aircraft Ground Dynamics (main left)

Originally considered as a tool for the early design stages, MBS is now being employed throughout the aircraft development cycle. Figure 2.5 shows the major characteristic issues of aircraft design, [51].

The focal point of this very brief list lies on the current state and common use of CAE software and the general environment the development takes place; other aspects, e.g. production design, are neglected. Contrary to other engineering disciplines, for example aerodynamics, where different tools are being employed depending on the task and the level of detail required, multibody simulation covers practically all areas of that specific discipline of system dynamics and thus serves, for various purposes, throughout the aircraft design process: in the conceptual design phase as well as in preliminary and detail design.

2.3.7 Methods of Modelling Aeroelastic Effects in Multibody Systems

Several approaches exist to include aerodynamic and aeroelastic effects in aircraft ground dynamics. In this section, an overview will be provided over the common methods and their specific characteristics.

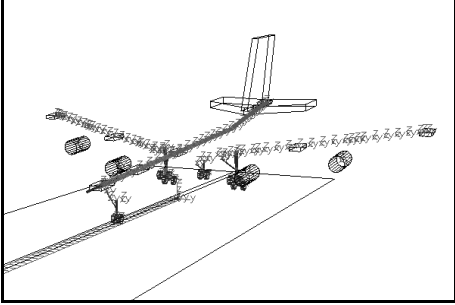
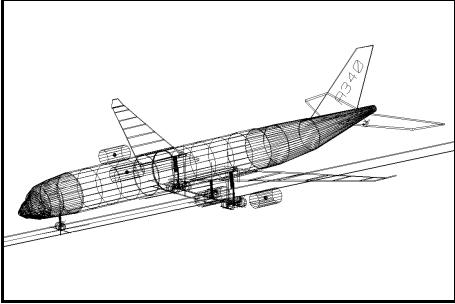
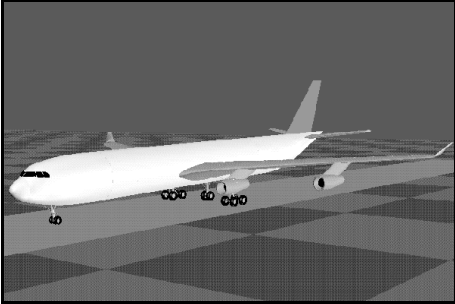
Aircraft Design	
Phase	Characteristics
<p>Conceptual Design</p> 	<ul style="list-style-type: none"> • dynamic and fluid multidisciplinary design process • large number of design alternatives • guide and evaluate design requirements of the overall aircraft configuration • low level of detail • study of “global” or significant interactions • small, self-contained group of contributors
<p>Preliminary Design</p> 	<ul style="list-style-type: none"> • major configuration fixed • occasional reshapes of the overall design • increasing level of detail and of understanding of the design • commencement of sub-system analysis and design by specialists • validation of the aircraft concept (predictions of the conceptual design phase)
<p>Detail Design</p> 	<ul style="list-style-type: none"> • full-scale development by large number of monodisciplinary designers and analysts • ramified organisational structure • high level of detail (analysis and design) • high level of confidence required • regular checks of design goals • field test results (esp. of components) become available

Figure 2.5 Main Characteristics of an Aircraft Design Process

Scaled Gravity Method

The method of scaled gravity assumes that during a landing sequence, a constant lift (in most cases equal to the actual aircraft weight) is acting on the aircraft. This approach usually holds for the initial impact of transport aircraft with a sufficiently stiff airframe structure. As already indicated, this is the universal method to account for aerodynamic forces by the certification requirements FAR 25 Sec. 25.473(b) “Landing load conditions and assumptions”, [52]: “Aeroplane lift, not exceeding aeroplane weight, may be assumed unless the presence of systems or procedures significantly affects the lift.”

This method is simple, fast and robust. It is not only applied for certification purposes, but most design and load studies are being performed with this approach as well.¹⁴ The problem: Analysing the structural dynamic response of the airframe is encumbered with the fact that the physics of the modelled procedure are not adequately represented, e.g. the aircraft approaches with undeformed wings or wings bent downwards because of their (residual) structural weight instead of upwards because of aerodynamic lift. Experience has shown that dynamic behaviour and loading conditions of aircraft and landing gear are very sensitive to small variations of the scenario or perturbations of the procedure.

Distributed Aerodynamic MBS Force Elements

Attempts have been made to account for airloads on the elastic structure in MBS modelling strategy by defining local force laws on markers of the elastic aircraft model, [28]. These MBS force elements are user defined and apply local forces and torques generated by analytic functions or interpolation of aerodynamic matrices. This approach solves some of the problems stated above: the airframe is being deflected by a +1g-load, the force law(s) can be state-dependent (e.g. to account for changes of the global or local angle of attack) and may even contain unsteady terms, and pilot control inputs and ground effect can be included.

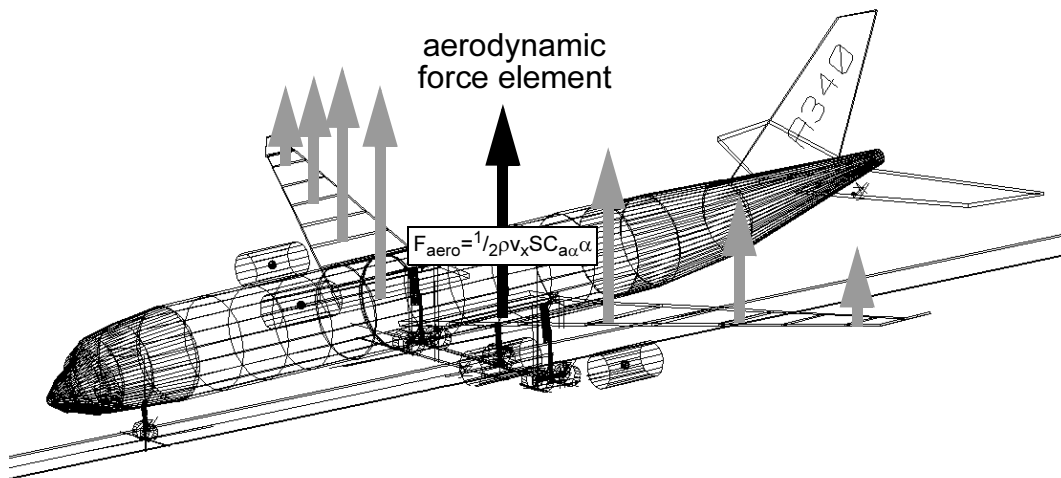


Figure 2.6 *Distributed Aerodynamic MBS Force Elements on MBS Model*

The advantage gained by this method is nevertheless limited. In the majority of applications, the implied aerodynamic force laws are highly simplified. Additionally, an aerodynamic force law is usually defined for a stripwise section of the wing. Although this is a reasonable solution for a clean wing with a high aspect ratio, modelling of configurations with low aspect ratio or wings with extended flaps and slats results in a poor

14. To prevent the aircraft from being “repelled” by the ground and starting to float again in a landing sequence, gravity is usually “switched on” at the lowest point of damper deflection or when the energy of landing impact has been consumed, and the subsequent landing roll takes place under +1g-conditions.

approximation of the distributed airloads. In general, these simplified aerodynamic force laws offer a physically more appropriate approximation than the method of gravity vector scaling. For transport aircraft models, accuracy of results is often improved as well, but still remains within the limits of general, qualitative investigations.

The attempt to set up more detailed force laws to obtain reliable quantitative results is cumbersome and work-intensive. Additionally, applicability is usually restricted to the model or case in question. The laws must be derived from CFD calculations or wind tunnel measurements of the high-lift configuration (e.g. total lift) or have to be defined using empirical data (e.g. useful for control surface deflections). Modelling the influence of local elastic deformations on the aerodynamic forces appears to be possible as well, but will require extensive modelling effort. Partially automated modelling techniques have been developed to lower the necessary effort, [53], but a model set-up still requires extensive investment of both, specialist knowledge and manual work. Possible enhancements to MBS for advanced aeroelastic force elements will be briefly covered in Section 5.3.1.

The approach of aerodynamic or aeroelastic force elements is not easy to apply effectively in an actual aircraft design process: the generation of detailed, reliable models is tedious, the necessary data has to be processed or must be available in a form that supports this MBS modelling technique, and finally every change of the design that influences the aerodynamic, structural or flight mechanical properties of the aircraft may require a new, labour-intensive model revision.

Co-Simulation

A widely used method in the regime of fluid/structure interaction, co-simulation can be used for multibody simulations as well. The underlying concept is straightforward: the CFD- and MBS-code communicate their specific solution at a discrete, often pre-defined time step; each code then proceeds with the new data set for the other regime. The principle is sketched in Figure 2.7, where model state and required measurements are transmitted from the MBS code to the CFD tool. The CFD solver generates a solution for the given state and passes back the resulting aerodynamic forces, which are included into the MBS model. The MBS code then advances in its time-integration until the next communication time step where the procedure is repeated, [54].

This approach is quite powerful: it is possible to access most capabilities of the tools involved; even highly nonlinear unsteady effects can (theoretically) be accounted for. It is nevertheless very time-consuming, too: the number of required CFD analyses and, if applicable, updates of the aerodynamic mesh demand their fair share of CPU time. Additional questions of interest are the convergence of solutions and general stability of both, the numerical solvers of the respective codes and of the process itself, [55].

For applications in aircraft ground dynamics, the quality of CFD solutions is additionally limited: analyses of full aircraft models in high-lift configuration remains a challenging task, especially for advanced CFD codes (Euler, Navier-Stokes).¹⁵

Less elaborate CFD solvers like high-level panel codes have the advantage of considerably lower computation times and more robust solutions, even for aircraft models

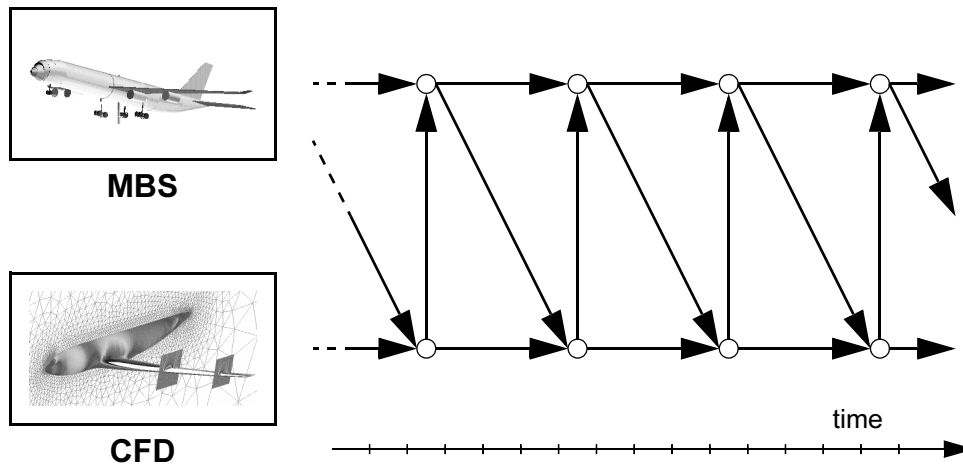


Figure 2.7 Inter-Process Communication (IPC) Between MBS and CFD

with high-lift devices deployed. Although the solution may not have the degree of detail precision that can usually be provided by more complex CFD tools, the quality of the results is often sufficient for this specific purpose, but with about one hour per analysis¹⁶ for a full model of a transport aircraft, the duration of a simulation in the time-domain is still unacceptable in present design processes: a standard, straightforward IPC analysis of a landing sequence, for example, would take about two weeks of CPU time to finish.

2.4 Computational Fluid Dynamics

2.4.1 Overview

Computational aerodynamics is the latest of the three main branches of aerodynamic science. The development of accurate numerical algorithms for solving aerodynamic problems on the computer has revolutionised modern aircraft design, but the other two branches, experimental and theoretical aerodynamics, remain essential approaches in the field of aircraft aerodynamics. Contributing to the idea of a concurrent, virtual design process of aeroplanes (with the focus on the field of aircraft ground dynamics), this work concentrates on computational methods, although most, if not all, of the required data could also be achieved by experiments.

Computational fluid dynamics is arguably the most important numerical research and design tool for aerodynamic analysis and evaluation. Similar to the science of

15. The preponderance of research activities and applications in IPC concentrate on Euler or Navier-Stokes codes on the CFD side (e.g. for analysis of the highly manoeuvrable fighter aircraft).
16. CPU time estimation is given for a high-performance desktop computer (workstation, Power-PC). Necessity to use supercomputers to run an analysis would be counterproductive, as it undermines the principle of decentralised, rapid and flexible interdisciplinary design.

mechanics, the fundamentals of aero- and hydrodynamics were developed in the age of enlightenment. Major achievements in theoretical aerodynamics are in fact attributed to personalities which had a strong influence on the progress of classical mechanics as well; among them *Euler*, who derived the equations of motion for an inviscid fluid (Euler equations), and the mathematical contributions of *Lagrange* and *Laplace*. With the work of *Navier* and *Stokes*, who independently introduced the effects of friction, the fundamental equations to analyse viscous flow fields have been found, [56].

Although the basic aerodynamic equations were known and well established in the middle of the 19th century, no general solution for this system of nonlinear partial differential equations (PDE) has been found so far. Thus, scope and level of detail of aerodynamic problems which could be solved remained limited. With the development of digital computers, it became possible to obtain numerical solutions for the full nonlinear Navier-Stokes equations (NSE). In the 1970ies, more complicated configurations such as slat-flap systems could already be analysed in detail, but with the computational and storage power available at that time, these CFD applications were mainly restricted to two-dimensional flows. By 1990, storage and speed capacity of computers had reached a level where three-dimensional flow field solutions became feasible, even for more elaborated problems. Since then, the widespread use of advanced computer architectures, e.g. vector or parallel processing, as well as the dramatic increase in computational power because of faster processors and more powerful storage systems enhanced the possibilities of CFD significantly. On the software side, sophisticated approaches further increased the performance and handling of CFD codes, such as hybrid grid methods which combine the modelling advantages of unstructured meshes with the performance and accuracy advantage of structured grids, or multigrid solver acceleration to speed up iterative solving algorithms.

Current research activities in CFD include unsteady aerodynamics, e.g. the analysis of highly manoeuvrable aircraft at high angles of attack, the aerodynamics of deformable structures (fluid / structure interaction), validation and calibration of CFD computations with laboratory or flight measurements and the embedding of CFD in multidisciplinary optimisation processes.

2.4.2 Fundamentals of Computational Fluid Dynamics

The fundamental governing equations of fluid dynamics - continuity, momentum and energy equations - are the basis of CFD.¹⁷ In their full form, they include the effects of friction, thermal conduction and mass diffusion. These equations can be simplified by approximate assumptions, of course at the cost of neglecting certain effects. From this point of view, three different levels of abstraction can be distinguished:

- Navier-Stokes methods are widely regarded as the ultimate answer to fluid dy-

17. Computational fluid dynamics comprises a manifold variety of methods and approaches. A comprehensive overview of all methods is well beyond the scope of this work. This section gives but a rough outline of methods which may be of interest for aerodynamic MBS preprocessing.

dynamic problems. The partial differential equations of the NSE are solved directly by PDE solution methods. The range of validity is only limited by the model used for the viscous stresses. The numerical methods can be roughly divided into finite difference, finite volume and finite element methods, [57]. The form of NSE most commonly used are the Reynolds averaged Navier-Stokes equations (RANS), which do not support turbulence modelling or turbulent transition - these fields have to be handled by other approaches, e.g. by direct numerical simulation (DNS) or large-eddy simulation (LES).

An alternative approach, the Boltzmann gas lattice method (BGLM), models the microscopic physics of the particles that compose the macroscopic fluid. Thus, it solves the equations of the continuum (NSE) indirectly by mimicking the fluid dynamics at the molecular level.

- Euler methods

use the Euler equations instead of the full set of NSE.¹⁸ The Euler equations neglect friction and thermal conductivity; they are valid only for unsteady compressible inviscid flow. Consequently, drag, boundary layer separation and turbulence cannot be computed directly, although approximation methods exist to account for these effects subsequently.

Basically, the Euler equations can be generated by neglecting friction and thermodynamic terms of the NSE. Thus, some CFD codes allow to toggle between Euler and full Navier-Stokes analysis. Computational effort and CPU time of Euler analyses are significantly lower than for the full Navier-Stokes equations, but solving a complex problem will still take a couple of hours, if not days.

- Potential flow methods

(PFM) represent a special solution of the Euler equations: the Cauchy-Riemann equations imply that a vector (e.g. velocity) field which has no curl can be expressed as the gradient of a potential function. The introduction of the potential function facilitates the computation of the Euler equations significantly: four equations, three of them nonlinear, can be substituted by one linear (potential) equation.

18. Historically, the Navier-Stokes equations as well as the Euler equations did not include the energy equation, [56]. In modern literature, both terms have been expanded to include the entire system of flow equations: continuity, energy and momentum. In this work, the terms Navier-Stokes and Euler equations will be used in accordance with the latter notion.

The “physical consequences” are that the potential flow approach introduces significant approximations: potential flows are inviscid, incompressible and irrotational. Despite these restrictions, PFMs can be employed for a variety of applications, e.g. for low-speed aerodynamics. Several modelling approaches exist to create a numerical potential flow solver; among them lifting line methods, lifting surface methods and surface panel methods.¹⁹ Correction methods and processes exist to enhance the range of application of these approaches.

Potential flow methods require no discretisation of the flow field, which significantly simplifies the set-up of a CFD analysis model and accelerates the computation.

2.4.3 Computational High-Lift Aerodynamics

High-lift systems are required in aeronautics to reduce take-off and landing speed or produce higher manoeuvrability, for higher payload or aircraft weight constraints, maximum engine power limits, etc. Transport aircraft, which often cruise at transonic speeds, are fitted with various measures to increase the maximum lift coefficient, e.g. leading- and trailing-edge devices such as slats and flaps.

Accurate prediction of the aerodynamic properties of aircraft equipped with multi-element high-lift systems is still considered an open problem in computational aerodynamics. Potential flow methods are still widely employed to analyse, evaluate and optimise the design. In the past few years, however, the computational methods for high-lift have been expanding towards Navier-Stokes solvers, although less expensive methods which include strongly interactive boundary layers have proven to be almost as successful.

The method of computation depends on the data available, the complexity of the problem (2-D, 3-D, number of high-lift bodies, precision requirements, turbulence modelling, etc.) and, of course, on time and budget constraints. They can be split up into three fundamental classes:

- Inviscid Methods are able to satisfactorily compute three-dimensional high-lift systems with large vortex drag, e.g. with efficient panel methods. When flow separation becomes a non-negligible effect, or the viscous effects must be accounted for in general, the possibilities with inviscid methods are limited.
- Viscid-Inviscid Methods are basically coupling techniques between different

19. In this work, a distinction is made between methods which concentrate the panels on a straight or cambered chord line, subsumed as lifting surface methods, and methods which place the modelling panels on the physical surface of the airframe, denoted surface panel methods.

approaches, e.g. a viscous method for the boundary layer and an inviscid method for the far-field airflow, [58]. The progress of this approach relies primarily on the coupling algorithm. Successful realisations are the semi-inverse method, [59], quasi- and fully-simultaneous methods, [60], [61], and the semi-implicit method, [62].

- Navier-Stokes Methods for high-lift analyses include both unstructured and multi-block structured approaches. Navier-Stokes codes are very time consuming, and have been applied essentially to 2-D problems. Three-dimensional wings are being treated as well, but analysis of full 3-D configurations has still to become a standard application in an aircraft design process.

2.5 Fluid-Structure Interaction

Multibody simulation of a flexible aircraft exposed to airloads implies that it is possible to distribute these aerodynamic loads on the deformable MBS aircraft structure. In aerodynamics, the airflow around the aircraft's contour is analysed to deliver the resulting pressure on its surface, whereas structural analysis primarily concentrates on the internal structure of the airframe. Consequently, the discretisations of the modelled system are fundamentally different. The key task of aeroelastic interaction between fluid dynamics and structural mechanics is to establish a numerical transformation of physical quantities between both disciplines.

The underlying problem of fluid-structure coupling is to set up a relation which interconnects scalar or vectorial quantities located at discrete grid points with corresponding values at an arbitrary set of other grid points. The aerodynamic mesh usually contains the body's discretised contour as a boundary condition of the solution. The structural representation for elastomechanical modelling does not necessarily have elements, or grid points, in the wetted surface area. A fluid-structure coupling therefore faces boundary conditions (the scalar and vectorial quantities) at the respective reference points, which have to be transformed from one domain to the other and back by adequate interpolation methods to achieve a local²⁰ but smooth interpolation.

Besides the vast assortment of interpolation algorithms published in the pertinent literature, coupling and interpolation libraries exist as ready-to-serve solutions. Among the most advanced multidisciplinary tool kits, offering far more than interpolation routines, are:

- MDICE (Multi-Disciplinary Computing Environment), which is a commercial

20. In this context, "local" interpolation means that a displacement of a sampling point has only minimal, if any, impact on the interpolation at distant sampling points (compactly supported basis functions).

product spun off from the US - DoD project FASIT (Fluid and Solid Interface Toolkit). MDICE has been developed by CFD Research Corporation with funding from NASA Glenn Research Center and the Air Force Research Laboratory - Air Vehicles Directorate at Wright-Patterson Air Force Base.

The FASIT project produced a library of generic tools for mapping fluid mesh geometries onto structural meshes and vice-versa. MDICE itself has been derived from the software system VCE "Visual Computing Environment", that had been developed by NASA Lewis Research Center to enable coupling among various flow-analysis codes. The focus lies on connexion of and data exchange between CAD, CFD and FEA software tools.

- MpCCI (Mesh-based parallel Code Coupling Interface), which is based on the coupling interfaces COCOLIB (Coupling Communication Library) developed during the EC-funded CIPAR project and on GRISLi-CI developed during the GRISLi project (funded by the German Federal Ministry for Education and Research). MpCCI has been developed by the Institute for Algorithms and Scientific Computing (SCAI). SCAI had been a research facility of GMD Gesellschaft für Mathematik und Datenverarbeitung mbH. Since the fusion of GMD with Fraunhofer-Gesellschaft in 2001, further development is carried out by Fraunhofer SCAI. Pallas GmbH in Brühl, Germany, is exclusive distributor for MpCCI. The main objective of MpCCI is to provide open, high-performant tools to interpolate between two- or three-dimensional surface or volume meshes and to synchronise multidisciplinary analyses where such interpolation is required.

Both program packages provide an object-oriented computing environment for generic multidisciplinary applications. In these environments, computer programs can operate concurrently and cooperatively to solve a multidisciplinary problem. Fluid-structure coupling is one of the main applications of both program packages. The proven interpolation routines can significantly facilitate the job to interconnect the structural and aerodynamic model.²¹ It would be also possible to use MpCCI, respectively MDICE, as a direct connexion tool between CFD and MBS, but computation times for the resulting IPC process will far beyond acceptable limits.

21. For several reasons, for all fluid-structure interpolation topics this work concentrates solely on MpCCI routines; among them: MpCCI provided all necessary functionality and it was free software at the time the interpolation computations were performed.



3 Solution Strategy

3.1 The Problem of Aeroelastic Effects in Aircraft Ground Analysis

“Lessons learned” in the development of the actual generation of civil transport aircraft indicate that it is no longer sufficient to optimise the aircraft solely with respect to pre-defined (and pre-known) critical conditions and the applicable certification cases. If an aircraft is to be developed in a virtual design environment, then analysis, simulation and testing tools must be capable to provide answers to complex interdisciplinary questions in this “domain” as well.

In short: The next generation of CAE tools in aviation will have to provide comprehensive interdisciplinary analysis and simulation capabilities. This is also true for multi-body simulation of aircraft ground dynamics.

3.1.1 Shortcomings of Conventional Simulation Capabilities

In aircraft ground dynamics, the loads applied on landing gear and airframe as well as the dynamic behaviour of the aircraft itself depend strongly on the particular circumstances - the obvious influence factors such as aircraft configuration, attitude and sinking speed are important for a rough estimation, but for more detailed, reliable and comprehensive results the actual scenario has to be modelled and analysed with a high degree of complexity, too. As an example, the actual timing of lift dumper deployment during a landing has a significant impact on the applied loads: activated at the right (or, rather, wrong) moment during rebound after a hard landing, the sudden loss of lift may cause the aeroplane to drop back into already compressed shock-absorbers, resulting in considerably higher loads on gear and airframe than at the landing impact itself. The effect is well-known, but being able to find the most critical condition(s) and to quantify the results is a challenging task.

So far, in most aircraft ground dynamics analyses, and in fact most aircraft developments in general, aircraft and landing gear designers have concentrated on certification requirements. If these requirements could be met, most critical conditions would be covered. New aircraft developments, however, may raise other, or additional, requirements:

- **Economy:** The certification requirements have been set up to ensure a high safety standard of aircraft, not to ensure best performance or low operating costs. In the case of the aforementioned problem of lift dumper deployment, for example, it does not necessarily affect the safe operation of the aircraft. The fatigue performance of the landing gear will probably decrease, but with proper maintenance the components in question will be replaced in time to avoid any risk. Nevertheless, the impact on maintenance, and consequently operation costs can be significant.

- **Applicability:** For very large aircraft, some certification requirements (many of which are basing on empirical data) do not represent reality. For the Airbus A380, for example, the lateral loads due to turning, respectively curving, are exaggerated, whereas other critical conditions like the torsion load on the main landing gear leg in a sharp turn (e.g. during push-back from the gate) are not adequately covered.
- **New problems:** Improvements in aircraft design, e.g. sophisticated lightweight constructions leading to increased structural flexibility, can cause new or so far uncritical phenomena to become an important issue. They have to be detected and counteracted as early as possible.
- **New concepts:** The point stated above is even more valid for unconventional designs, e.g. blended wing bodies. Doubts about the validity of analysis results which cannot be crosschecked with empirical data and uncertainty about the regulations which will finally be applied are among the major concerns everytime a new, unconventional configuration is being evaluated.

Advanced aircraft ground dynamics simulations will have to cover these additional requirements as well. Comprehensive and detailed physical modelling and analysis has to ensure that all realistic, “flyable” conditions and scenarios can be simulated and evaluated.

Experiences gained in research projects²² have identified two major areas of improvement of aircraft ground dynamics analysis and simulation, [33], [63]. These are

- for highly dynamic scenarios (take-off, landing and high-speed ground run simulations): consideration of aerodynamic effects on the flexible aircraft structure,
- for the low-speed regime (push-back, sharp slow turning and curving): realistic tyre data, properties and models for high slip and torque conditions at low speeds.

These findings are in line with the opinion of the U.S. Committee of Aeronautical Technologies which states in their study on “Aeronautical Technologies for the 21st Century” for aerodynamic aspects of takeoff and landing flight dynamics that current analysis capabilities are not sufficient to detect and avoid “undesirable dynamic characteristics”, concluding: “It is important that sufficiently accurate techniques be applied to predict dynamic characteristics from the beginning of the design effort”, [64].

3.1.2 Importance of Simulation of Aerodynamic / Aeroelastic Effects

In general, an aircraft in trimmed, straight flight generates a lift equal but opposed to its weight force. This is valid, of course, for a landing approach as well. Even during the first moments of touch-down, the aircraft attitude remains almost unchanged. Therefore, it is obviously an acceptable simplification to analyse landing impacts under the assumption of “lift equals weight” and to omit (or, for some cases, reduce)

22. ELGAR, Flexible Aircraft I - III; see Section 2.2.2, page 17.

the effects of gravity.²³ This is, in fact, the method used in the certification requirements - and it has worked well for stiff (rigid) aircraft structures. For a simulation environment covering the level of detail and precision as sketched in the paragraph above, this is no longer sufficient:

- Scaling of the gravity vector can only be used for the analysis of the landing impact itself. More complex scenarios, e.g. those including a final approach or considering the rebound after impact, can not be simulated realistically.
- The deformation of the structure during the landing impact starts from the unstressed 0g-configuration, not from the pre-stressed +1g-state like in reality.
- The airloads resulting from an elastic airframe (esp. wing) deformation have significant influence on the dynamic behaviour. They may damp as well as excite the aircraft motion or deformation, see Figure 3.1.²⁴
- Aircraft control surface deflections, e.g. pilot control inputs or lift dumper deployment, can not be accounted for realistically.
- The influence of ground effect is neglected altogether.

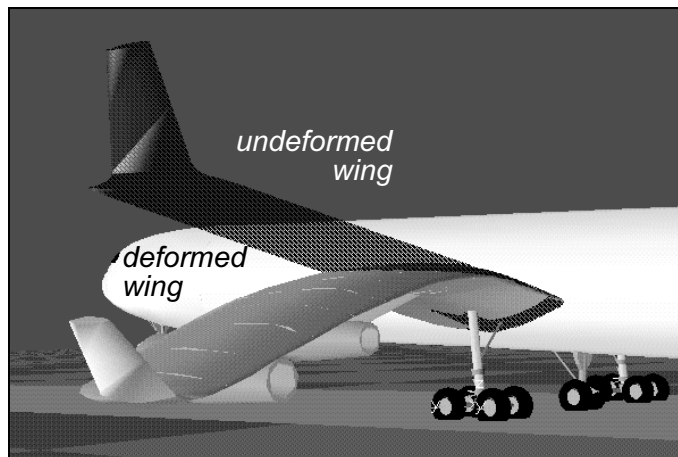


Figure 3.1 Deflection of an A340-300 Wing at a Hard Touch-Down (10 fps-landing at MLW)

As a consequence, further progress in aircraft ground dynamics analysis in terms of increased precision and reliability of results and enhanced modelling capabilities (e.g. complex scenarios) will only be possible if the airloads acting on the elastic aircraft structure can be accounted for.

3.1.3 Requirements on an Aeroelastic Enhancement to MBS

With MBS being a rather universal tool for system dynamics, an aeroelastic enhancement to MBS should be able to cover this broad range as well to avoid inefficient and

23. Please refer to Section 2.3.7, “Scaled Gravity Method”, for more details.

24. For an impact at a descent rate of 10 fps, as shown in Figure 3.1, deflection of the wing at its tip can be as much as 2.8 m.

error-prone “switching” between different approaches. This claim, of course, involves a design conflict between precision and computation times. If we further take into account that this tool has to suit the aircraft manufacturer’s design processes, satisfy the demands of the various fields of application sketched above, will be applied by users who are no aerodynamic specialists and should blend in a multidisciplinary optimisation (MDO) process, the following requirements can be derived:

- Strategy
 - physical approach for non-heuristic evaluation;
 - use of customary CAE software tools;
 - access of existing knowledge (e.g. modelling);
 - compatibility to interdisciplinary aircraft design processes.
- Scope
 - incorporating rigid body motion (reproduction of the aircraft flight mechanics);
 - influence of pilot control inputs, respectively control surface deflection;
 - influence of elastic deformations on aerodynamic loading conditions;
 - influence of aerodynamic damping and excitation effects due to elastic deformation (no eigendynamics required);
 - consideration of ground effect.
- Efficiency
 - precision of aerodynamic, respectively aeroelastic analysis in line with modelling depth of MBS;
 - standardised and (as far as feasible) automated generation of input data;
 - easy handling for users without extensive knowledge in aerodynamics;
 - robustness;
 - acceptable computation times.

3.2 Aerodynamic Preprocessing as a Possible Solution

A lot of research activities are underway in the field of fluid/structure coupling and combined analysis. Most work concentrates on high-precision analysis of the flexible aircraft in cruise or on the manoeuvring fighter aircraft at high angles of attack. For aerodynamic and aeroelastic effects in aircraft ground dynamics, the level of detail necessary is significantly lower than for those applications, requiring neither most precise transonic aerodynamics nor to account for highly nonlinear aerodynamic effects. There remains, nevertheless, the problem of aerodynamic representation of the full aircraft with flap-slat-systems deployed, the need of robust and “fool-proof” applicability and, last but not least, the critical demand on computation times. It is therefore not favourable to adopt an existing solution and to undertake a minor trim to fit the specific requirements. This applies for current activities of fluid-structure coupling on IPC basis as well as for other methods which may provide the necessary functionality, e.g. approaches from aeroelasticity (flutter analysis), [65], or aeroservoelasticity, [66].

A similar problem of how to integrate a complex correlation into MBS existed previously for the consideration of deformable bodies in multibody simulation. It was solved

by generating a modal representation of the deformable component from computational structural mechanics (CSM) programs such as FEA which could be included into the MBS equations of motion, [47], [67]. The derivation of modal coupling submatrices is performed in a preprocessing step to the MBS analysis; the necessary data is stored in an input file to MBS, e.g. in SID format which is the standard input format for this functionality, [68]. This method has two main advantages: the extension of the MBS system is moderate which results in acceptable CPU time demands even for large models, and it allows efficient multidisciplinary working as, once created, it is possible to reuse the input file over and over again as long as the structural properties of the modelled component and its operational conditions are not altered.

The underlying principle of the approach proposed in this work is to use a similar strategy and to interrelate aerodynamics and structural mechanics in a preprocessing step to the dynamic analysis, see Figure 3.2. In the following sections, it will be described how the necessary aerodynamic terms can be derived in a second pre-calculation process following the extraction of elastic properties and how they have to be implemented into the MBS equations of motion.

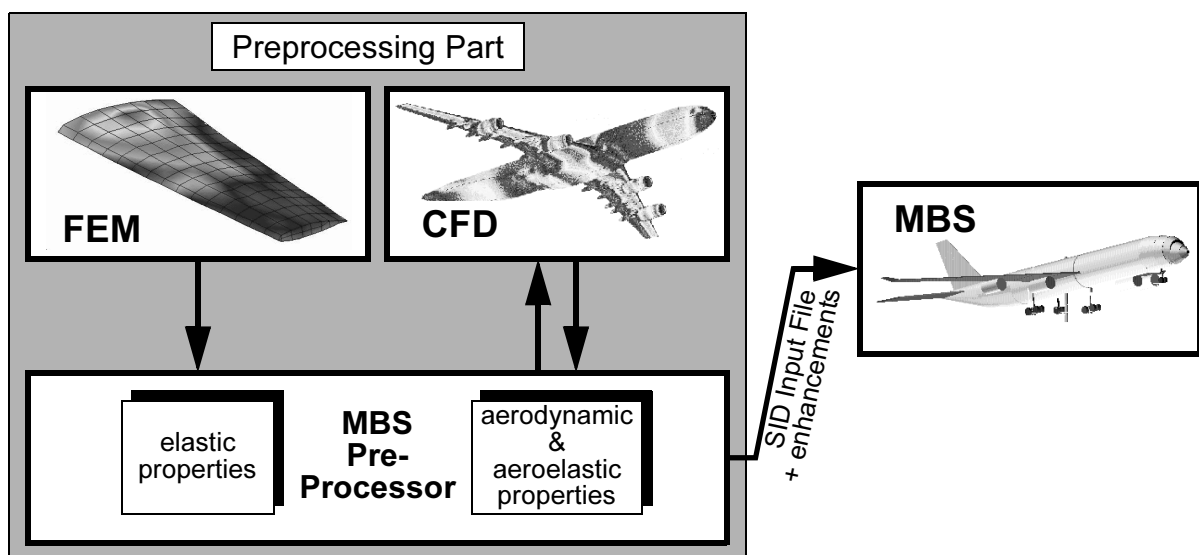


Figure 3.2 Flow Scheme of Aeroelastic Preprocessing

The proposed approach of aeroelastic preprocessing builds up on the method of linearised hybrid multibody dynamics, using modal representation of FEA structures, [69]. The resulting rigid body and elastic degrees of freedom are interconnected with modal aerodynamic influence increments. Additional modal aerodynamic matrices provide aircraft control. The resulting aerodynamic or aeroelastic effects are obtained by superposition of the modal influence increments.

The approach can be applied to all applications where the prerequisites of approximately linear aerodynamic conditions around a given working point and of basically decoupled influence factors hold. It will be demonstrated that this procedure allows efficient modelling of aeroelastic effects in system dynamics evaluations with only negligible influence on the analysis performance.

4 Deformable Bodies in Multibody Simulation Systems

The approach of aeroelastic preprocessing has its roots in the way deformable bodies are represented in almost all modern MBS codes. This chapter recapitulates this modelling technique, the method of modal reduction, before the approach of aeroelastic preprocessing is introduced in the following chapters.

4.1 Classification of Multibody Systems

The configuration of a multibody system is identified by a set of system variables, the generalised coordinates, which determine the mathematic description of the system, i.e. its equations of motion (EqM).

- EqM in descriptor form identify the configuration of the multibody system by using a set of Cartesian coordinates that describe the locations and orientations of the bodies in the system (absolute coordinates). Each body has three translational and three rotational degrees of freedom. The connectivity between bodies is introduced by a set of nonlinear algebraic constraint equations, which is usually adjoined to the system equations by Lagrangian multipliers. Absolute coordinates deliver the equations of motion, as a set of DAEs, in descriptor form.
- EqM in state-space form eliminate the constraints from the equations of motion by using a set of minimal coordinates. The system variables are chosen such that the constraints on the system's motion are satisfied, respectively that the system is defined in a univocal representation. Thus, the equations of motion form a set of ODEs. Integration is more facile than for DAEs, and less variables have to be determined. Because of the compact representation, however, the generation of the equations of motion is expensive, especially for systems with closed loops.
- Partially reduced EqM are a mixture of both forms, descriptor and state-space form. Each kinematic connexion of the system contributes to the equations of motion with its actual degrees of freedom only. Systems with a tree-like topology are represented by a set of minimal coordinates. Systems with kinematic loops possess a set of independent coordinates for all connexions but loop-closing joints; these are incorporated by side condi-

tions, the algebraic constraint equations. Thus, partially reduced equations of motion are in state-space representation for tree-like system topologies and in descriptor form for systems with kinematic loops.

4.2 Equations of Motion of Hybrid Multibody Systems

In a multibody system described by n generalised coordinates \mathbf{q} , the equations of motion can be written as

$$\mathbf{M}(\mathbf{q})\ddot{\mathbf{q}}(t) = \mathbf{f}(\mathbf{q}, \dot{\mathbf{q}}, \boldsymbol{\lambda}, t) - \mathbf{G}^T(\mathbf{q}, t)\boldsymbol{\lambda}, \quad (6a)$$

$$0 = \mathbf{g}(\mathbf{q}, t), \quad (6b)$$

where $\mathbf{M}(\mathbf{q})$ is the $n \times n$ symmetric and positive definite mass, or inertia matrix, $\mathbf{f}(\mathbf{q}, \dot{\mathbf{q}}, \boldsymbol{\lambda}, t)$ is the $n \times 1$ vector of applied and gyroscopic forces, $\boldsymbol{\lambda}$ represents the $m \times 1$ vector of Lagrangian multipliers, and

$$\mathbf{G}(\mathbf{q}, t) = \frac{\partial \mathbf{g}(\mathbf{q}, t)}{\partial \mathbf{q}} \quad (7)$$

is the $m \times n$ constraint matrix, derived from the vector of constraints \mathbf{g} .

The set of algebraic equations of Eq. (6b), and consequently the constraint matrix $\mathbf{G}(\mathbf{q}, t)$, either comprises all constraints of kinematic connexions that act among the coordinates of \mathbf{q} in the case of absolute coordinates, or only those of loop-closing kinematic connexions for relative coordinates. Minimal coordinates and, for tree-like system topology, relative coordinates deliver the equations of motion in state-space form,

$$\mathbf{M}(\mathbf{q})\ddot{\mathbf{q}}(t) = \mathbf{f}(\mathbf{q}, \dot{\mathbf{q}}, t), \quad (8)$$

rather than in the descriptor form of Eqs. (6a) and (6b).

For multibody systems containing deformable bodies, the vector of generalised coordinates \mathbf{q} contains the “classical” rigid body states of the system \mathbf{q}_R as well as additional deformation coordinates \mathbf{q}_E ,

$$\mathbf{q} = (\mathbf{q}_R^T, \mathbf{q}_E^T)^T, \quad (9)$$

expanding the equations of motion to

$$\begin{bmatrix} \mathbf{M}_R & \mathbf{M}_{RE} \\ \mathbf{M}_{ER} & \mathbf{M}_E \end{bmatrix} \begin{bmatrix} \mathbf{q}_R \\ \mathbf{q}_E \end{bmatrix} = \mathbf{f}(\mathbf{q}, \dot{\mathbf{q}}, \boldsymbol{\lambda}, t) - \mathbf{G}^T(\mathbf{q}, t)\boldsymbol{\lambda}, \quad (10a)$$

$$0 = \mathbf{g}(\mathbf{q}, t). \quad (10b)$$

Because of this dispersed structure, it is possible to concentrate on the representation of aerodynamic effects on a single deformable body.

4.3 Deformable Bodies

In comparison to FEA analysis, which has its focus on the deformation of a structure or component, the emphasis of multibody simulation lies on the dynamic behaviour of the overall system. Applications are usually characterised by a quantity of bodies, undergoing large, nonlinear transformations and rotations. MBS modelling and solution strategies are optimised to deal with this specific problem robustly and efficiently. The representation of deformable bodies in MBS is adjusted to the requirements and characteristics of this kind of application. The implementation of elastic bodies into MBS is, for example, explained in the publications of Shabana, [47], Schwertassek and Wallrapp, [69], and Rulka, [70]; the following paragraphs refer to these works.

Most approaches represent the time-dependent movement of a deformable body by a large rigid body motion (the body being represented by its body fixed reference frame) which is superposed by a small deformation. The (unconstrained) gross motion of the body reference frame, with its six degrees of freedom, can be described by a set of six independent second-order differential equations of motion. The exact configuration of the deformable body itself can be identified by an infinite number of elastic coordinates. The most prevalent computational method of structural mechanics, FEA, still introduces a large number of elastic degrees of freedom ($>10^6$ DOFs for a typical application) - too many to solve reasonably in a complex multibody system. Approximation methods are needed to reduce the number of elastic degrees of freedom in an appropriate way, i.e. to account for those effects of body deflection that have significant influence on the dynamics of the system.

A common strategy is to use Bernoulli's principle of separation of variables to describe the state- and time-dependent displacement field of the deformable body by state-dependent base functions and time-dependent elastic coordinates. Thus, the original set of partial differential equations representing the dynamics of the deformable body is converted; the equations of motion now form a set of ordinary differential equations. Approximation methods, e.g. Rayleigh-Ritz or Galerkin methods, [71], can be employed to reduce the system to a finite number of coordinates. With the introduction of base functions, the equations of motion of the deformable body contain state-independent volume integrals which are responsible for the coupling between rigid body motion and elastic deformation. They can be computed prior to integration of the equations of motion itself.

The quality of the solution depends strongly upon the "quality" of the base functions. Of the three different types of base functions, [72], the use of eigenfunctions has gained preponderance in technical applications. Eigenmodes usually form the core set of base functions, possibly enhanced by staticmodes or inertia relief modes, e.g. to account for local deformations due to large point loads on the structure or geometric boundary conditions.

Various methods exist to process suitable base functions, to optimise the approximation to the particularities of the application and to compensate for errors; an overview is given by Sachau, [73]. The approach used in this report falls back on the works of Rulka, [70], and Wallrapp, [74], and is based on eigen- and staticmode analysis per-

formed in nonlinear FEA software tools using the consistent mass approach of FEA formulation to integrate the volume integrals of the modal coefficient matrices.

4.4 Presumptions of Deformable Bodies in MBS

The modal representation of deformable bodies in MBS implies several presumptions and model conditions which have to be observed, [48].

- The elastic body may undergo large overall body motion, as indicated by the displacement vector \mathbf{r}_{IB} , Figure 4.1. This motion may be accompanied by small elastic deformations \mathbf{r}_{def} of the body, which are given in respect to the reference location on the undeformed body $\mathbf{r}_{BV(0)}$.
- The state of deformation of a body is measured in its reference system. The reference configuration of the body is the undeformed state which has to be unequivocal and time-independent. This precludes the consideration of elastic bodies with material creep effects.
- The body is not exposed to internal force effects, e.g. on polarised materials in electromagnetic fields.
- The state variables of deformation (elastic coordinates) are assumed to be small on position and velocity level; on acceleration level, however, they may be significant. Thus, the mass matrix of the deformable body remains symmetric.

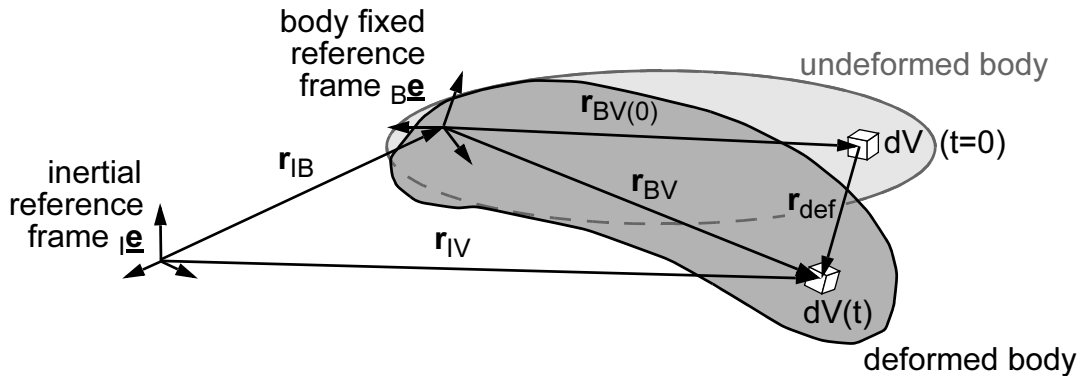


Figure 4.1 Deformation of a Deformable Body

4.5 Representation of Deformable Bodies

The approach of separating the large gross motion of the body from its small elastic deformations, see Figure 4.1, allows to write the absolute position \mathbf{r}_{IV} of a volume element dV as

$$\mathbf{r}_{IV} = \mathbf{r}_{IB} + \mathbf{r}_{BV} \cdot \quad (11)$$

The state of deformation of a deformable body can be described by specifying, for every volume element dV of the body, the position vector of the volume element \mathbf{r}_{BV} in respect to the position vector $\mathbf{r}_{BV(0)}$ of dV in the undeformed reference configuration and time t , [75]:

$$\mathbf{r}_{BV} = \mathbf{r}_{BV}(\mathbf{r}_{BV(0)}, t), \quad (12)$$

thus introducing the displacement vector \mathbf{r}_{def} :

$$\mathbf{r}_{BV}(t) = \mathbf{r}_{BV(0)} + \mathbf{r}_{\text{def}}(\mathbf{r}_{BV(0)}, t). \quad (13)$$

Introducing this approach into the equations of motion generates a set of partial differential equations; a general, explicit solution is apparently impossible. Bernoulli's principle of separation of variables allows converting the equations of motion to a set of ordinary differential equations. For the deformation vector \mathbf{r}_{def} , this step yields

$$\mathbf{r}_{\text{def}} = \mathbf{\Psi} \mathbf{z}_E(t). \quad (14)$$

\mathbf{z}_E denotes the vector of elastic coordinates, which is a single-row combination of the single elastic coordinates z_{Ei} of the base functions,

$$\mathbf{z}_E(t) = (z_{E1}, z_{E2}, \dots)^T, \quad (15)$$

and $\mathbf{\Psi}$ is the Jacobian matrix of the elastic states,

$$\mathbf{\Psi} = \frac{\partial \mathbf{r}_{BV}}{\partial \mathbf{z}_E} d\mathbf{z}_E. \quad (16)$$

In general, a nonlinear dependency exists between the position \mathbf{r}_{BV} of dV on the body and the elastic deformation. This would require that the modal coefficient matrices had to be computed for every new set of elastic coordinates; but with the presumptions given above, the equations of motion of the elastic deformation can be linearised. The modal coefficient matrices then become state-independent and can be computed prior to the integration of the equations of motion.

4.6 Kinematics of the Deformable Body

With the separation of nonlinear overall motion and small elastic deformation, the absolute position \mathbf{r}_{IV} of a volume element dV was given by Eq. (11). Under consideration of the definition of the Jacobian $\mathbf{\Psi}$ with its correlations

$$\mathbf{r}_{BV} = \mathbf{\Psi} \mathbf{z}_E + \mathbf{r}_{BV(0)}, \quad (17a)$$

$$\dot{\mathbf{r}}_{BV} = \mathbf{\Psi} \dot{\mathbf{z}}_E, \quad (17b)$$

$$\ddot{\mathbf{r}}_{BV} = \mathbf{\Psi} \ddot{\mathbf{z}}_E, \quad (17c)$$

the kinematic relations of the position vector \mathbf{r}_{IV} from the inertial reference frame to the control element dV , the element's absolute translational velocity \mathbf{v}_V and its absolute translational acceleration \mathbf{a}_V can be written as²⁵

$$\mathbf{r}_{IV} = \mathbf{r}_{IB} + \mathbf{r}_{BV}, \quad (18a)$$

$$\mathbf{v}_{IV} = \mathbf{v}_{IB} - \tilde{\mathbf{r}}_{BV} \boldsymbol{\omega}_{IB} + \dot{\mathbf{r}}_{BV} = (\mathbf{E}, -\tilde{\mathbf{r}}_{BV}, \boldsymbol{\Psi}) \begin{pmatrix} \mathbf{v}_{IB} \\ \boldsymbol{\omega}_{IB} \\ \dot{\mathbf{z}}_E \end{pmatrix}, \quad (18b)$$

$$\mathbf{a}_{IV} = \mathbf{a}_{IB} - \tilde{\mathbf{r}}_{BV} \boldsymbol{\alpha}_{IB} + \tilde{\boldsymbol{\omega}}_{IB} \tilde{\boldsymbol{\omega}}_{IB} \mathbf{r}_{BV} + 2 \tilde{\boldsymbol{\omega}}_{IB} \dot{\mathbf{r}}_{BV} + \ddot{\mathbf{r}}_{BV} \quad (18c)$$

$$= (\mathbf{E}, -\tilde{\mathbf{r}}_{BV}, \boldsymbol{\Psi}) \begin{bmatrix} \mathbf{a}_{IB} \\ \boldsymbol{\alpha}_{IB} \\ \ddot{\mathbf{z}}_E \end{bmatrix} (\tilde{\boldsymbol{\omega}}_{IB} \tilde{\boldsymbol{\omega}}_{IB} \mathbf{r}_{BV} + 2 \tilde{\boldsymbol{\omega}}_{IB} \dot{\mathbf{r}}_{BV}).$$

4.7 Nonlinear Equations of Motion of the Single Deformable Body

The equations of motion for a deformable body can now be derived from the motion of a control volume element dV , as performed by Rulka, [48]. With the density ρ of the control element, its overall motion can be given by the theorem of impulse:

$$(\rho \cdot \mathbf{a}_{dV} - \mathbf{f}_\rho) dV = 0. \quad (19)$$

Vector \mathbf{a}_{dV} denotes the absolute acceleration of dV , \mathbf{f}_ρ the resulting (stress) forces acting on the element (unit: force per volume).

The stress forces \mathbf{f}_ρ consist of applied forces \mathbf{f}_{app} , external constraint forces $\mathbf{f}_{cstr, e}$ and internal constraint forces $\mathbf{f}_{cstr, i}$:

$$\mathbf{f}_\rho = \mathbf{f}_{app} + \mathbf{f}_{cstr, e} + \mathbf{f}_{cstr, i}. \quad (20)$$

Applying the principle of virtual velocities, the internal constraint forces disappear if the absolute velocity \mathbf{v}_{dV} of the control volume includes all internal constraints (set of minimal coordinates):

$$\int_V \delta \mathbf{v}_{dV} (\rho \mathbf{a}_{dV} - \mathbf{f}_{app} - \mathbf{f}_{cstr, e}) dV = 0. \quad (21)$$

If a vector of velocity coordinates of the elastic body $\dot{\mathbf{z}}_e$ is introduced,

$$\dot{\mathbf{z}}_e = (\mathbf{v}_{IB}^T, \boldsymbol{\omega}_{IB}^T, \dot{\mathbf{z}}_E^T)^T, \quad (22)$$

25. The kinematics of the body are developed in respect to the body's reference frame ${}_B\mathbf{e}$, Figure 4.1.

Eq. (21) may be written as

$$\delta \dot{\mathbf{z}}_e^T \int_V \left(\frac{\partial \mathbf{v}_{dV}}{\partial \dot{\mathbf{z}}_e} \right)^T (\rho \mathbf{a}_{dV} - \mathbf{f}_{app} - \mathbf{f}_{cstr,e}) dV = 0. \quad (23a)$$

Considering that only virtual velocities may be applied which are in line with the boundary conditions (see above), we can write

$$\int_V \left(\frac{\partial \mathbf{v}_{dV}}{\partial \dot{\mathbf{z}}_e} \right)^T (\rho \mathbf{a}_{dV} - \mathbf{f}_{app} - \mathbf{f}_{cstr,e}) dV = 0. \quad (23b)$$

The required kinematic values, \mathbf{v}_{dV} and \mathbf{a}_{dV} , are given by Eqs. (18b,c). Therefore, the partial derivation of \mathbf{v}_{dV} in Eq. (23b) can be read from Eq. (18b):

$$\frac{\partial \mathbf{v}_{dV}}{\partial \dot{\mathbf{z}}_e} = (\mathbf{E}, -\tilde{\mathbf{r}}_{BV}, \Psi). \quad (24)$$

Substitution of $\partial \mathbf{v}_{dV} / \partial \dot{\mathbf{z}}_e$ and \mathbf{a}_{dV} by Eq. (18c) and Eq. (24) yields

$$\int_V \begin{bmatrix} \mathbf{E} \\ -\tilde{\mathbf{r}}_{BV}^T \\ \Psi^T \end{bmatrix} [\rho (\mathbf{a}_{IB} - \tilde{\mathbf{r}}_{BV} \alpha_{IB} + \tilde{\omega}_{IB} \tilde{\omega}_{IB} \mathbf{r}_{BV} + 2 \tilde{\omega}_{IB} \dot{\mathbf{r}}_{BV} + \Psi \ddot{\mathbf{z}}_E) - \mathbf{f}_{app} - \mathbf{f}_{cstr,e}] dV = 0, \quad (25)$$

respectively

$$\int_V \rho \begin{bmatrix} \mathbf{E} & \tilde{\mathbf{r}}_{BV}^T & \Psi \\ \tilde{\mathbf{r}}_{BV} & \tilde{\mathbf{r}}_{BV}^T \tilde{\mathbf{r}}_{BV} & \tilde{\mathbf{r}}_{BV} \Psi \\ \Psi^T & \Psi^T \tilde{\mathbf{r}}_{BV}^T & \Psi^T \Psi \end{bmatrix} dV \begin{bmatrix} \mathbf{a}_{IB} \\ \alpha_{IB} \\ \ddot{\mathbf{z}}_E \end{bmatrix} + \int_V \rho \left(\begin{bmatrix} \tilde{\omega}_{IB} \tilde{\omega}_{IB} \mathbf{r}_{BV} + 2 \tilde{\omega}_{IB} \dot{\mathbf{r}}_{BV} \\ \tilde{\omega}_{IB} \tilde{\mathbf{r}}_{BV}^T \tilde{\mathbf{r}}_{BV} \omega_{IB} + 2 \tilde{\mathbf{r}}_{BV}^T \dot{\tilde{\omega}}_{IB} \omega_{IB} \\ \omega_{IB}^T \otimes \tilde{\Psi}^T \tilde{\mathbf{r}}_{BV} \omega_{IB} + 2 \Psi^T \tilde{\mathbf{r}}_{BV} \omega_{IB} \end{bmatrix} - \begin{bmatrix} \mathbf{E} \\ \tilde{\mathbf{r}}_{BV} \\ \Psi^T \end{bmatrix} (\mathbf{f}_{app} + \mathbf{f}_{cstr,e}) \right) dV = 0 \quad (26)$$

in resolved form.²⁶ With the coefficient matrices

$$\mathbf{m} = \int_V \rho dV, \quad \mathbf{C}_r = \int_V \rho \Psi^T \tilde{\mathbf{r}}_{BV}^T dV, \quad (27a)$$

$$\mathbf{m} \mathbf{r}_{BV} = \int_V \rho \mathbf{r}_{BV} dV, \quad \mathbf{M}_E = \int_V \rho \Psi^T \Psi dV, \quad (27b)$$

$$\mathbf{m} \dot{\mathbf{r}}_{BV} = \int_V \rho \dot{\mathbf{r}}_{BV} dV, \quad \mathbf{O}_E = \int_V \rho \tilde{\Psi}^T \tilde{\mathbf{r}}_{BV}^T dV, \quad (27c)$$

$$\mathbf{J} = \int_V \rho \tilde{\mathbf{r}}_{BV}^T \tilde{\mathbf{r}}_{BV} dV, \quad \mathbf{G}_E = 2 \int_V \rho \Psi^T \dot{\tilde{\mathbf{r}}}_{BV} dV, \quad (27d)$$

26. The \otimes -multiplier is defined as $\mathbf{b}^T \otimes \mathbf{A} = [b_1, b_2, b_3] \otimes \begin{bmatrix} \mathbf{A}_1 \\ \mathbf{A}_2 \\ \mathbf{A}_3 \end{bmatrix} = b_1 \mathbf{A}_1 + b_2 \mathbf{A}_2 + b_3 \mathbf{A}_3$, [70].

$$\mathbf{C}_t = \int_V \rho \boldsymbol{\Psi}^T dV, \quad \mathbf{G}_R = 2 \int_V \rho \tilde{\mathbf{r}}_{BV} \dot{\tilde{\mathbf{r}}}_{BV} dV, \quad (27e)$$

Eq. (26) can be written as

$$\begin{aligned} \textcircled{1} \begin{bmatrix} m\mathbf{E} & m\mathbf{r}_{BV}^T & \mathbf{C}_t^T \\ m\mathbf{r}_{BV} & \mathbf{J} & \mathbf{C}_r \\ \mathbf{C}_t & \mathbf{C}_r & \mathbf{M}_E \end{bmatrix} \begin{bmatrix} \mathbf{a}_{IB} \\ \boldsymbol{\alpha}_{IB} \\ \ddot{\mathbf{z}}_E \end{bmatrix} &= \textcircled{2} \begin{bmatrix} m\mathbf{g} \\ m\mathbf{r}_{BCCG}\mathbf{g} \\ \mathbf{C}_t\mathbf{g} \end{bmatrix} - \textcircled{3} \begin{bmatrix} m\tilde{\boldsymbol{\omega}}_{IB}\tilde{\boldsymbol{\omega}}_{IB}\mathbf{r}_{BV} + 2m\tilde{\boldsymbol{\omega}}_{IB}\dot{\mathbf{r}}_{BV} \\ \tilde{\boldsymbol{\omega}}_{IB}\mathbf{J}\boldsymbol{\omega}_{IB} + \mathbf{G}_R\boldsymbol{\omega}_{IB} \\ \boldsymbol{\omega}_{IB}^T \otimes \mathbf{O}_E\boldsymbol{\omega}_{IB} + \mathbf{G}_E\boldsymbol{\omega}_{IB} \end{bmatrix} - \textcircled{4} \begin{bmatrix} 0 \\ 0 \\ \frac{\partial \Pi}{\partial \mathbf{z}_E} \end{bmatrix} \\ &- \textcircled{5} \begin{bmatrix} \sum_k \mathbf{f}_{app,k} \\ \sum_k \mathbf{I}_{app,k} + \sum_k \mathbf{r}_{Bf}\mathbf{f}_{app,k} \\ \sum_k \boldsymbol{\Psi}_{Ik}\mathbf{I}_{app,k} + \sum_k \boldsymbol{\Psi}_{fk}\mathbf{f}_{app,k} \end{bmatrix} - \textcircled{6} \begin{bmatrix} \sum_k \mathbf{f}_{cstr,e,k} \\ \sum_k \mathbf{I}_{cstr,e,k} + \sum_k \mathbf{r}_{Bf}\mathbf{f}_{cstr,e,k} \\ \sum_k \boldsymbol{\Psi}_{Ik}\mathbf{I}_{cstr,e,k} + \sum_k \boldsymbol{\Psi}_{fk}\mathbf{f}_{cstr,e,k} \end{bmatrix} \end{aligned} \quad (28)$$

with the mass matrix (①), gravity effects (②), centrifugal and gyroscopic terms (③), internal stress (④), and the vectors of applied forces (⑤) and external constraint forces (⑥). In this equation, \mathbf{r}_{BCCG} denotes the position vector from the body reference frame B to the centre of gravity, \mathbf{r}_{Bf} the position vector from B to the point of action of the respective force and Π the potential of internal elastic deformation forces. The Jacobian matrices $\boldsymbol{\Psi}_f$ and $\boldsymbol{\Psi}_l$ are defined by

$$\boldsymbol{\Psi}_f = \frac{\partial \mathbf{r}_{Bf}}{\partial \mathbf{z}_E}, \quad (29a)$$

$$\boldsymbol{\Psi}_l = \frac{\partial \boldsymbol{\omega}_{Bf}}{\partial \mathbf{z}_E}. \quad (29b)$$

All necessary integrations of coefficient matrices, Eq. (27a), can be performed independently from the overall body motion. They are nevertheless still dependent on the elastic coordinates \mathbf{z}_E .

4.8 Linearisation of the Elastic Deformation

The Jacobian $\boldsymbol{\Psi}$, and consequently the modal coefficient matrices as well, are derived by differentiating \mathbf{r}_{BV} for \mathbf{z}_E , Eq. (16). Therefore, the deformation vector \mathbf{r}_{def} has to be developed to second order terms to receive the first order modal coefficient matrices. The linearisation of \mathbf{r}_{def} yields, then:

$$\mathbf{r}_{def} \cong \left(\boldsymbol{\Psi}_0 + \frac{1}{2} \boldsymbol{\Psi}_1 \mathbf{z}_E \right) \mathbf{z}_E. \quad (30)$$

Discretisation of a continuum, however, leads to a large number of elastic coordinates \mathbf{z}_E . Base functions, which represent significant deformation modes of the flexible body, can be used to reduce the number of elastic coordinates. Applying the Ritz approach,²⁷ which approximates the deformation field of the body with a linear superposition of n_q base functions ϕ_i ,

$$\mathbf{r}_{\text{def}} \cong \sum_{i=1}^{n_q} \phi_i z_{Ei} \quad (31)$$

the Jacobian matrix of elastic states can be substituted by mode shapes of the deformable body. The mode matrix Φ ,

$$\Phi = [\phi_1, \phi_2, \dots, \phi_{n_q}], \quad (32)$$

then replaces the Jacobian matrix Ψ of Eq. (30):

$$\mathbf{r}_{\text{def}} \cong \left(\Phi_0 + \frac{1}{2} \Phi_1 \mathbf{z}_E \right) \mathbf{z}_E. \quad (33)$$

Φ_0 and Φ_1 are mode shape matrices of the zero and first order expansion of Φ . They can be derived from FEA analyses, [76].

The approach of modal representation of a deformable body is quite common: In FEA analysis, the linearised equations of motion of a non-damped system are given by

$$\mathbf{M}_F \ddot{\mathbf{u}}_F + \mathbf{K}_F \mathbf{u}_F = \mathbf{f}_F, \quad (34)$$

where \mathbf{M}_F and \mathbf{K}_F are the symmetric mass and stiffness matrix, \mathbf{u}_F represents the vector of nodal coordinates and \mathbf{f}_F is the vector of nodal forces. An eigenvalue analysis delivers natural frequencies ω_m and eigenvectors \mathbf{u}_{Fm} :

$$(\mathbf{K}_F - \omega_m^2 \mathbf{M}_F) \mathbf{u}_{Fm} = 0. \quad (35)$$

Additionally, a static analysis for a pre-defined load vector \mathbf{f}_{Fs} may be performed to receive the corresponding deformation \mathbf{u}_{Fs} :

$$\mathbf{K}_F \mathbf{u}_{Fs} = \mathbf{f}_{Fs}. \quad (36)$$

Eq. (35) and Eq. (36) deliver the eigen- and staticmodes, \mathbf{u}_{Fm} and \mathbf{u}_{Fs} , respectively, from which the base functions ϕ_i forming the mode matrix Φ_F can be selected,

$$\Phi_F = [\phi_1, \phi_2, \dots, \phi_q] = [\mathbf{u}_{Fm1}, \dots, \mathbf{u}_{Fs1}, \dots]. \quad (37)$$

27. Following the suggestion of Bremer / Pfeiffer, [71], the term ‘‘Ritz approach’’ is maintained although mode shapes selected as base functions may consist of eigenmodes, staticmodes and inertia relief modes. Esp. in English literature, the use of staticmodes is often named ‘‘Craig-Bampton-Method’’.

With

$$\mathbf{u}_F = \Phi_F \mathbf{z}_E, \quad (38a)$$

$$\dot{\mathbf{u}}_F = \Phi_F \dot{\mathbf{z}}_E, \quad (38b)$$

$$\ddot{\mathbf{u}}_F = \Phi_F \ddot{\mathbf{z}}_E, \quad (38c)$$

and the transformation into modal form by

$$\hat{\mathbf{M}}_e = \Phi_F^T \mathbf{M}_F \Phi_F, \quad (39a)$$

$$\hat{\mathbf{K}}_e = \Phi_F^T \mathbf{K}_F \Phi_F \quad (39b)$$

and

$$\hat{\mathbf{f}}_e = \Phi_F^T \mathbf{f}_F, \quad (39c)$$

Eq. (34), the equations of motion of the linearised system, can now be transferred into modal coordinates:

$$\hat{\mathbf{M}}_e \ddot{\mathbf{z}}_E + \hat{\mathbf{D}}_e \dot{\mathbf{z}}_E + \hat{\mathbf{K}}_e \mathbf{z}_E = \hat{\mathbf{f}}_e. \quad (40)$$

Modal damping $\hat{\mathbf{D}}_e$ is included in this equation under the assumption of stiffness-proportional damping, either with a global or a mode-specific damping coefficient, e.g. using Lehr's damping factor ζ_i to receive

$$\hat{\mathbf{D}}_e = \text{diag}(\hat{d}_i), \quad (41)$$

where \hat{d}_i depends on the i^{th} diagonal elements $\hat{M}_{e,ii}$ and $\hat{K}_{e,ii}$ of the modal mass and stiffness matrices $\hat{\mathbf{M}}_e$, $\hat{\mathbf{K}}_e$:

$$\hat{d}_i = 2\zeta_i \sqrt{\hat{K}_{e,ii} \hat{M}_{e,ii}}. \quad (42)$$

FEA software tools provide all results necessary to derive the zero-order terms Φ_0 of the mode matrix in their standard structural analysis solutions; the first-order terms, Φ_1 , have to be created in an additional FEA analysis sequence, [77]. Eq. (40) only accounts for the elastic deformation of the body. Including rigid body modes would allow to represent the translational and rotational gross motion of the body as well, but only in linearised form. Therefore, this elastic representation has to be coupled with the nonlinear equation of (gross) motion of the body's reference frame.

Eq. (28) delivers the necessary terms. The coefficient matrices can be expressed by Taylor expansion of the volume integrals, delivering zero and first order coefficient matrices which are independent from the elastic coordinates, e.g.

$$\mathbf{C}_t(\mathbf{z}_E) = \mathbf{C}_{t,0} + \mathbf{C}_{t,1,i} z_{E,i}. \quad (43)$$

The coefficient matrices can therefore be computed prior to the dynamic analysis and stored, e.g. in an MBS input file.²⁸ The modal representation of the deformable body is therefore available for other simulations as well.²⁹ The derivation of the zero and first order coefficient matrices of a modally reduced deformable body can be found in the literature, e.g. Wallrapp ([68], [76]).

Now, the equations of motion can be written as

$$\begin{bmatrix} m\mathbf{E} & m\mathbf{r}_{\text{BV}}^T & \mathbf{C}_t^T \\ m\mathbf{r}_{\text{BV}} & \mathbf{J} & \mathbf{C}_r \\ \mathbf{C}_t & \mathbf{C}_r & \hat{\mathbf{M}}_e \end{bmatrix} \begin{bmatrix} \mathbf{a}_{\text{IB}} \\ \boldsymbol{\alpha}_{\text{IB}} \\ \ddot{\mathbf{z}}_E \end{bmatrix} = \begin{bmatrix} m\mathbf{g} \\ m\mathbf{r}_{\text{BCG}}\mathbf{g} \\ \mathbf{C}_t\mathbf{g} \end{bmatrix} - \begin{bmatrix} m\tilde{\boldsymbol{\omega}}_{\text{IB}}\tilde{\boldsymbol{\omega}}_{\text{IB}}\mathbf{r}_{\text{BV}} + 2m\tilde{\boldsymbol{\omega}}_{\text{IB}}\dot{\mathbf{r}}_{\text{BV}} \\ \tilde{\boldsymbol{\omega}}_{\text{IB}}\mathbf{J}\boldsymbol{\omega}_{\text{IB}} + \mathbf{G}_R\boldsymbol{\omega}_{\text{IB}} \\ \boldsymbol{\omega}_{\text{IB}}^T \otimes \mathbf{O}_E\boldsymbol{\omega}_{\text{IB}} + \mathbf{G}_E\boldsymbol{\omega}_{\text{IB}} \end{bmatrix} - \begin{bmatrix} 0 \\ 0 \\ \mathbf{k}_\sigma + \hat{\mathbf{K}}_e\mathbf{z}_E + \hat{\mathbf{D}}_e\dot{\mathbf{z}}_E \end{bmatrix} \quad (44)$$

$$- \begin{bmatrix} \sum_k \mathbf{f}_{\text{app},k} \\ \sum_k \mathbf{I}_{\text{app},k} + \sum_k \mathbf{r}_{\text{Bf}}\mathbf{f}_{\text{app},k} \\ \sum_k \boldsymbol{\Phi}_{\text{Ik}}\mathbf{I}_{\text{app},k} + \sum_k \boldsymbol{\Phi}_{\text{fk}}\mathbf{f}_{\text{app},k} \end{bmatrix} - \begin{bmatrix} \sum_k \mathbf{f}_{\text{cstr},e,k} \\ \sum_k \mathbf{I}_{\text{cstr},e,k} + \sum_k \mathbf{r}_{\text{Bf}}\mathbf{f}_{\text{cstr},e,k} \\ \sum_k \boldsymbol{\Phi}_{\text{Ik}}\mathbf{I}_{\text{cstr},e,k} + \sum_k \boldsymbol{\Phi}_{\text{fk}}\mathbf{f}_{\text{cstr},e,k} \end{bmatrix}$$

with \mathbf{k}_σ accounting for possible pre-stress conditions, or, with mass matrix \mathbf{M} and the respective forces \mathbf{f}_i as substitutions,

$$\mathbf{M}\ddot{\mathbf{z}} = \mathbf{M} \begin{bmatrix} \mathbf{a}_{\text{IB}} \\ \boldsymbol{\alpha}_{\text{IB}} \\ \ddot{\mathbf{z}}_E \end{bmatrix} = \mathbf{f}_{\text{grav}} + \mathbf{f}_{\text{gyro}} + \mathbf{f}_{\text{elast}} + \mathbf{f}_{\text{app}} + \mathbf{f}_{\text{cstr}} \quad (45)$$

It can easily be seen that the lower line of Eq. (44), representing the small elastic deformation of the body, is linked with the equations of the nonlinear gross motion by the coupling terms of the mass matrix only. We will use this circumstance later in the introduction of aeroelastic coupling matrices.

28. The file format SID is an acknowledged, standardised data format, [68].

29. ... under the assumption that the elastic properties of the body, its major dynamic deformations during the analysis as well as the boundary conditions remain the same.

5 The Approach of Aeroelastic Preprocessing

5.1 The Principle of Superposition

Evaluating the overall dynamic behaviour of a vehicle as a multibody system, the dominant motion will be the translational and rotational displacements of the bodies itself. As already mentioned in the previous chapter, elastic deformations of bodies will usually be comparatively small. In most analyses, nevertheless, they must not be neglected - their influence on the dynamics of the system can be significant. A similar situation can be found for the incorporation of aerodynamic and aeroelastic effects in multibody simulation: the main aerodynamic forces³⁰ will generally depend on the attitude of the aircraft and on control inputs by the pilot rather than on aerodynamic effects due to airframe deformation. Again, the latter may have a decisive influence on the overall system which has to be accounted for.

Three main sources of aerodynamic forces can be identified: the aerodynamic conditions of the undeformed aircraft, deflections of primary or secondary flight control surfaces and a displacement of wetted surfaces because of elastic airframe deformations. The principle of aerodynamic superposition will be applied to generate the prevailing airloads and their distribution over the aircraft structure.

In aerodynamics, the principle of superposition itself is by no means new - actually, it dates back to 1789, when Laplace introduced his well-known equation³¹

$$\nabla^2 G = 0 \quad (46)$$

which was soon recognised to deliver a solution to the Euler equations for inviscous, irrotational flow by a linear combination of elementary solutions (sources, sinks, doublets, etc.).

Besides the mathematical field of application, linear superposition of aerodynamic effects has for long been established as an accepted method in various aeronautic disciplines, among them flight mechanics, aeroelasticity and aeroservoelasticity; and it still serves well nowadays, mainly in conceptual and preliminary design tasks where the level of detail is quite similar to the precision required in the application targeted with this approach. A very common example is to approximate the aerodynamic forces and moments by the linear expressions in their Taylor series expansions, leading to the concept of stability and control derivatives, [78]. This approximation has been found to work extremely well for quasi-steady subsonic flows at low to moderate angles of attack.

30. To facilitate the reading of the following, general sections, aerodynamic moments are only mentioned when they shall be explicitly addressed; in all other cases, aerodynamic force and moment effects are subsumed under the expression "aerodynamic forces".

31. The equation was originally developed to model the rings of planet Saturn (with G as the gravity potential), but their significance to mathematic physics became apparent very quickly.

5.1.1 Prerequisites and Assumptions of Superposed Aerodynamics

Naturally, a superposition of linearised aerodynamic effects represents a considerable simplification of the actual aerodynamics of the aeroplane. Therefore, it seems only reasonable to have a closer look at the prevailing conditions for an aircraft on or close to the ground as well as on the assumptions which have to hold so a satisfying reproduction of reality is achieved.

Aerodynamics for aircraft ground dynamics simulation shows only little affinity to most CFD analysis performed in the development process of an aircraft, where the focus is on the aerodynamics of the aircraft in cruise flight. Much closer resemblance can be found with the discipline of high-lift aerodynamics, which also shares most of the principal characteristics. The main features of aerodynamics for aircraft ground dynamics are:

- The aircraft is being analysed in its high-lift configuration, with flaps and slats extended and the landing gear deployed.
- Freestream velocity lies within the range of classical subsonic flow (usually $Ma \leq 0.3$). Compressibility effects are of secondary importance: often, they are either neglected or accounted for by standard correction methods.
- Overall aerodynamic conditions as well as determining effects are of (quasi-)steady nature. Fluid-structure interactions influence the aircraft motion only and do not develop eigendynamics (e.g. oscillations).

Further requirements have to be complied with in order to receive reasonable, realistic results from this approach:

- For all deformable bodies which are exposed to aerodynamic loads, the assumptions of modal representation of their elasticity have to be valid. This includes:
 - the body undergoes only deformations which are small in its elastic coordinates,
 - the body has linear-elastic deformation properties (possible local nonlinearities such as non-homogenous or non-isentropic material properties do not necessarily conflict with this requirement) and
 - adequate representation of the body's flexibility by the selected mode shapes (base functions).
- Aerodynamic forces on the aircraft stand in a basically linear relation to the state of the system (attitude, control surface deflection), respectively they may be linearised near or interpolated between given working points.
- Aerodynamic history effects such as a time lag between cause (e.g. structural deformation) and effect (e.g. resulting airloads) do not influence the overall dynamic behaviour of the aircraft and can be neglected.

5.1.2 Superposition of Aerodynamic Effects

Formally, aerodynamic loads can be easily introduced in multibody systems with deformable bodies by adding a (generalised) aerodynamic force, \mathbf{f}_{aero} , to the right-hand-side of the equations of motion, Eq. (6a):

$$\mathbf{M}\ddot{\mathbf{q}} = \mathbf{f}_{\text{grav}} + \mathbf{f}_{\text{gyro}} + \mathbf{f}_{\text{elast}} + \mathbf{f}_{\text{app}} + \mathbf{f}_{\text{cstr}} + \mathbf{f}_{\text{aero}}. \quad (47)$$

Under the prerequisites and assumptions given in the previous section, the vector of aerodynamic forces can be divided up into three parts, distinguishing

- rigid body aerodynamics $\mathbf{f}_{\text{aeroR}}$, i.e. the aerodynamic forces acting on the aircraft in its undeformed reference configuration;
- aerodynamic force increments $\mathbf{f}_{\text{aeroE}}$ deriving from deflections of the aircraft structure;
- aircraft control forces $\mathbf{f}_{\text{aeroC}}$ due to deflections of control surfaces (primary or secondary controls, lift dumping devices etc.).

The resulting aerodynamic forces and their distribution on the aircraft structure are found by superposing these airloads linearly, as indicated in Figure 5.1.

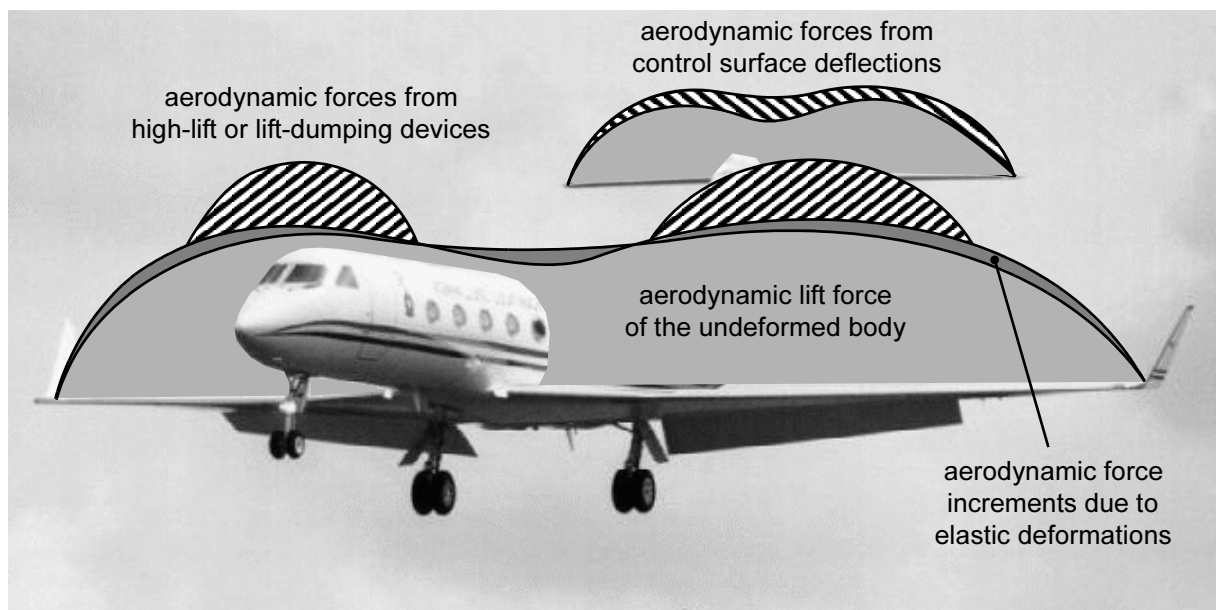


Figure 5.1 Superposition of Aerodynamic Effects

The basic equations of motion for the single deformable body now read:

$$\mathbf{M}\ddot{\mathbf{z}} = \mathbf{M} \begin{bmatrix} \mathbf{a}_{|B} \\ \boldsymbol{\alpha}_{|B} \\ \ddot{\mathbf{z}}_E \end{bmatrix} = \mathbf{f}_{\text{grav}} + \mathbf{f}_{\text{gyro}} + \mathbf{f}_{\text{elast}} + \mathbf{f}_{\text{app}} + \mathbf{f}_{\text{cstr}} + \mathbf{f}_{\text{aeroR}} + \mathbf{f}_{\text{aeroC}} + \mathbf{f}_{\text{aeroE}}. \quad (48)$$

Basically, the first two rows of Eq. (48), referring to translational and rotational motion of the body, represent the classical approach of linear flight mechanics, [78], [79]. The third row, containing the degrees of freedom of body flexibility, ensures a body deformation corresponding to the actual state of the system (boundary conditions, applied and constrained forces, centrifugal and gravity forces, etc.). Both parts of the equations of motion are connected by the coupling terms of the mass matrix. The aerodynamic forces may contain position- and velocity-depending values, which, under consideration of the pre-defined requirements, is sufficient for reliable and meaningful results in aircraft ground dynamics analysis.

5.1.3 Comparison Between Linearised and Nonlinear Aerodynamics

Comparison between linearised and nonlinear aerodynamics revealed a good conformance of results, [80]. In the test, static aerodynamic deflection of a model of the AMP wing was analysed in a multibody simulation. It compared a nonlinear co-simulation between dynamic simulation and an Euler code to a simulation where aerodynamics consisted of the linearised Euler results.

The AMP wing is a scaled wind tunnel model of a typical large transport aircraft wing, with a wing span of 1.05 m, a wing sweep of 30° at the 25% chord and a mass of approx. 8 kg. The wing has an asymmetric profile with a zero-lift angle of attack of -1.8° . The dynamic simulation was performed with SIMPACK. Elastic properties were obtained from a 600 DOF MSC.NASTRAN model, aerodynamics were computed with FLOWer, using a CFD model of about 10000 cells.

With a freestream velocity of $Ma = 0.78$, compressibility effects have already been present in this test. Even close to the limits of linear representation, conformance can be considered as fair, with the largest difference in deflection at about 12%. The undeformed state and both, linearised and nonlinear results, are shown in Figure 5.2. Differences are to be expected lower in the regime of incompressible airflow ($Ma < 0.3$).

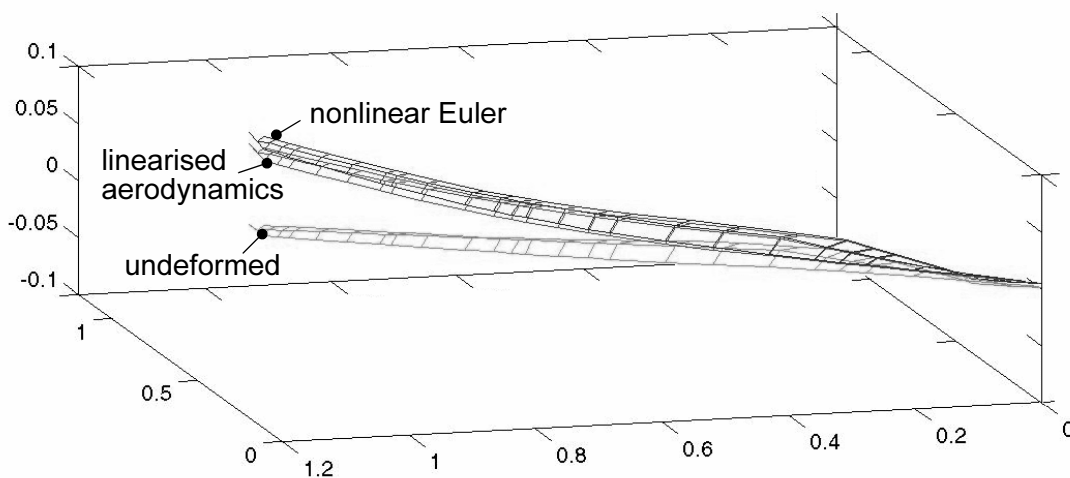


Figure 5.2 AMP Wing - Unloaded and with Linearised and Nonlinear Aerodynamics

5.2 The Principle of Modal Aerodynamics for Multibody Systems

Elastic deformation and aerodynamic forces deriving from body deflection are closely connected. Figure 5.3 resumes the basic principle of elastic body representation in MBS given in Chapter 4 in a visual form. The deformability of the body is reduced to a limited number of deformation forms, the base functions of the Ritz approach. The actual body deformation, depending on the state of the system, its boundary conditions and applied and constrained forces, is found by a linear superposition of these basic, independent deformation modes. An elastic coordinate represents a time-dependent weighting factor which determines the contribution of its corresponding mode to the overall deformation.

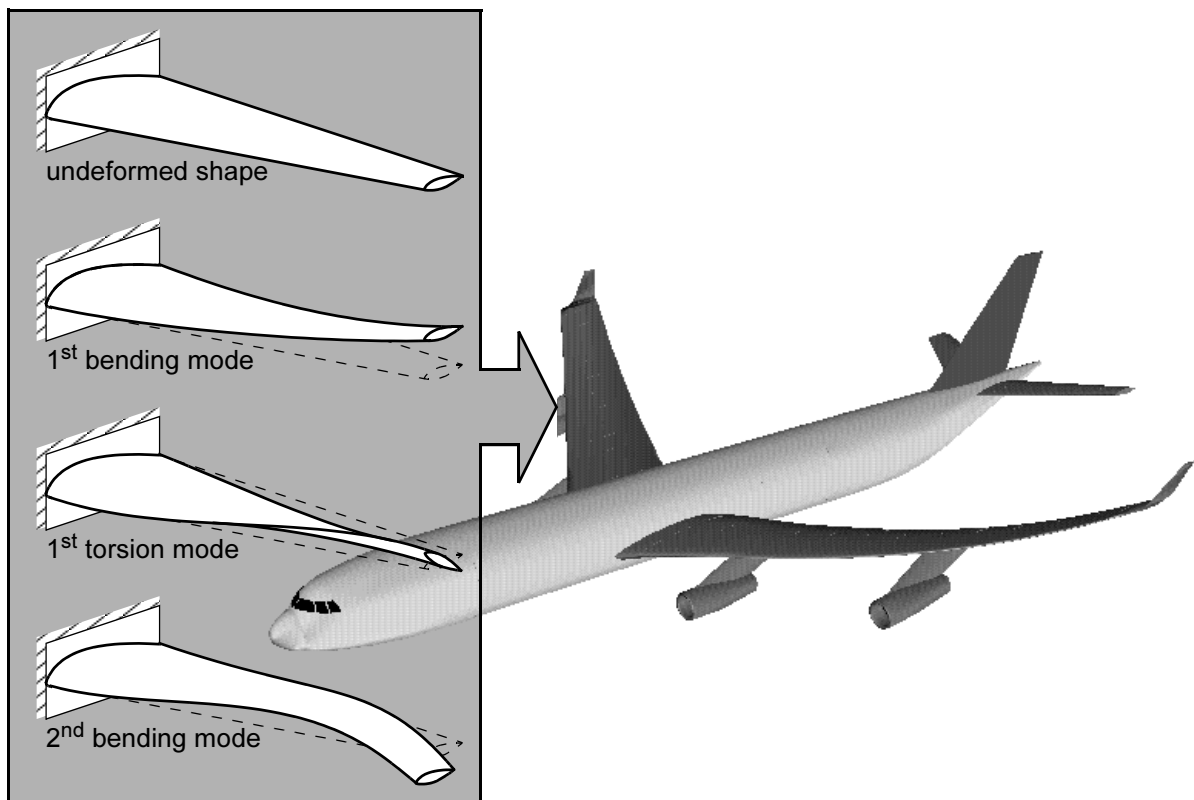


Figure 5.3 Superposition of Basic Deformation Modes of a Deformable Body

It should be noticed that aeroelastic effects on a deformable MBS body can only be caused by these modes of deformation, i.e. they are “linked” to the base functions, eigen- and staticmodes of the deformable body, which are selected in the process of generating the modal coefficient matrices. Therefore, it seems to be only reasonable to superpose the aerodynamic influences of elastic deformation as well. If the effects of a body deflection, given by a base function of the Ritz approach, on the aerodynamic conditions was known, the elastic and aerodynamic “modes” could be inter-related - a deflection of the body would automatically deliver the corresponding aerodynamic state of forces on the body, and vice versa, which allows to compute the generalised aerodynamic forces due to body deflection, $\mathbf{f}_{\text{aeroE}}$. Accordingly, this approach may be termed “modal aerodynamics for multibody systems”.

This approach of connecting normalised aerodynamic modes with other quantities affecting the aircraft's dynamic behaviour is not necessarily limited to elastic deformations. Rigid body and control deflection modes, i.e. generalised rotations, or displacements, of the rigid airframe body and its control surfaces, can be added to deliver the rigid body aerodynamics $\mathbf{f}_{\text{aeroR}}$ and aircraft control forces $\mathbf{f}_{\text{aeroC}}$. The precondition is that the aerodynamic conditions can be linearised - over the entire working range or sectionwise, respectively may be interpolated between reference points.

The effects of an aerodynamic mode, even if it derives from a local displacement or control input, may have impact on the overall airload distribution, but it is required that the various aerodynamic modes are decoupled, i.e. every aerodynamic mode is independent (qualitatively and quantitatively) from the state of another aerodynamic mode; a requirement which is met close enough to receive reasonable precision in the range of applications targeted here, [81].

5.3 Representation of Aerodynamics in the Equations of Motion

5.3.1 Multibody System Aerodynamics in Descriptor Form

In the conventional approach to define additional aerodynamic force laws to an MBS model, the equations of motion of the multibody system are enhanced by additional algebraic equations, containing the force laws of the aerodynamic conditions. In the form of Eqs. 6a and (6b), the equations of motion can be written as

$$\mathbf{M}(\mathbf{q})\ddot{\mathbf{q}}(t) = \mathbf{f}(\mathbf{q}, \dot{\mathbf{q}}, \boldsymbol{\lambda}, t) - \mathbf{G}^T(\mathbf{q}, t)\boldsymbol{\lambda}, \quad (49a)$$

$$0 = \mathbf{g}(\mathbf{q}, t), \quad (49b)$$

$$\dot{\mathbf{q}}_f = \mathbf{f}_f(\mathbf{q}, \dot{\mathbf{q}}, t, \dots) . \quad (49c)$$

Aerodynamics are included in descriptor form, i.e. by additional algebraic equations added to the system, Eq. (49c), where the additional forces \mathbf{f}_f are related to the internal force states \mathbf{q}_f of the system. Coupling of aerodynamic effects with the elastic states of a deformable body is performed during the time-integration process, which leads to considerable computational expense, especially in the number of right hand-side (RHS) calls.

Descriptor form representations of aerodynamic effects of flexible bodies are not limited to (manually defined) force elements. Two other approaches will deliver the same results, but will ease the manual handling:

- Aerodynamic force elements or underlying algebraic equations can be generated by preprocessing tools, creating an MBS input which is attached to the already existing force elements. For the MBS code, there is no difference to conventional force elements defined manually by the user with the standard GUI of the code. In fact, this approach simply represents an additional preprocessing deck for force elements,

which is explicitly adjusted to read, handle and process the aerodynamic data from which the individual forces on the structural nodes are derived.

- The second approach is to generate a separate module which contains the algebraic equations and which may also have internal processes to take advantage of the afore-known structure of this specialised task. For some applications in which the aerodynamic conditions experience only small perturbations from the reference state throughout the simulation, this module can even be disconnected from the MBS solution sequence of a timestep and be employed as an external aerodynamic solver: for each timestep, the airloads are computed only once for the estimated aircraft attitude, which speeds up computation times significantly.

The differences in respect to the formal representation, however, are marginal - they all belong to the conventional approach to introduce force elements (respectively the equivalent equations), which are basically dependent from the state vector, \mathbf{q} , and its first derivative with respect to time, $\dot{\mathbf{q}}$.

5.3.2 Multibody System Aerodynamics in State-Space Representation

In state-space representation, aeroelastic effects are accounted for without adding additional algebraic equations to the equations of motion. Aerodynamics of a deformable body have to be included on equation level, often referred to as “close coupling”. Regarding the equations of motion of the single, deformable body, Eq. (44), this has to be adjusted to the modal representation of the elastic degrees of freedom. Introducing the modal aerodynamic forces of the rigid aircraft in reference configuration $\hat{\mathbf{f}}_{aRref}$ and the modal aerodynamic matrices $\hat{\mathbf{Q}}_s$ and $\hat{\mathbf{Q}}_v$, the equation of motion can be written as

$$\begin{aligned} \begin{bmatrix} m\mathbf{E} & m\mathbf{r}_{BV}^T & \mathbf{C}_t^T \\ m\mathbf{r}_{BV} & \mathbf{J} & \mathbf{C}_r^T \\ \mathbf{C}_t & \mathbf{C}_r & \hat{\mathbf{M}}_e \end{bmatrix} \begin{bmatrix} \mathbf{a}_{IB} \\ \boldsymbol{\alpha}_{IB} \\ \ddot{\mathbf{z}}_E \end{bmatrix} &= \mathbf{f}_{grav} + \mathbf{f}_{gyro} + \mathbf{f}_{app} + \mathbf{f}_{cstr} + \mathbf{f}_{elast} + \mathbf{f}_{aero} \\ &= \mathbf{f}_{grav} + \mathbf{f}_{gyro} + \mathbf{f}_{app} + \mathbf{f}_{cstr} \\ &\quad - \begin{bmatrix} 0 \\ 0 \\ \mathbf{k}_\sigma + \hat{\mathbf{K}}_e \mathbf{z}_E + \hat{\mathbf{D}}_e \dot{\mathbf{z}}_E \end{bmatrix} - \begin{bmatrix} \mathbf{f}_a \\ \mathbf{l}_a \\ \hat{\mathbf{f}}_{aRref} + \hat{\mathbf{Q}}_s \mathbf{z}_a + \hat{\mathbf{Q}}_v \dot{\mathbf{z}}_a \end{bmatrix} \end{aligned} \quad (50)$$

with \mathbf{z}_a as the state vector of the body’s aerodynamic properties, i.e. translations, rotations, control inputs and deformation states.

As already indicated in Section 4.8, the elastic deformation of the body is linked with the equations of the nonlinear gross motion by the coupling terms of the mass matrix \mathbf{C}_t , \mathbf{C}_r only. For an introduction of modal aerodynamics, this circumstance has two important consequences:

- We can introduce state- and velocity-dependent aerodynamic and aeroelastic effects without having to alter any of the modal coefficient matrices. This fact simplifies preparation and processing of aeroelastic MBS input data, resulting in a straightforward algorithm for the required preprocessing routines to the MBS tool. Additionally, the structural input data sets are not connected to the aerodynamic data, which simplifies a comfortable, consistent data handling - especially in complex interdisciplinary design tasks.
- In combination with the aerodynamic state vector, the modal matrices $\hat{\mathbf{Q}}_s$ and $\hat{\mathbf{Q}}_v$ effectuate a deflection of the airframe under aerodynamic loads by generating a condition which can be compared to an internal stress condition of the deformable structure - they do not apply any external (aerodynamic) forces on the structure. Thus, if the equations of motion were enhanced by $\hat{\mathbf{f}}_{aRref}$, $\hat{\mathbf{Q}}_s$ and $\hat{\mathbf{Q}}_v$ only, an aircraft in a simulation of straight, level flight would flex, correctly representing the deflection under the acting flight loads, but immediately start to enter a dive on a parabolic trajectory. Additional terms are required in the upper two rows of Eq. (50) to ensure adequate rigid body motion: \mathbf{f}_a and \mathbf{l}_a , which subsume the rigid body airloads \mathbf{f}_{aR} , \mathbf{l}_{aR} , the aerodynamic effects of control inputs \mathbf{f}_{aC} , \mathbf{l}_{aC} , and the increments of elastic body deformation \mathbf{f}_{aE} , \mathbf{l}_{aE} . Similarly, $\hat{\mathbf{Q}}_s$ and $\hat{\mathbf{Q}}_v$ can be split into their respective components, the modal aerodynamic matrices of rigid body motion $\hat{\mathbf{Q}}_{sR}$, control surface deflection $\hat{\mathbf{Q}}_{sC}$ and elastic deformations $\hat{\mathbf{Q}}_{sE}$, respectively $\hat{\mathbf{Q}}_{vR}$, $\hat{\mathbf{Q}}_{vC}$ and $\hat{\mathbf{Q}}_{vE}$ for the first-order terms.

5.4 Modal Representation of Rigid Body Aerodynamics

With Eq. (50), the rigid body portion of aerodynamic loads can be written as

$$\mathbf{f}_{aeroR} = - \begin{bmatrix} \mathbf{f}_{aRB} \\ \mathbf{l}_{aRB} \\ \hat{\mathbf{f}}_{aRref} \end{bmatrix} - \begin{bmatrix} \mathbf{f}_{aR}(\mathbf{z}_R, \dot{\mathbf{z}}_R) \\ \mathbf{l}_{aR}(\mathbf{z}_R, \dot{\mathbf{z}}_R) \\ \hat{\mathbf{Q}}_{sR}\mathbf{z}_a + \hat{\mathbf{Q}}_{vR}\dot{\mathbf{z}}_a \end{bmatrix}. \quad (51)$$

As described above, the equation above can be split into two parts: the rigid body motion (first two rows) and the effects of the loads distributed on the deformable body.

The vector of aerodynamic rigid body states consists of angle of attack α , the yaw angle β and the roll angle γ , Figure 5.4. In reference configuration, the aircraft is analysed at or at least close to its +1-g level flight attitude, with the initial freestream parameters α_0 , β_0 and γ_0 .³²

32. For the conventional, symmetrical aircraft (and a reasonable choice of the aircraft reference system), no sideslip will be applied in the reference analysis. This will leave the angle of attack α_0 as the only non-zero reference parameter of \mathbf{z}_R , as the parameters α and β are sufficient to define the direction of action of the freestream velocity vector. The time-derivative of the roll angle, the roll rate $\dot{\gamma}$, is nevertheless required for first-order terms.

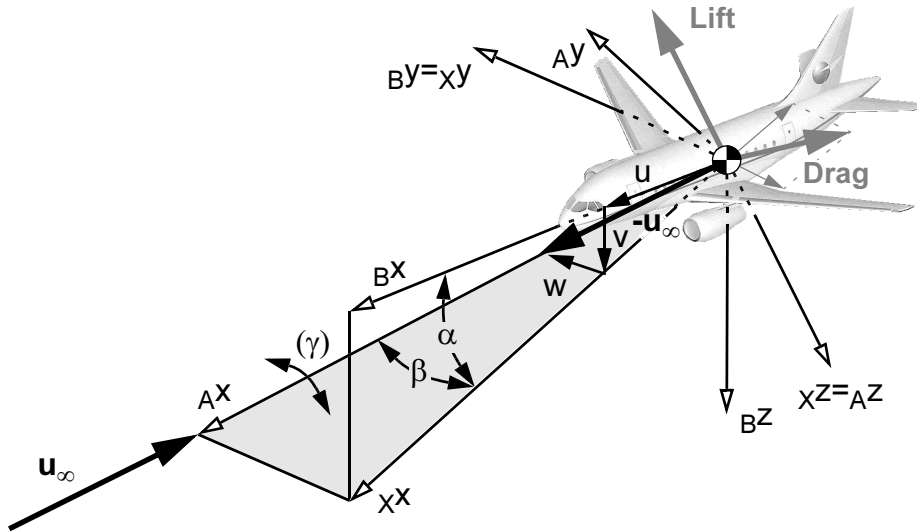


Figure 5.4 Flight Attitude Measurements for the Vector of Rigid Body States

The aerodynamic forces will be determined in the experimental coordinate system $\underline{x}\mathbf{e}$, which requires to transform them into the body-fixed frame $\underline{B}\mathbf{e}$ in the computation with the transformation matrix \mathbf{A}_{BX} .³³ All rotations are defined in the right-handed sense about the rotation axis. The vector of aerodynamic rigid body states \mathbf{z}_R then reads

$$\mathbf{z}_R = \begin{bmatrix} \gamma - \gamma_0 \\ \alpha - \alpha_0 \\ \beta - \beta_0 \end{bmatrix}. \quad (52)$$

5.4.1 Aerodynamics of the Reference Configuration

The rigid body aerodynamic terms of the reference configuration, \mathbf{f}_{aRB} and \mathbf{l}_{aRB} , can be directly derived from the reference CFD analysis. By transforming them to the body frame,

$$\underline{B}\mathbf{f}_{aRB} = \mathbf{A}_{BX} \underline{X}\mathbf{f}_{aRB}, \quad (53a)$$

and, with a possible offset vector \mathbf{r}_{BX} between both systems $\underline{x}\mathbf{e}$ and $\underline{B}\mathbf{e}$,

$$\underline{B}\mathbf{l}_{aRB} = \mathbf{A}_{BX}(\mathbf{r}_{BX} \times \underline{X}\mathbf{f}_{aRB} + \underline{X}\mathbf{l}_{aRB}), \quad (53b)$$

they can be inserted into Eq. (51).

33. The coordinate systems used here follow the standard definitions of LN 9300, resp. ISO 1151, [82]-[85]. An overview of the systems used in this report can be found in the Annex (see Figure 5.4 for illustration). LN 9300 / ISO 1151 are also used for the denotation of components, which are explained in the Annex, too.

The distributed modal aerodynamic force vector $\hat{\mathbf{f}}_{\text{aRref}}$ can be determined by mapping the local aerodynamic forces and moments onto the modally reduced structural model.³⁴ The resulting aerodynamic force vector $\mathbf{f}_{\text{aRref}}$ has to be transformed into modal form by a left-multiplication of the mode matrix Φ_{F} :

$$\hat{\mathbf{f}}_{\text{aRref}} = \Phi_{\text{F}} \mathbf{f}_{\text{aRref}}. \quad (54)$$

5.4.2 State-dependent Aerodynamics of the Rigid Body

For deviations from the defined reference attitude, the resulting force increments can be derived from the CFD analyses of the undeformed aircraft with a unit rotation around a specific axis. With the assumption of basically linear aerodynamic conditions, it is possible to compute the derivatives for each axis.

The aerodynamic effects of rigid body motion can be represented by a force and a moment at the origin of the aircraft reference frame, and represent each component in dependence to the respective angle of rotation or angular velocities, e.g. the non-dimensional derivative of vertical force in dependence from the angle of attack, ${}_A C_{Z\alpha}$, which is related to the classical derivative of the lift coefficient $C_{L\alpha}$ ³⁵:

$$C_{L\alpha} = \frac{\partial C_L}{\partial \alpha} = -{}_A C_{Z\alpha}. \quad (55)$$

Aerodynamic increments of rigid body rotations thus yield

$$\mathbf{f}_{\text{aR}} = q(\mathbf{u}_{\infty}) \mathbf{S}_{\text{ref}} \mathbf{A}_{\text{BX}} \left(\begin{array}{c} \left[\begin{array}{ccc} C_{X\gamma} & C_{X\alpha} & C_{X\beta} \\ C_{Y\gamma} & C_{Y\alpha} & C_{Y\beta} \\ C_{Z\gamma} & C_{Z\alpha} & C_{Z\beta} \end{array} \right] \mathbf{z}_{\text{R}} + \left[\begin{array}{ccc} C_{X\dot{\gamma}} & C_{X\dot{\alpha}} & C_{X\dot{\beta}} \\ C_{Y\dot{\gamma}} & C_{Y\dot{\alpha}} & C_{Y\dot{\beta}} \\ C_{Z\dot{\gamma}} & C_{Z\dot{\alpha}} & C_{Z\dot{\beta}} \end{array} \right] \dot{\mathbf{z}}_{\text{R}} \end{array} \right) \quad (56a)$$

for the force vector of rigid body motion, and

$$\mathbf{l}_{\text{aR}} = \mathbf{r}_{\text{BX}} \times \mathbf{f}_{\text{aR}} + q(\mathbf{u}_{\infty}) c_{\text{ref}} \mathbf{S}_{\text{ref}} \mathbf{A}_{\text{BX}} \left(\begin{array}{c} \left[\begin{array}{ccc} C_{L\gamma} & C_{L\alpha} & C_{L\beta} \\ C_{M\gamma} & C_{M\alpha} & C_{M\beta} \\ C_{N\gamma} & C_{N\alpha} & C_{N\beta} \end{array} \right] \mathbf{z}_{\text{R}} + \left[\begin{array}{ccc} C_{L\dot{\gamma}} & C_{L\dot{\alpha}} & C_{L\dot{\beta}} \\ C_{M\dot{\gamma}} & C_{M\dot{\alpha}} & C_{M\dot{\beta}} \\ C_{N\dot{\gamma}} & C_{N\dot{\alpha}} & C_{N\dot{\beta}} \end{array} \right] \dot{\mathbf{z}}_{\text{R}} \end{array} \right) \quad (56b)$$

for the moment vector, with all derivatives given in respect to the experimental reference frame ${}_X \mathbf{e}_-$.

34. For aspects of interpolation between modally reduced CSM and CFD, refer to Section 6.3

35. An equivocality of indices exists for $C_{L\alpha}$ and the derivative of the rolling moment coefficient in respect to the angle of attack of the same notation. In cases where the meaning is not obvious, it will be described in the accompanying text.

It should be noted that Eqs. (56a) and (56b) represent the formal approach of rigid body CG aerodynamics - not all derivatives have to be determined to receive a reasonable solution, respectively are of physical importance. The decision which derivatives should actually be taken into consideration, however, depends strongly upon the application and the deriving simulation scenario.

We can assume the velocity-dependent derivatives to be quasi-steady, [86]. Thus, the derivative values for the working point(s) of the simulation may be processed prior to the dynamic analysis as well.

5.4.3 Load Distribution on the Elastic Airframe

The aerodynamic influence matrices $\hat{\mathbf{Q}}_{sR}$ and $\hat{\mathbf{Q}}_{vR}$ of Eq. (51) represent transformation matrices which concatenate the actual flow conditions given by the vector of aerodynamic rigid body states \mathbf{z}_R , respectively its derivative to time $\dot{\mathbf{z}}_R$, with the modal forces on the n_n nodes of the structural MBS-model. Similar to the other modal matrices, they may be computed prior to the simulation.

Two basic pieces of information provide these matrices: the distribution of the aerodynamic forces \mathbf{f}_{aRref} and moments \mathbf{l}_{aRref} in the aircraft's reference attitude on the nodes of the structural model of the deformable body, and the gradient of \mathbf{f}_{aRref} and \mathbf{l}_{aRref} in reference to the coordinates of \mathbf{z}_R and $\dot{\mathbf{z}}_R$,

$$\begin{aligned} \nabla \mathbf{f}_{aRref}(\mathbf{z}_R, \dot{\mathbf{z}}_R) &= [\mathbf{f}_{aRref\gamma}, \mathbf{f}_{aRref\alpha}, \mathbf{f}_{aRref\beta}, \mathbf{f}_{aRref\dot{\gamma}}, \mathbf{f}_{aRref\dot{\alpha}}, \mathbf{f}_{aRref\dot{\beta}}] \\ &= \left[\frac{\partial}{\partial \gamma} \mathbf{f}_{aRref}, \frac{\partial}{\partial \alpha} \mathbf{f}_{aRref}, \frac{\partial}{\partial \beta} \mathbf{f}_{aRref}, \frac{\partial}{\partial \dot{\gamma}} \mathbf{f}_{aRref}, \frac{\partial}{\partial \dot{\alpha}} \mathbf{f}_{aRref}, \frac{\partial}{\partial \dot{\beta}} \mathbf{f}_{aRref} \right], \end{aligned} \quad (57a)$$

and

$$\begin{aligned} \nabla \mathbf{l}_{aRref}(\mathbf{z}_R, \dot{\mathbf{z}}_R) &= [\mathbf{l}_{aRref\gamma}, \mathbf{l}_{aRref\alpha}, \mathbf{l}_{aRref\beta}, \mathbf{l}_{aRref\dot{\gamma}}, \mathbf{l}_{aRref\dot{\alpha}}, \mathbf{l}_{aRref\dot{\beta}}] \\ &= \left[\frac{\partial}{\partial \gamma} \mathbf{l}_{aRref}, \frac{\partial}{\partial \alpha} \mathbf{l}_{aRref}, \frac{\partial}{\partial \beta} \mathbf{l}_{aRref}, \frac{\partial}{\partial \dot{\gamma}} \mathbf{l}_{aRref}, \frac{\partial}{\partial \dot{\alpha}} \mathbf{l}_{aRref}, \frac{\partial}{\partial \dot{\beta}} \mathbf{l}_{aRref} \right]. \end{aligned} \quad (57b)$$

These gradients are still dependent on the dynamic pressure q . To decouple \mathbf{f}_{aRref} and \mathbf{l}_{aRref} from the influence of freestream velocity \mathbf{u}_∞ (and density ρ) and to establish a consistent representation, the partial derivatives will be transformed to a non-dimensional form, with $i = [\alpha, \beta, \gamma, \dot{\alpha}, \dot{\beta}, \dot{\gamma}]$:

$$\mathbf{c}_{aRfi} = \frac{\mathbf{f}_{aRrefi}}{q \mathbf{S}_{ref}}, \quad \mathbf{c}_{aRli} = \frac{\mathbf{l}_{aRrefi}}{q c_{ref} \mathbf{S}_{ref}}. \quad (58)$$

The lower case letter c has been chosen for these derivatives as they can be regarded as vectors of the corresponding local derivatives in respect to an aerodynamic unit load distribution.

To be included into the equations of motion, these derivatives have to be transformed into modal coordinates by a left-multiplication of the mode matrix Φ_F :

$$\hat{\mathbf{c}}_{aRfi} = \Phi_F^T \mathbf{c}_{aRfi}, \quad \hat{\mathbf{c}}_{aRli} = \Phi_F^T \mathbf{c}_{aRli}. \quad (59)$$

The modal derivatives can now be combined with the modal aerodynamic submatrices $\hat{\mathbf{Q}}_{sRf}$, $\hat{\mathbf{Q}}_{sRI}$, $\hat{\mathbf{Q}}_{vRf}$ and $\hat{\mathbf{Q}}_{vRI}$:

$$\hat{\mathbf{Q}}_{sRf} = [\hat{\mathbf{c}}_{aRf\gamma}, \hat{\mathbf{c}}_{aRf\alpha}, \hat{\mathbf{c}}_{aRf\beta}], \quad \hat{\mathbf{Q}}_{sRI} = [\hat{\mathbf{c}}_{aRI\gamma}, \hat{\mathbf{c}}_{aRI\alpha}, \hat{\mathbf{c}}_{aRI\beta}], \quad (60a)$$

$$\hat{\mathbf{Q}}_{vRf} = [\hat{\mathbf{c}}_{aRf\dot{\gamma}}, \hat{\mathbf{c}}_{aRf\dot{\alpha}}, \hat{\mathbf{c}}_{aRf\dot{\beta}}], \quad \hat{\mathbf{Q}}_{vRI} = [\hat{\mathbf{c}}_{aRI\dot{\gamma}}, \hat{\mathbf{c}}_{aRI\dot{\alpha}}, \hat{\mathbf{c}}_{aRI\dot{\beta}}]. \quad (60b)$$

As its name already indicates, the vector of aerodynamic rigid body states \mathbf{z}_R consists of time-dependent states of the body in question. This implies that the force vector \mathbf{f}_{aeroR} is a variable in the integration process. Its components are determined by a preceded routine which, similar to a sensor measurement, computes the actual state values, i.e. α , β and γ , of the solution step.

It seems reasonable to ask the question: "What's the advantage?", as, compared to the approach to include rigid body aerodynamics by force elements, this formulation for the aerodynamics of the rigid body does not distinctly reduce computation times or simplify the analysis algorithm on the MBS side. It is nevertheless a method to include rigid body aerodynamics in a closed, formalistic representation which facilitates an (semi-)automated processing of aerodynamic data: its main advantage is that it allows for a user-friendly integration of the aerodynamics of a deformable structure into MBS by a preprocessing file which has only to be generated once for a given configuration - dealing with numerous force elements acting on the structural nodes is avoided. Additionally, this approach is consistent with the procedure for control inputs and, more important, the aerodynamic influences of structural deformation, where in fact advantages in computation times are achieved.

5.5 Aerodynamic Effects of Control Surface Deflections

The aerodynamic effects of control inputs can be treated similar to rigid body aerodynamics: forces and moments are generated by control surface deflections instead of the changes in attitude of the aircraft in reference to the airflow. The state vector of control surface deflections \mathbf{z}_C is composed of a characteristic specification of each control which is considered. In most simulation cases, this will be the actual value of angular deflection of a control surface, but other references are possible as well, e.g. from stick motion or FCS data.

Thus, \mathbf{z}_C reads

$$\mathbf{z}_C = [\delta_1, \delta_2, \dots, \delta_{n_C}]^T. \quad (61)$$

A total of n_c controls is being considered; these can be primary or secondary flight controls, high lift or lift dumping devices, etc.

Each control contained in \mathbf{z}_C requires (at least) one CFD analysis step in the preprocessing computation. Processing of this data delivers the results necessary for rigid body motion and the elastic response of the airframe.

5.5.1 Effects of Control Surface Deflections on Rigid Body Motion

Similar to the representation of rigid body aerodynamics, the effects of control inputs on the rigid body motion are constituted in derivative form:

$$\mathbf{f}_{aC} = q(\mathbf{u}_\infty) \mathbf{S}_{ref} \mathbf{A}_{BX} \left(\text{diag}(\mathbf{s}_s^T(\mathbf{z}_C)) \begin{bmatrix} C_{X\delta_1} & C_{X\delta_2} & \dots & C_{X\delta_{n_c}} \\ C_{Y\delta_1} & C_{Y\delta_2} & \dots & C_{Y\delta_{n_c}} \\ C_{Z\delta_1} & C_{Z\delta_2} & \dots & C_{Z\delta_{n_c}} \end{bmatrix} \mathbf{z}_C + \text{diag}(\mathbf{s}_v^T(\dot{\mathbf{z}}_C)) \begin{bmatrix} C_{X\dot{\delta}_1} & \dots & C_{X\dot{\delta}_{n_c}} \\ C_{Y\dot{\delta}_1} & \dots & C_{Y\dot{\delta}_{n_c}} \\ C_{Z\dot{\delta}_1} & \dots & C_{Z\dot{\delta}_{n_c}} \end{bmatrix} \dot{\mathbf{z}}_C \right), \quad (62a)$$

$$\mathbf{l}_{aC} = \mathbf{r}_{BX} \times \mathbf{f}_{aC} \quad (62b)$$

$$+ q(\mathbf{u}_\infty) c_{ref} \mathbf{S}_{ref} \mathbf{A}_{BX} \left(\text{diag}(\mathbf{s}_s^T(\mathbf{z}_C)) \begin{bmatrix} C_{L\delta_1} & C_{L\delta_2} & \dots & C_{L\delta_{n_c}} \\ C_{M\delta_1} & C_{M\delta_2} & \dots & C_{M\delta_{n_c}} \\ C_{N\delta_1} & C_{N\delta_2} & \dots & C_{N\delta_{n_c}} \end{bmatrix} \mathbf{z}_C + \text{diag}(\mathbf{s}_v^T(\dot{\mathbf{z}}_C)) \begin{bmatrix} C_{L\dot{\delta}_1} & \dots & C_{L\dot{\delta}_{n_c}} \\ C_{M\dot{\delta}_1} & \dots & C_{M\dot{\delta}_{n_c}} \\ C_{N\dot{\delta}_1} & \dots & C_{N\dot{\delta}_{n_c}} \end{bmatrix} \dot{\mathbf{z}}_C \right).$$

The vectors \mathbf{s}_s and \mathbf{s}_v contain adjustment factors which allow to account for losses of control effectiveness at larger flap deflection angles; each of the n_c factors of \mathbf{s}_s and \mathbf{s}_v is assigned to a specific control deflection δ_i and restrains the applied airloads due to control inputs at large deflection angles, Figure 5.5, usually by empirical functions.

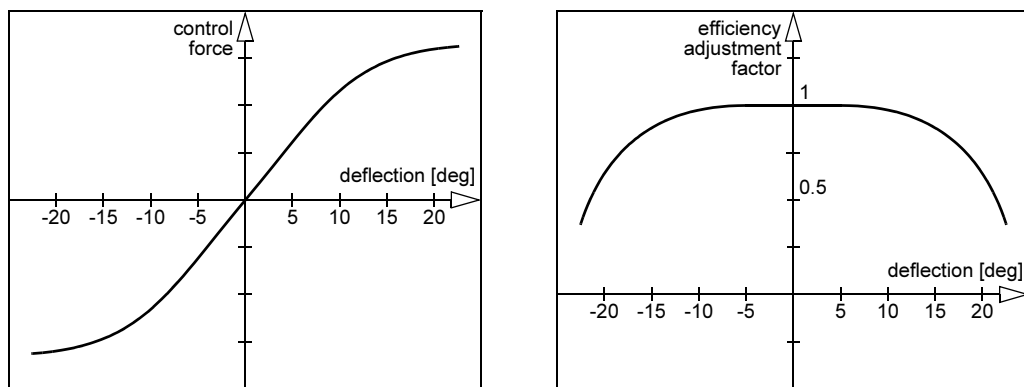


Figure 5.5 Example of Control Efficiency Function and Corresponding Efficiency Factor

5.5.2 Distribution of Control Loads on the Elastic Airframe

For the distribution of aerodynamic control loads on the flexible structure, again the “sensitivity” of the aerodynamic properties is being considered; this time in respect to a rotational deflection of a control δ_i and its rotational velocity $\dot{\delta}_i$ for $i = [1, 2, \dots, n_c]$,

$$\begin{aligned} \nabla \mathbf{f}_{aCref} &= [\mathbf{f}_{aCref\delta_1}, \mathbf{f}_{aCref\delta_2}, \dots, \mathbf{f}_{aCref\delta_{n_c}}, \mathbf{f}_{aCref\dot{\delta}_1}, \dots, \mathbf{f}_{aCref\dot{\delta}_{n_c}}] \quad (63a) \\ &= \left[\frac{\partial}{\partial \delta_1} \mathbf{f}_{aCref,1}, \frac{\partial}{\partial \delta_2} \mathbf{f}_{aCref,2}, \dots, \frac{\partial}{\partial \delta_{n_c}} \mathbf{f}_{aCref,n_c}, \frac{\partial}{\partial \dot{\delta}_1} \mathbf{f}_{aCref,1}, \dots, \frac{\partial}{\partial \dot{\delta}_{n_c}} \mathbf{f}_{aCref,n_c} \right] \end{aligned}$$

and

$$\begin{aligned} \nabla \mathbf{l}_{aCref} &= [\mathbf{l}_{aCref\delta_1}, \mathbf{l}_{aCref\delta_2}, \dots, \mathbf{l}_{aCref\delta_{n_c}}, \mathbf{l}_{aCref\dot{\delta}_1}, \dots, \mathbf{l}_{aCref\dot{\delta}_{n_c}}] \quad (63b) \\ &= \left[\frac{\partial}{\partial \delta_1} \mathbf{l}_{aCref,1}, \frac{\partial}{\partial \delta_2} \mathbf{l}_{aCref,2}, \dots, \frac{\partial}{\partial \delta_{n_c}} \mathbf{l}_{aCref,n_c}, \frac{\partial}{\partial \dot{\delta}_1} \mathbf{l}_{aCref,1}, \dots, \frac{\partial}{\partial \dot{\delta}_{n_c}} \mathbf{l}_{aCref,n_c} \right]. \end{aligned}$$

The aerodynamic reference force vector $\mathbf{f}_{aCref,i}$ for the i^{th} control input is the difference between the aerodynamic forces on the aircraft in reference configuration with a unit deflection of the corresponding control(s) and the force vector of the aircraft in rigid body reference attitude \mathbf{f}_{aRref} .

Non-dimensionalised by

$$\mathbf{c}_{aCfi} = \frac{\mathbf{f}_{aCref\delta_i}}{qS_{ref}}, \quad \mathbf{c}_{aCli} = \frac{\mathbf{l}_{aCref\delta_i}}{qC_{ref}S_{ref}}, \quad (64)$$

and transformed into modal coordinates

$$\hat{\mathbf{c}}_{aCfi} = \Phi_F^T \mathbf{c}_{aCfi}, \quad \hat{\mathbf{c}}_{aCli} = \Phi_F^T \mathbf{c}_{aCli}, \quad (65)$$

the modal aerodynamic matrices $\hat{\mathbf{Q}}_{sCf}$, $\hat{\mathbf{Q}}_{sCl}$, $\hat{\mathbf{Q}}_{vCf}$ and $\hat{\mathbf{Q}}_{vCl}$ are derived, denoting

$$\hat{\mathbf{Q}}_{sCf} = [\hat{\mathbf{c}}_{aCf\delta_1}, \hat{\mathbf{c}}_{aCf\delta_2}, \dots, \hat{\mathbf{c}}_{aCf\delta_{n_c}}], \quad \hat{\mathbf{Q}}_{sCl} = [\hat{\mathbf{c}}_{aCl\delta_1}, \hat{\mathbf{c}}_{aCl\delta_2}, \dots, \hat{\mathbf{c}}_{aCl\delta_{n_c}}], \quad (66a)$$

$$\hat{\mathbf{Q}}_{vCf} = [\hat{\mathbf{c}}_{aCf\dot{\delta}_1}, \hat{\mathbf{c}}_{aCf\dot{\delta}_2}, \dots, \hat{\mathbf{c}}_{aCf\dot{\delta}_{n_c}}], \quad \hat{\mathbf{Q}}_{vCl} = [\hat{\mathbf{c}}_{aCl\dot{\delta}_1}, \hat{\mathbf{c}}_{aCl\dot{\delta}_2}, \dots, \hat{\mathbf{c}}_{aCl\dot{\delta}_{n_c}}]. \quad (66b)$$

This, of course, is the formal derivation of $\hat{\mathbf{Q}}_C$; in most practical applications, the velocity terms of control input effects will be neglected, omitting the terms of Eq. (66b).

Not neglected, although it may appear so at first glance, is the interdependence of control effects and the aircraft’s overall behaviour - the aerodynamic forces of a control deflection remain in fact constant, regardless of aircraft motion, but they are counteracted by the velocity-dependent terms of rigid body aerodynamic. The maximum roll rate, for example, is achieved when the aerodynamic forces of full aileron deflection are counterbalanced by the roll-rate dependent damping moment of $C_{L\dot{\gamma}}$.

5.6 Aerodynamic Effects of Structural Deformations

5.6.1 Aerodynamic Force Increments of Elastic Aircraft Deformation

The most apparent influence of elastic deformations of the airframe on the overall airloads on the aircraft generally derives from wing torsion. Wing torsion can be caused by aerodynamic loads on the wing, or by dynamic loads as they may result from a touch-down, e.g. for the current standard configuration of civil transports, the engines which are placed well in front of the elastic axis of the wing can raise high torsional loads on the wing box. Twisting of the wing leads to changes in the local angle of attack, thus significantly altering the aerodynamic conditions. Other deformation modes which may influence the airloads are wing bending and fuselage bending. Figure 5.6 displays the local flow conditions at a outboard section of a wing which is twisted by a 1st-order torsion mode.

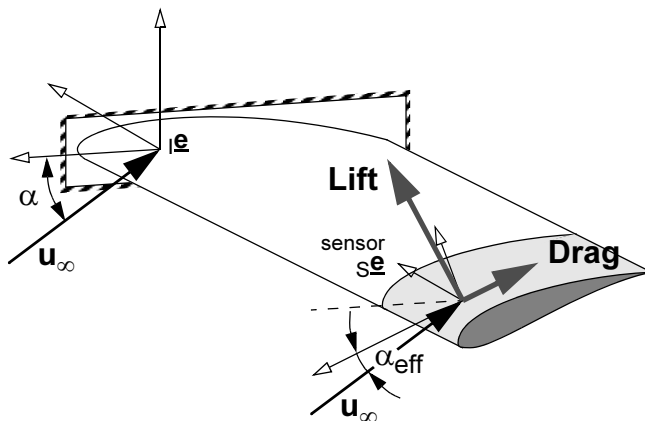


Figure 5.6 Lift and Drag of a Wing Section Under Consideration of Wing Torsion

Obviously, aerodynamic effects of airframe deflection can only appear for those deformation modes which are considered as base functions in the set-up of the SID data file of the flexible body. Thus, the state vector of aerodynamic effects of body deformation corresponds to the vector of elastic coordinates \mathbf{z}_E , but not all deformation modes have impact on the aerodynamics. The advantages of a consistent approach nevertheless suggest to employ \mathbf{z}_E instead of creating a reduced aerodynamic state vector which contains required elastic coordinates only.

To obtain the aerodynamic data corresponding to the state of body displacement, an aerodynamic analysis has to be performed for every aeroelastic mode considered where the reference configuration of the aircraft is superposed with the unit displacement or velocity field of the specific mode. Figure 5.7 shows a mesh of the aircraft³⁶ which is trimmed to the deformation field of a base function, here the first wing torsion mode. The force vectors symbolise the deriving force increments in respect to the

36. Figure 5.7 is intended to demonstrate the principle idea of modal aerodynamics. The underlying mesh derives from CAD, not from a CFD analysis - in practical applications, variation of the flow field is advantageous over an actual displacement of the CFD mesh of the aircraft.

undeformed reference solution; they may act on whole components, on sections, stripes, user defined patches or the single panel.

Converting the modal deformations so they can be applied onto the CFD model is simple and straightforward: the eigenvector of a mode which is to be considered in the analysis of aerodynamic effects of structural deformation in fact contains the “unit” displacements and rotations which are used as a reference for elastic body representation. Interpolating these values onto the aerodynamic model results in a deformation of the CFD mesh which automatically delivers the appropriate airloads as a result of the CFD analysis, respectively the desired aeroelastic increments when compared to the undeformed reference conditions.

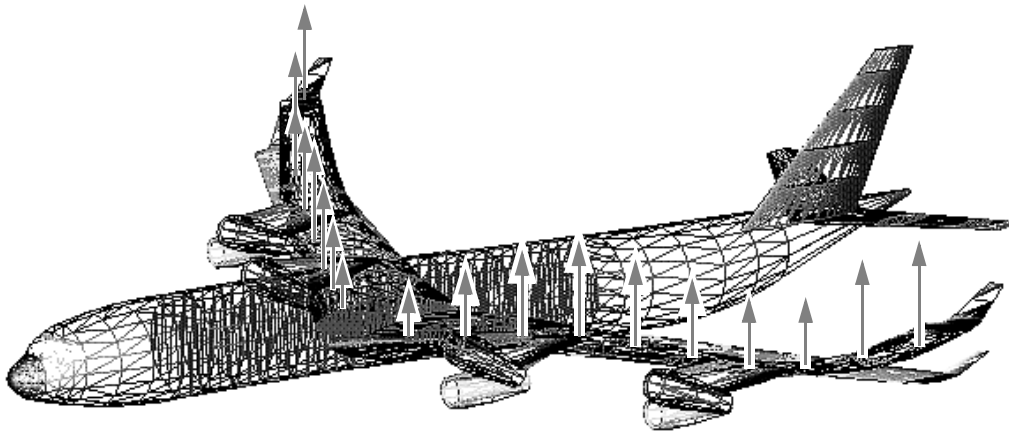


Figure 5.7 Aerodynamic Analysis of Flexible Body Deformed by Characteristic Base Function (1st Wing Torsion Mode - deformation is overscaled)

To receive a good result from the CFD analysis, it may nevertheless be advantageous to “normalise” the eigenvector so the deformations and rotations applied on the CFD model are physically reasonable: low-order modes may contain local deflections, whereas stiff higher-order modes deliver only infinitesimal differences in the aerodynamic properties compared to the reference configuration. Reference computations have shown that good results are obtained when the applied deformation lies within the range of 70-100% of the maximum deformation expected to occur in the simulation. Due to the linear relation, the aeroelastic increments received by the analysis of scaled deflections can then be rescaled to correspond to the actual elastic properties of the body as they are represented in the equations of motion.

5.6.2 Aerodynamic Effects Due to Aerodynamic Damping / Excitation

Kinematic velocities interrelate the kinematic motion of an airfoil, or an airfoil section, to physically plausible changes in the airflow conditions around that component. An obvious example is the consideration of translational motion, where the displacement rate \mathbf{d}_{def} of a (stiff) wingtip section is vectorially added to the freestream velocity \mathbf{u}_{∞} , Figure 5.8.

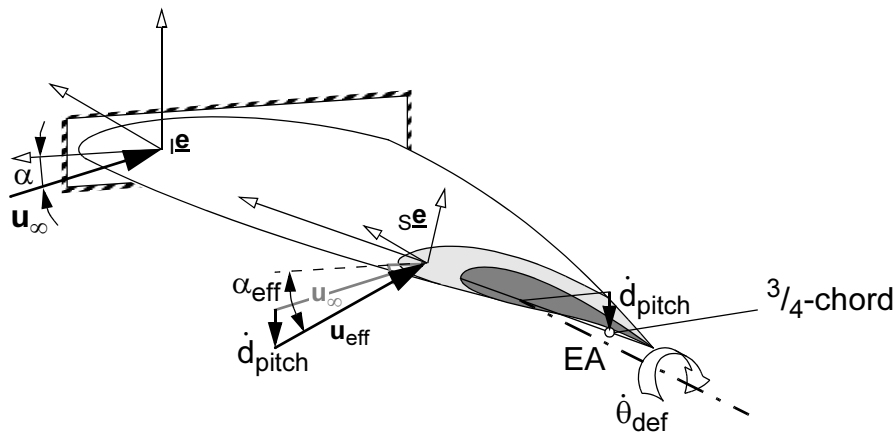


Figure 5.9 Kinematic Velocities at a Wing Section Under Consideration of Dynamic Wing Torsion

Similar to the method to derive aerodynamic force increments for structural deformation, the approach of kinematic velocities can also be used to compute the aerodynamic influence matrix \mathbf{Q}_{VE} of aerodynamic damping or excitation from a CFD model. The eigenvectors of the FEA normal mode analysis delivering the base functions for the fundamental matrix will be used to determine the local “deformation velocity” at the nodes of the structural model as a function of the first derivative of the vector of elastic coordinates with respect to time, $\dot{\mathbf{z}}_E$. This information is processed to local disturbances of the flow field around the airframe, e.g. by defining airflow velocity components normal to CFD model panels as boundary conditions of the aerodynamic solution. Thus, the aerodynamic force and moment increments of these aeroelastic modes can be computed, Figure 5.10.

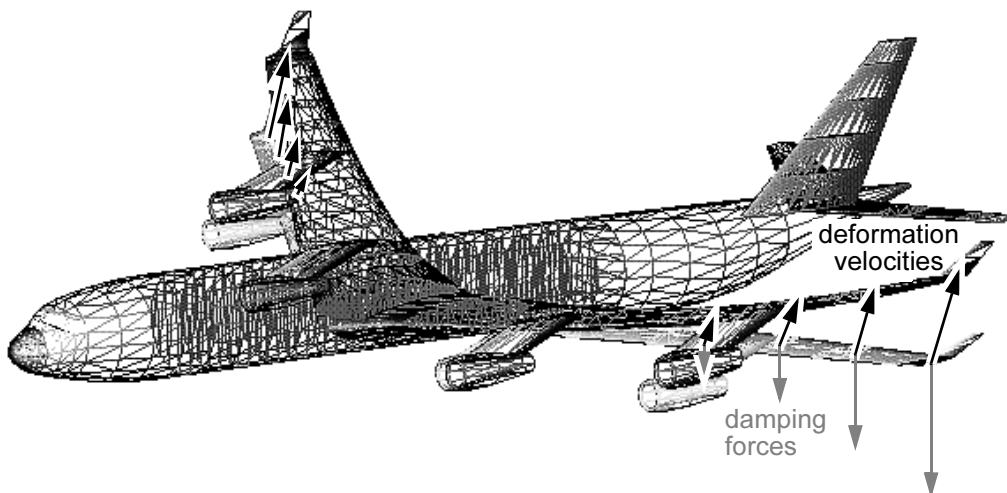


Figure 5.10 Analysis of Aerodynamic Damping/Excitation by Characteristic Base Function (1st Wing Bending Mode)

It should perhaps be added that the deformed state of the airframe structure is only depicted for illustration - obviously, kinematic velocities are applied on the undeformed model.

For the derivation of deformation velocities, we will utilise the fact that the modal representation of the flexible airframe structure is based on a combination of linearly amplified displacement fields. If the structure is deformed on the basis of a displacement mode ϕ_i , the nodal displacements of the structural grid \mathbf{u}_F are

$$\mathbf{u}_F = \phi_i z_{Ei} \cdot \quad (70)$$

As a result of the linear relation between the time derivative of the elastic coordinate, the "elastic velocity" \dot{z}_{Ei} , and the nodal velocities $\dot{\mathbf{u}}_F$,

$$\dot{\mathbf{u}}_F = \phi_i \dot{z}_{Ei}, \quad (71)$$

it is possible to directly interrelate \dot{z}_{Ei} and the corresponding nodal deformation velocities which are required for the aeroelastic preprocessing analysis, i.e. for a unit elastic velocity.³⁷

The corresponding deformation velocities can be easily determined for every node of the flexible MBS structure, as is may be demonstrated in a brief example of a cantilever beam, Figure 5.11. This beam performs a harmonic oscillation with an eigenfrequency of ω_0 . The eigenvector ϕ contains the deformations at the nodes N_i , $i \in [1;2;3;4]$:

$$\phi = \begin{pmatrix} u_{ref,1} \\ u_{ref,2} \\ u_{ref,3} \\ u_{ref,4} \end{pmatrix} \cdot \quad (72)$$

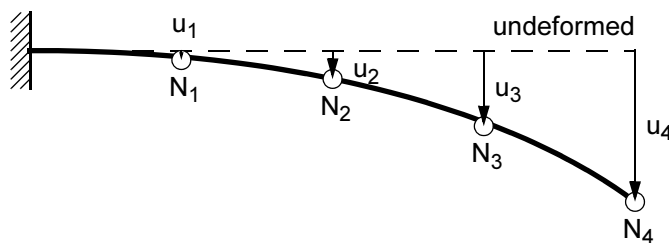


Figure 5.11 1st Bending Mode of a Cantilever Beam

A node N_i then performs a harmonic oscillation with an amplitude of $u_{ref,i}$,

$$u_i(t) = u_{ref,i} \sin(\omega_0 t), \quad (73)$$

37. Scaling of the applied velocities to the physical properties of the model is also possible, but is advantageously applied later on in the form of a constant (scaling) factor of the deriving velocity field.

and has a velocity of

$$\mathbf{v}_i(t) = \dot{\mathbf{u}}_i(t) = \frac{\partial \mathbf{u}_i(t)}{\partial t} = \omega_0 \mathbf{u}_{\text{ref},i} \cos(\omega_0 t). \quad (74)$$

Its velocity when passing the zero-point (undeformed position) is

$$\mathbf{v}_i(t=0) = \mathbf{v}_{0,i} = \omega_0 \mathbf{u}_{\text{ref},i}. \quad (74a)$$

In modal coordinates, using Eq. (38a) for a single mode ϕ which delivers

$$\mathbf{u}(t) = \phi \mathbf{z}_E(t), \quad (75)$$

Eq. (73) can be written as

$$\mathbf{z}_E(t) = \sin(\omega_0 t). \quad (76)$$

Thus, Eq. (74) yields

$$\dot{\mathbf{z}}_E(t) = \omega_0 \cos(\omega_0 t). \quad (77)$$

Therefore, the modal velocity $\dot{\mathbf{z}}_{E,0}$ at neutral position equals the frequency of oscillation

$$\dot{\mathbf{z}}_{E,0} = \dot{\mathbf{z}}_E(t=0) = \omega_0. \quad (78)$$

For the approach of modal aerodynamics, we are only interested in the aerodynamic forces and moments which are caused by a unit deflection velocity, for example

$$\dot{\mathbf{z}}_E = \omega_{\text{ref}} = 1 \quad [\text{Hz}], \quad (79)$$

which, at neutral position of the mode, leads to a kinematic velocity \mathbf{v}_{kin} for all nodes of the mCSM model. \mathbf{v}_{kin} is thus defined by the eigenvector (and the underlying modal unit values $\dot{\mathbf{z}}_E$, \mathbf{z}_E , which only introduce an user-defined scaling factor):

$$\mathbf{v}_{\text{kin}} = \mathbf{u}_{\text{ref}} \omega_{\text{ref}} = \phi \dot{\mathbf{z}}_E \mathbf{z}_E. \quad (80)$$

Applying kinematic velocities onto the CFD model can use the same interpolation which has been set up for transmuting structural deflections from mCSM to CFD. The kinematic translational velocities may be taken directly from the eigenvectors of the deflection modes considered, only the (local) kinematic rotations may need an adjustment, according to the position of the reference point on the CFD panel or surface element to which the kinematic rotation is applied.³⁸

Now, the aerodynamic damping or excitation forces due to this unit deformation rate can be computed. Contrary to the “traditional” derivation of the modal damping matrix $\hat{\mathbf{D}}_e$ of deformable body representation (Eqs. (41) and (42)), which is simply derived

38. The main velocity-dependent effects of a twisting structure, e.g. by wing torsion, are usually covered by the translational velocities of CFD surface elements, especially for elements distant from the elastic axis (e.g. panels near leading and trailing edge). Kinematic rotations become interesting when nodal forces derive from large CFD elements, e.g. stiff wing sections.

from stiffness-proportional damping, additional solution sequences are needed to receive the required data for the velocity-dependent part of \mathbf{Q}_{VE} .

The transformation from nodal deformation velocities to the appropriate boundary conditions of the CFD analysis depends in a nonlinear way on the reference velocity; thus, strictly speaking, the solution is applicable for this specific reference airspeed only, even if the resulting aerodynamic derivatives and matrices are transformed to a non-dimensional form. For small variations in airspeed Δu_∞ , however, we can reasonably assume a linear relation - and therefore, a valid solution - as long as the approximation

$$\sin \frac{\Delta u_\infty}{u_\infty} \approx \frac{\Delta u_\infty}{u_\infty} \quad (81)$$

holds. In the targeted field of application, that is the simulation of aircraft landing sequences, the most violent structural deformations occur at the landing impact, which delivers a convenient design point for the preprocessing analysis. It has nevertheless to be kept in mind that the quality of solution deteriorates when the aircraft decelerates. For applications where the structure is exposed to significant vibrations at other velocities than approach speed as well, it has to be considered if a changeover to one or more additional sets of aeroelastic matrices or interpolation between sampling points has to be performed.

5.6.3 Effects of Structural Deformation on Overall Body Motion

Because of the linear conditions, the derivatives of overall behaviour of the aircraft in respect to the elastic coordinates can be determined by the difference between the airloads of the reference configuration and those of the solution for a unit displacement given by the eigenvector of the considered base function. For each coordinate $j = [x, y, z]$, the corresponding rigid body forces of the deformed structure, f_{Ej} , are extracted from the aerodynamic analysis to deliver the respective derivative C_{Jz_i} , with $J = [X, Y, Z]$, for the displacement mode ϕ_i :

$$C_{Jz_i} = \frac{1}{z_i} \left(\frac{f_{Ej}}{q_\infty S_{ref}} - C_{J\alpha} \alpha_0 - C_{J\beta} \beta_0 - C_{J\gamma} \gamma_0 \right), \quad (82a)$$

where z_i is the "weighting factor" of the eigenvector displacement used for the CFD analysis (usually selected as $z_i = 1$, especially when the eigenvectors are normalised in respect to the mass matrix).

Similarly, the derivatives for the aerodynamic moments, with $J = [L, M, N]$, are calculated by

$$C_{Jz_i} = \frac{1}{z_i} \left(\frac{l_{Ej}}{q_\infty c_{ref} S_{ref}} - C_{J\alpha} \alpha_0 - C_{J\beta} \beta_0 - C_{J\gamma} \gamma_0 \right). \quad (82b)$$

For the deformation-velocity dependent aerodynamic derivatives C_{Jz_i} , the elastic coordinate z_i has to be replaced by its time derivative \dot{z}_i (the steady-state terms

$C_{J\alpha}\alpha_0$, $C_{J\beta}\beta_0$ and $C_{J\gamma}\gamma_0$ remain unchanged, as the aerodynamic conditions of the deforming aircraft are still measured against the steady reference configuration).

Accordingly, the aerodynamic force and moment increments of elastic body deformation read

$$\mathbf{f}_{aE} = q(\mathbf{u}_\infty) \mathbf{S}_{\text{ref}} \mathbf{A}_{\text{BX}} \left(\begin{bmatrix} C_{Xz_1} & C_{Xz_2} & \dots & C_{Xz_{n_q}} \\ C_{Yz_1} & C_{Yz_2} & \dots & C_{Yz_{n_q}} \\ C_{Zz_1} & C_{Zz_2} & \dots & C_{Zz_{n_q}} \end{bmatrix} \mathbf{z}_E + \begin{bmatrix} C_{X\dot{z}_1} & C_{X\dot{z}_2} & \dots & C_{X\dot{z}_{n_q}} \\ C_{Y\dot{z}_1} & C_{Y\dot{z}_2} & \dots & C_{Y\dot{z}_{n_q}} \\ C_{Z\dot{z}_1} & C_{Z\dot{z}_2} & \dots & C_{Z\dot{z}_{n_q}} \end{bmatrix} \dot{\mathbf{z}}_E \right) \quad (83a)$$

and

$$\mathbf{l}_{aE} = \mathbf{r}_{\text{BX}} \times \mathbf{f}_{aE} + q(\mathbf{u}_\infty) c_{\text{ref}} \mathbf{S}_{\text{ref}} \mathbf{A}_{\text{BX}} \left(\begin{bmatrix} C_{Lz_1} & C_{Lz_2} & \dots & C_{Lz_{n_q}} \\ C_{Mz_1} & C_{Mz_2} & \dots & C_{Mz_{n_q}} \\ C_{Nz_1} & C_{Nz_2} & \dots & C_{Nz_{n_q}} \end{bmatrix} \mathbf{z}_E + \begin{bmatrix} C_{L\dot{z}_1} & C_{L\dot{z}_2} & \dots & C_{L\dot{z}_{n_q}} \\ C_{M\dot{z}_1} & C_{M\dot{z}_2} & \dots & C_{M\dot{z}_{n_q}} \\ C_{N\dot{z}_1} & C_{N\dot{z}_2} & \dots & C_{N\dot{z}_{n_q}} \end{bmatrix} \dot{\mathbf{z}}_E \right). \quad (83b)$$

5.6.4 Distribution of Loads Caused by Elastic Airframe Deformations

To close the loop between elastic deformation and resulting airloads, these loads have to be distributed on the deformable structure as well. The advantage of the approach of modal aerodynamics is that the same algorithm can be used as applied for the effects of rigid body aerodynamics and control surface deflections.

Here, the aerodynamic reference force vector $\mathbf{f}_{a\text{Eref},i}$ corresponding to the base function ϕ_i is the difference between the aerodynamic forces on the aircraft, deformed according to the specific mode, and the force vector of the aircraft in rigid body reference attitude $\mathbf{f}_{a\text{Rref}}$.

Thus,

$$\begin{aligned} \nabla \mathbf{f}_{a\text{Eref}} &= [\mathbf{f}_{a\text{Cref}z_1}, \mathbf{f}_{a\text{Cref}z_2}, \dots, \mathbf{f}_{a\text{Cref}z_{n_c}}, \mathbf{f}_{a\text{Cref}\dot{z}_1}, \dots, \mathbf{f}_{a\text{Cref}\dot{z}_{n_c}}] \\ &= \left[\frac{\partial}{\partial z_1} \mathbf{f}_{a\text{Cref},1}, \frac{\partial}{\partial z_2} \mathbf{f}_{a\text{Cref},2}, \dots, \frac{\partial}{\partial z_{n_c}} \mathbf{f}_{a\text{Cref},n_c}, \frac{\partial}{\partial \dot{z}_1} \mathbf{f}_{a\text{Cref},1}, \dots, \frac{\partial}{\partial \dot{z}_{n_c}} \mathbf{f}_{a\text{Cref},n_c} \right] \end{aligned} \quad (84a)$$

and

$$\begin{aligned} \nabla \mathbf{l}_{a\text{Cref}} &= [\mathbf{l}_{a\text{Cref}z_1}, \mathbf{l}_{a\text{Cref}z_2}, \dots, \mathbf{l}_{a\text{Cref}z_{n_c}}, \mathbf{l}_{a\text{Cref}\dot{z}_1}, \dots, \mathbf{l}_{a\text{Cref}\dot{z}_{n_c}}] \\ &= \left[\frac{\partial}{\partial z_1} \mathbf{l}_{a\text{Cref},1}, \frac{\partial}{\partial z_2} \mathbf{l}_{a\text{Cref},2}, \dots, \frac{\partial}{\partial z_{n_c}} \mathbf{l}_{a\text{Cref},n_c}, \frac{\partial}{\partial \dot{z}_1} \mathbf{l}_{a\text{Cref},1}, \dots, \frac{\partial}{\partial \dot{z}_{n_c}} \mathbf{l}_{a\text{Cref},n_c} \right] \end{aligned} \quad (84b)$$

Arranging these sensitivities according to their type and order, non-dimensionalising the resulting \mathbf{c}_{aE} -derivatives and transforming them to modal coordinates by left-mul-

tiplication of the fundamental matrix similar to the process of Sections 5.4.3 and 5.5.2 yields the modal aerodynamic matrices $\hat{\mathbf{Q}}_{sEf}$, $\hat{\mathbf{Q}}_{sEI}$, $\hat{\mathbf{Q}}_{vEf}$ and $\hat{\mathbf{Q}}_{vEI}$.

From the numerical side, the term $\hat{\mathbf{Q}}_{sEf} + c_{ref} \hat{\mathbf{Q}}_{sEI}$ can be considered as an “aerodynamic stiffness matrix”; $\hat{\mathbf{Q}}_{vEf} + c_{ref} \hat{\mathbf{Q}}_{vEI}$ accordingly represents an “aerodynamic damping matrix”. The only difference in this respect to the structural stiffness and damping matrices $\hat{\mathbf{K}}_e$ and $\hat{\mathbf{D}}_e$ is that, in the equations of motion, the former possess an additional state-, respectively velocity-dependent factor, the dynamic pressure of the airflow. In most applications, this factor can be assumed to be constant throughout a time-integration step, which further simplifies (and accelerates) the calculation.

The modal aerodynamics enhancement of the elastic deformation part applies, as already mentioned, nothing but the equivalent of an internal stress condition of the body in question. This internal stress enforces a deflection of the body which complies with the loading state of the body. The internal stress caused by aerodynamic forces, which is introduced by the described enhancements to the third row of the EqM, can be integrated over the body and should consequently correspond to the aerodynamic forces and moments of the rigid body motion part. For numerical stability, however, the overall forces on the aircraft of the rigid body part (first two rows) and the elastic deformation part (third row) does not necessarily have to match. For a physically correct solution, both should be as close as possible, but small differences, for example because of rounding differences, have no effect on the numerical robustness of the solution or on computation times.

5.7 The Enhanced Equations of Motion of the Deformable Body

Including the results of Sections 5.4 to 5.6 into the equations of motion of the single deformable body, we receive

$$\begin{bmatrix} m\mathbf{E} & m\mathbf{r}_{BV}^T & \mathbf{C}_t^T \\ m\mathbf{r}_{BV} & \mathbf{J} & \mathbf{C}_r \\ \mathbf{C}_t & \mathbf{C}_r & \hat{\mathbf{M}}_e \end{bmatrix} \begin{bmatrix} \mathbf{a}_{IB} \\ \boldsymbol{\alpha}_{IB} \\ \ddot{\mathbf{z}}_E \end{bmatrix} = \mathbf{f}_{grav} + \mathbf{f}_{gyro} + \mathbf{f}_{elast} + \mathbf{f}_{app} + \mathbf{f}_{cstr} \quad (85)$$

$$\begin{bmatrix} q(\mathbf{u}_\infty) \mathbf{S}_{ref} \mathbf{A}_{BX} \begin{pmatrix} \begin{bmatrix} C_{X\gamma} & C_{X\alpha} & C_{X\beta} \\ C_{Y\gamma} & C_{Y\alpha} & C_{Y\beta} \\ C_{Z\gamma} & C_{Z\alpha} & C_{Z\beta} \end{bmatrix} \mathbf{z}_R + \begin{bmatrix} C_{X\dot{\gamma}} & C_{X\dot{\alpha}} & C_{X\dot{\beta}} \\ C_{Y\dot{\gamma}} & C_{Y\dot{\alpha}} & C_{Y\dot{\beta}} \\ C_{Z\dot{\gamma}} & C_{Z\dot{\alpha}} & C_{Z\dot{\beta}} \end{bmatrix} \dot{\mathbf{z}}_R \\ \mathbf{r}_{BX} \times \mathbf{f}_{aR} + q(\mathbf{u}_\infty) c_{ref} \mathbf{S}_{ref} \mathbf{A}_{BX} \begin{pmatrix} \begin{bmatrix} C_{L\gamma} & C_{L\alpha} & C_{L\beta} \\ C_{M\gamma} & C_{M\alpha} & C_{M\beta} \\ C_{N\gamma} & C_{N\alpha} & C_{N\beta} \end{bmatrix} \mathbf{z}_R + \begin{bmatrix} C_{L\dot{\gamma}} & C_{L\dot{\alpha}} & C_{L\dot{\beta}} \\ C_{M\dot{\gamma}} & C_{M\dot{\alpha}} & C_{M\dot{\beta}} \\ C_{N\dot{\gamma}} & C_{N\dot{\alpha}} & C_{N\dot{\beta}} \end{bmatrix} \dot{\mathbf{z}}_R \\ q\mathbf{S}_{ref} (\hat{\mathbf{Q}}_{sRf} + c_{ref} \hat{\mathbf{Q}}_{sRI}) \mathbf{z}_R + q\mathbf{S}_{ref} (\hat{\mathbf{Q}}_{vRf} + c_{ref} \hat{\mathbf{Q}}_{vRI}) \dot{\mathbf{z}}_R \end{pmatrix} \end{bmatrix}$$

$$\left[\begin{array}{l}
 \mathbf{q}(\mathbf{u}_\infty) \mathbf{S}_{\text{ref}} \mathbf{A}_{\text{BX}} \left(\text{diag}(\mathbf{s}_s^T(\mathbf{z}_C)) \begin{bmatrix} C_{X\delta_1} & C_{X\delta_2} & \dots & C_{X\delta_{n_c}} \\ C_{Y\delta_1} & C_{Y\delta_2} & \dots & C_{Y\delta_{n_c}} \\ C_{Z\delta_1} & C_{Z\delta_2} & \dots & C_{Z\delta_{n_c}} \end{bmatrix} \mathbf{z}_C + \text{diag}(\mathbf{s}_v(\dot{\mathbf{z}}_C)) \begin{bmatrix} C_{X\dot{\delta}_1} & \dots & C_{X\dot{\delta}_{n_c}} \\ C_{Y\dot{\delta}_1} & \dots & C_{Y\dot{\delta}_{n_c}} \\ C_{Z\dot{\delta}_1} & \dots & C_{Z\dot{\delta}_{n_c}} \end{bmatrix} \dot{\mathbf{z}}_C \right) \\
 \mathbf{r}_{\text{BX}} \times \mathbf{f}_{\text{aC}} + \mathbf{q}(\mathbf{u}_\infty) c_{\text{ref}} \mathbf{S}_{\text{ref}} \mathbf{A}_{\text{BX}} \left(\text{diag}(\mathbf{s}_s^T(\mathbf{z}_C)) \begin{bmatrix} C_{L\delta_1} & \dots & C_{L\delta_{n_c}} \\ C_{M\delta_1} & \dots & C_{M\delta_{n_c}} \\ C_{N\delta_1} & \dots & C_{N\delta_{n_c}} \end{bmatrix} \mathbf{z}_C + \text{diag}(\mathbf{s}_v^T(\dot{\mathbf{z}}_C)) \begin{bmatrix} C_{L\dot{\delta}_1} & \dots & C_{L\dot{\delta}_{n_c}} \\ C_{M\dot{\delta}_1} & \dots & C_{M\dot{\delta}_{n_c}} \\ C_{N\dot{\delta}_1} & \dots & C_{N\dot{\delta}_{n_c}} \end{bmatrix} \dot{\mathbf{z}}_C \right) \\
 \mathbf{q} \mathbf{S}_{\text{ref}} \text{diag}(\mathbf{s}_s^T(\mathbf{z}_C)) (\hat{\mathbf{Q}}_{\text{sCf}} + c_{\text{ref}} \hat{\mathbf{Q}}_{\text{sCl}}) \mathbf{z}_C + \mathbf{q} \mathbf{S}_{\text{ref}} \text{diag}(\mathbf{s}_v^T(\dot{\mathbf{z}}_C)) (\hat{\mathbf{Q}}_{\text{vCf}} + c_{\text{ref}} \hat{\mathbf{Q}}_{\text{vCl}}) \dot{\mathbf{z}}_C
 \end{array} \right]$$

$$\left[\begin{array}{l}
 \mathbf{q}(\mathbf{u}_\infty) \mathbf{S}_{\text{ref}} \mathbf{A}_{\text{BX}} \left(\begin{bmatrix} C_{Xz_1} & C_{Xz_2} & \dots & C_{Xz_{n_q}} \\ C_{Yz_1} & C_{Yz_2} & \dots & C_{Yz_{n_q}} \\ C_{Zz_1} & C_{Zz_2} & \dots & C_{Zz_{n_q}} \end{bmatrix} \mathbf{z}_E + \begin{bmatrix} C_{X\dot{z}_1} & C_{X\dot{z}_2} & \dots & C_{X\dot{z}_{n_q}} \\ C_{Y\dot{z}_1} & C_{Y\dot{z}_2} & \dots & C_{Y\dot{z}_{n_q}} \\ C_{Z\dot{z}_1} & C_{Z\dot{z}_2} & \dots & C_{Z\dot{z}_{n_q}} \end{bmatrix} \dot{\mathbf{z}}_E \right) \\
 \mathbf{r}_{\text{BX}} \times \mathbf{f}_{\text{aE}} + \mathbf{q}(\mathbf{u}_\infty) c_{\text{ref}} \mathbf{S}_{\text{ref}} \mathbf{A}_{\text{BX}} \left(\begin{bmatrix} C_{Lz_1} & C_{Lz_2} & \dots & C_{Lz_{n_q}} \\ C_{Mz_1} & C_{Mz_2} & \dots & C_{Mz_{n_q}} \\ C_{Nz_1} & C_{Nz_2} & \dots & C_{Nz_{n_q}} \end{bmatrix} \mathbf{z}_E + \begin{bmatrix} C_{L\dot{z}_1} & C_{L\dot{z}_2} & \dots & C_{L\dot{z}_{n_q}} \\ C_{M\dot{z}_1} & C_{M\dot{z}_2} & \dots & C_{M\dot{z}_{n_q}} \\ C_{N\dot{z}_1} & C_{N\dot{z}_2} & \dots & C_{N\dot{z}_{n_q}} \end{bmatrix} \dot{\mathbf{z}}_E \right) \\
 \mathbf{q} \mathbf{S}_{\text{ref}} (\hat{\mathbf{Q}}_{\text{sEf}} + c_{\text{ref}} \hat{\mathbf{Q}}_{\text{sEl}}) \mathbf{z}_E + \mathbf{q} \mathbf{S}_{\text{ref}} (\hat{\mathbf{Q}}_{\text{vEf}} + c_{\text{ref}} \hat{\mathbf{Q}}_{\text{vEl}}) \dot{\mathbf{z}}_E
 \end{array} \right]$$

6 Realisation Aspects of Aeroelastic Preprocessing

6.1 Basic Workflow of Aeroelastic Preprocessing

The sequences of aeroelastic preprocessing consist of analysing the aerodynamic properties of the rigid aircraft in reference configuration, the influence of rigid body motion and control surface deflections on the aerodynamics, the aerodynamics of the deformed body and additional cases such as ground effect, see Figure 6.1.

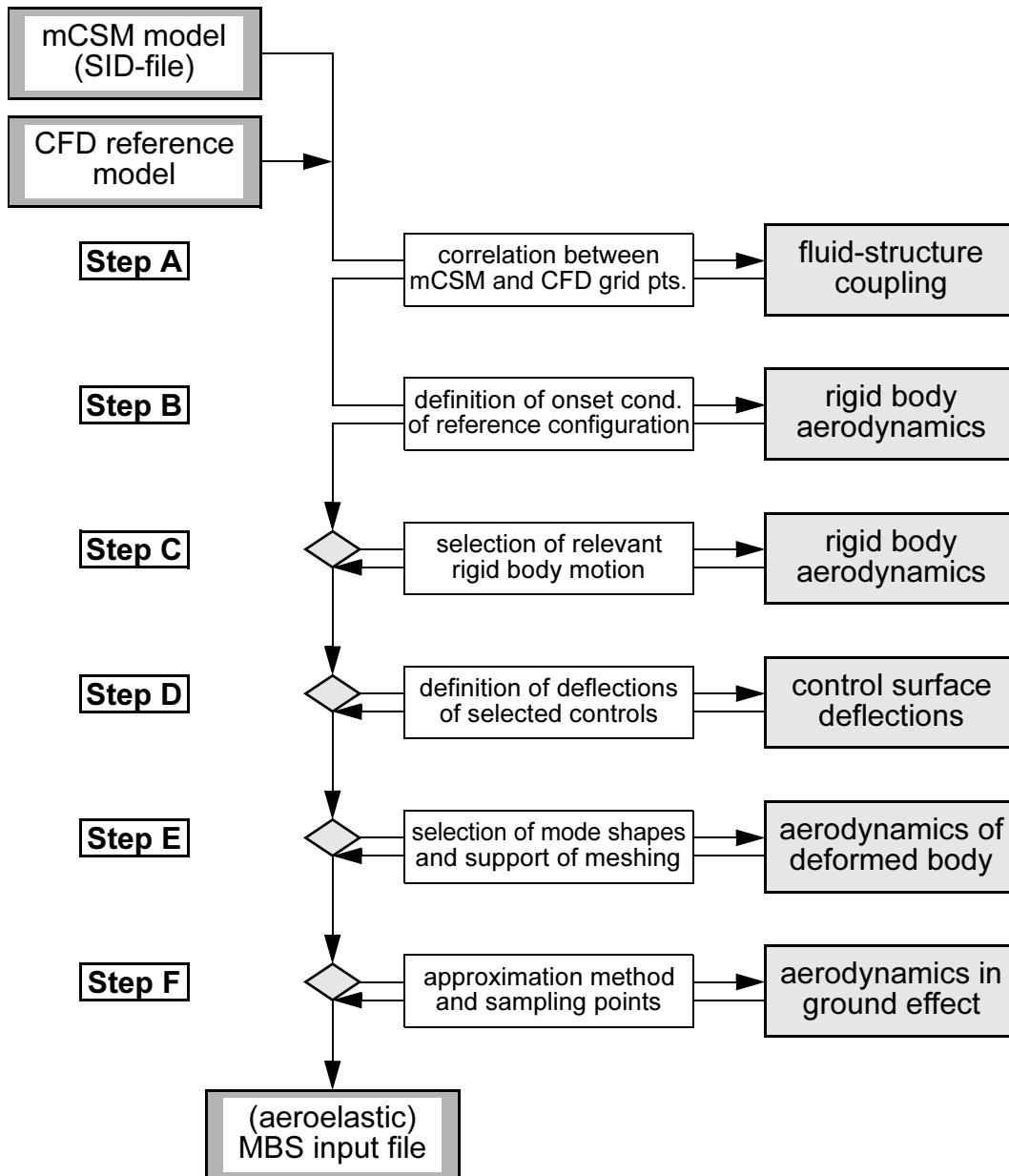


Figure 6.1 Overview of Workflow of Aeroelastic Preprocessing Using Modal Aerodynamics

The rhomboid “if”-symbol in Figure 6.1 indicates that steps C-F are not compulsory. Depending on the application, each of them may be skipped, but for detailed aircraft ground dynamics analysis, at least the effects of steps C, D and E have to be accounted for.

For aeroelastic preprocessing, two input files must be available:

- the modally reduced structural model and its base functions (SID input file);
- one or more CFD analysis file(s) of the aircraft in high-lift configuration.

The CFD reference cases should correspond to the MBS scenario. A landing sequence, for example, may use a CFD analysis file of the aircraft at approach angle of attack and an analysis file of the aircraft in derotated attitude. For MBS, the aerodynamic properties are then interpolated between these sampling points or switched by root functions. Additional sampling points can be used to improve accuracy.

Step A contains all necessary operations to couple the aerodynamic and the modally reduced computational structural mechanics (mCSM) model. This includes alignment of the CFD and CSM global coordinate systems, mapping of structural deformations onto the CFD grid and transformation of the aerodynamic forces to act on the mCSM model.

Step B defines the onset conditions (AoA, freestream Mach number, Reynold’s number, compressibility corrections, etc.) of the aircraft in reference configuration to compute the prevailing aerodynamic effects, i.e. the distributed rigid body lift forces and moments. Multiple sampling points can be defined to cover large changes of attitude, e.g. about the angle of attack, either by entering the sampling points of the parameter(s) in question via GUI (automated adaption of the reference model)³⁹ or by accessing multiple reference files. Interpolation or switching between sampling points is controlled in the MBS setup process.

Step C uses the same CFD model(s) as step A, but applies small unit rotations of the aircraft (roll, pitch, yaw). The difference to the respective reference configuration for rigid-body lift of step B delivers the aerodynamic force increment due to the unit rotation to determine the instationary derivatives,⁴⁰ e.g. $C_{A\dot{\alpha}}$. One CFD analysis has to be performed for each derivative.

Step D modifies the CFD model of step A with a unit deflection of an aerodynamic control surface. One analysis (and consequently model modification) is required for each control to be considered. Correction factors can be defined to include loss of control authority or efficiency at increased deflection angles.

39. Significant changes of characteristic properties, such as the AoA, may impair accuracy, as other model parameters, e.g. wake model(s), cannot be adapted to the new settings in this preprocessing step. This feature is intended for minor corrections to onset parameters, e.g. to achieve an adequately trimmed reference file, and should not be used for setting up multiple sampling points.

40. Although denoted instationary here to underline the difference to the stability derivatives computed in Step A, the method of incremental rotational velocities delivers quasi-steady derivatives rather than truly instationary derivatives (which nevertheless satisfies the requirements).

Step E applies elastic unity deflections of the structure on the CFD model to compute the influence of structural deformation on the aerodynamics. As in step C, one analysis is required for each considered deformation or deformation velocity mode. Comparison to the reference configuration delivers the aeroelastic influence matrices for the modally reduced structural model, i.e. the deformable body of the airframe, in dependence from the elastic coordinates. Generation of aeroelastic matrices is only possible for base functions which are selected for the SID input file, but may be limited to those deformation modes which are expected to have significant impact on the aerodynamics of the aircraft.

Step F accounts for the influence of ground effect. Several computations are carried out to examine the aircraft's sensitivity to ground effect for the given configuration and attitude and to determine interpolation points for an altitude dependent lift efficiency factor. Additional influence factors or effects can be added to this step.

6.2 Software Tools for Aeroelastic Preprocessing

When modelling an aircraft for a "multidisciplinary" multibody simulation, the basic structure (mainly bodies and connections) has to be set up in the MBS environment, usually using the MBS-GUI. Additional information from other disciplines are included when needed in the set-up process via MBS input files. These includes may either directly be output files of a specific CAx software application, e.g. a CAD generated IGES-file for graphical representation of a component, or have to be generated by MBS preprocessors which use output data of CAx software and process the information to MBS input data format, as described for elastic bodies in Sections 4.3 to 4.8.

The aeroelastic model data is not a decoupled, "stand-alone" solution as other CAx inputs but depends on the results of the FEA analysis, which is symbolised by the dashed arrow. The main quantities the aerodynamic analysis of the aircraft has to deliver are the rigid body derivatives of the aircraft attitudes, control inputs and manoeuvres (to account for the aircraft's overall motion), and the corresponding aerodynamic loads on the deformable structure (to be further processed to yield the aeroelastic matrices). Several strategies, and, associated with them, software tools and methods, may be used to deliver the required data. The criteria for a good solution are a set of general or operational demands (refer also to Section 3.1.3), and technical requirements. The most important are:

- Acceptance / commonness: The aerodynamic analysis has to be performed by an accepted and common software tool, preferable a CFD tool which is widely used in transport aircraft design processes. CFD models of the aircraft should be available as early as in the conceptual design phase and continuously refined in the course of the development process.

- **General precision:** The CFD analysis has to deliver reliable results for arbitrary high-lift configurations of transport aircraft, especially for low-speed aerodynamic derivatives and the surface pressure distribution.
- **Initial precision:** In addition to the precision which can be achieved in general, i.e. under consideration of underlying methodology, limitations of the tool employed and consecutive correction methods, the high-lift CFD analysis must possess a high degree of initial precision: it has to provide a reasonable accuracy without additional adjustments such as fine-tuning corrections with wind tunnel test data.
- **CFD-CSM interpolation:** The CFD modelling strategy must support a robust fluid-structure coupling for
CSM \leftrightarrow CFD: transformation of structural displacements (control surface deflections, deformations) onto the aerodynamic analysis model,
CFD \leftrightarrow CSM: transformation of aerodynamic forces and moments on the (modally condensed) structure.
- **Automated mesh adaptation:** Meshing of the aerodynamic model(s) must allow for (semi-)automated modifications to implement structural displacements on the CFD analysis.
- **Low computation times:** CFD-MBS preprocessing has to be performed within a reasonable timeframe. Performance target is to process a medium-sized model (including approximately 12 CFD analysis steps) in 12-16 hours to allow the preparation of an aerodynamic MBS input file in an overnight job.

6.2.1 Computational Structural Mechanics

For aeroelastic preprocessing for multibody simulation, any tool which generates the necessary data for deformable body representation (basically eigen- and staticmodes, see Chapter 4) in an auto-readable format can be used. An aeroelastic MBS preprocessing tool will nevertheless draw on the MBS input file for flexible bodies rather than on the underlying FEA output data: this source contains all necessary information⁴¹ and its format is “standardised”, i.e. independent from the FEA tool employed.

41. Besides the zero- and first-order modal matrices which are generated by the preprocessing routines of the MBS code, the MBS input file for flexible bodies contains in fact more information which can be used than the FEA output file from which it is generated; e.g. the nodes serving as reference points (markers) for MBS body representation, the user-decisions such as the selected eigen- and staticmodes which form the modal matrix and homogenising coordinate transformations.

Almost all standard FEA codes are able to effectively perform the required evaluations, e.g. static and normal mode analysis. Commercial MBS codes support a variety of FEA codes to generate the MBS input data for flexible body simulation, e.g. MSC.NASTRAN, ANSYS, I-DEAS, PERMAS, ABAQUS, MSC.MARC, all of which are supported by SIMPACK's preprocessor FEMBS. MSC.NASTRAN has nevertheless an almost ubiquitous distribution in aerospace industry, thus making it the primary tool for the targeted range of application.

6.2.2 Computational Fluid Dynamics

In CFD, the situation is less homogenous, and the selection of the appropriate tool for the aerodynamic analysis has more impact. As already indicated in the background information on CFD, a variety of methods and tools exist, each with its specific strengths and shortcomings, ranging from "quick-and-dirty" methods for first conceptual studies to high-precision approaches. Examples for CFD methods which may be applied in aeroelastic preprocessing are lifting line methods (LLM), lifting surface methods (LSM), surface panel methods (SPM) and Euler and Navier-Stokes methods.

It may be added that, besides the aerodynamic analysis itself, a critical part of efficient aeroelastic preprocessing is the coupling between the CSM and the CFD model. Instead of creating an own coupling routine, it might prove advantageous to fall back on other CSM-CFD interpolations from disciplines which also require fluid-structure interaction. Especially in aeroelasticity and aeroservoelasticity, quite similar objectives have to be met; in fact, a lot of effort is being spent to develop adequate fluid-structure interpolations. Using a CSM-CFD coupling which has already been set up for another design task, e.g. flutter analysis, could significantly facilitate the generation of an aeroelastic MBS input file. On the other hand, these methods raise a number of characteristics and limitations due to their specialised approaches, so we will concentrate on CFD methods to solve the aerodynamic problem and establish an adequate mCSM-CFD interpolation independently.

The rather elementary methods, LLM and most LSM approaches, are generally fast and robust to compute, analysis models are quickly set up and mCSM-CFD interpolation is usually good-natured, but there is only little confidence in the results - especially for a complex aircraft in high-lift configuration⁴² modelled from scratch, i.e. without measurement data to compare with. Sophisticated approaches like Euler and Navier-Stokes methods, on the other hand, lead to unacceptable computation times. Manipulation of the CFD model, as it is necessary to account for control surface deflection and structural deformation, is difficult to perform in a semi-automated fashion, and mCSM-CFD coupling is a demanding task.

So far, best overall results have been achieved with surface panel methods. SPMs are a common approach to investigate the low speed, high-lift regime of an aircraft's flight

42. Vortex lattice methods (VLM) are used for analysis and optimisation of high-lift systems, though, but 3D VLM models of the trimmed aircraft are hard to get hold of. As an example, Bombardier Aerospace uses a 2D VLM solver to optimise the alignment of high-lift devices before switching to an advanced code to analyse the full aircraft.

envelope. In fact, almost all manufacturers of transport aircraft use SPMs for analysis and optimisation of the high-lift aerodynamics of a new design. The models represent the actual geometric shape of the aircraft, contrary to LLM and most common LSM approaches.

With SPM being a standard tool for high-lift aerodynamics, adequate, currently updated models can be accessed in most design processes. The panels are located on the actual wetted surface of the aircraft, which considerably improves the significance of the data derived from geometrically modified analysis models. Although correction methods exist, e.g. compressibility corrections (Prandtl-Glauert, Karman-Tsien, Lieblein-Stockman, etc.), SPMs loose precision in the transonic regime.

Fluid-structure coupling is demanding but still straightforward. Adequate interpolation methods such as the stiff section approach, [88], have been developed and are available in interpolation libraries, e.g. COCOLIB / MpCCI. The handling is supported by the fact that potential flow methods do not require airflow meshing or mesh-adaption as Euler or Navier-Stokes codes do (the wake is usually attached to discrete grid points and automatically rearranged).

Adaptions of the aircraft surface mesh to structural unity displacements are feasible, but not recommended: SPM codes are sensitive to model inconsistencies like gaps, holes, warped panels, etc. Alternative methods exist to simulate the effects of a translational or rotational displacement of a surface panel or triangle without actually changing the geometry of the body mesh, e.g. modification of the local normal vector of the element or the local freestream velocity vector.

Surface panel codes still run on desktop computers. The computation time of a full aircraft model of average complexity is approximately 30-90 minutes on a high-end desktop, which still is acceptable: a batch job to set-up an aeroelastic MBS input file could be completed overnight.

With reasonable precision for high-lift models on one side and acceptable computational effort on the other, SPM tools represent the best compromise for the average application. Examples for adequate software tools which are used in the aeronautical industry for aerodynamic research and development in the low-speed regime are PAN AIR, [89], at Boeing, HISSS, [90], at EADS Military Aircraft or VSAERO, [91], at Airbus Deutschland. A less expensive alternative for MATLAB-users is to use the implemented vortex lattice method TORNADO.

6.3 Coupling of CFD Model and Modally Reduced CSM Model

The underlying purpose of the aeroelastic fluid-structure coupling is to provide a numerical transformation of physical values between the primarily self-contained domains of structural and aerodynamic analysis. The aerodynamic surface panel model discretises the wetted surface of the aircraft into a grid of panels, whereas the modally reduced structural model consists of a selection of user-defined nodes which are chosen from the FEA model nodes and in most cases belong to a primary part of

the load-bearing structure. The respective grids which are generated by these discretisations differ significantly. In most applications, the grids will not have a surface-surface intersection, i.e. there is no contact between or overlapping of the CFD and mCSM grid.

Coupling of the aerodynamic model and the modally reduced structural model consists of two main tasks:

- a non-conservative interpolation of the spatial coordinates of the (possibly deformed) mCSM model, or its first derivatives in respect to time, onto the CFD surface mesh of the aircraft, and
- a conservative interpolation of CFD surface element pressures, forces or aerodynamic derivatives onto the grid points of the mCSM model, respectively the corresponding marker elements of the deformable MBS body in question.

Figure 6.2 shows a non-conservative interpolation of a uni-directional value (left) and of a rotation (right) of source points s_i onto the target point t_k .

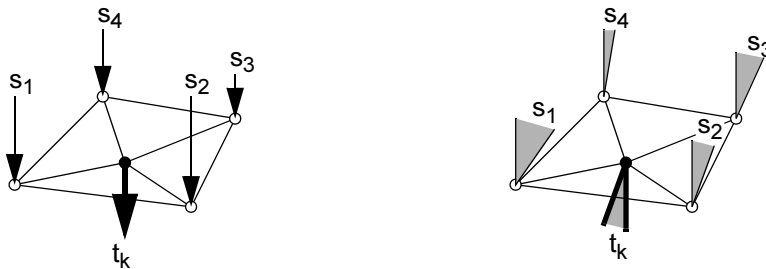


Figure 6.2 Interpolation of Four Source Points s_i to a Target Point t_k (Non-Conservative)

The source values (displacements, velocities) at structure nodes (mCSM grid points) have to be interpolated for each target point. Depending on the subsequent analysis algorithm, the targets can be either grid points of the CFD surface mesh (e.g. SPM panel corner points or panel control points). Vectors are usually interpolated component-wise.

A common circumstance of aeroelastic preprocessing is that a multitude of target points have to be served by few source points. As an example, a section of the modally reduced structural model, e.g. a wing, often consists of only a handful of grid points located on or close to the elastic axis, which have to be mapped onto the detailed CFD surface discretisation, Figure 6.3.

The range of possible source points is determined by the nodes of the FEA model which are selected for the SID input file in FEA-MBS preprocessing. Their number can be further reduced by partitioning, i.e. establishing a correlation between an assortment of source elements and the target elements these have to be mapped on, and by suppressing sampling points which provide little or erratic information about the deformation of the airframe contour, e.g. landing gear or engine attachment points.

For a slender, straight wing or a stretched fuselage, this leads to a quasi-1D-3D-coupling problem. Suitable interpolation methods are coupling via rigid interconnexions,

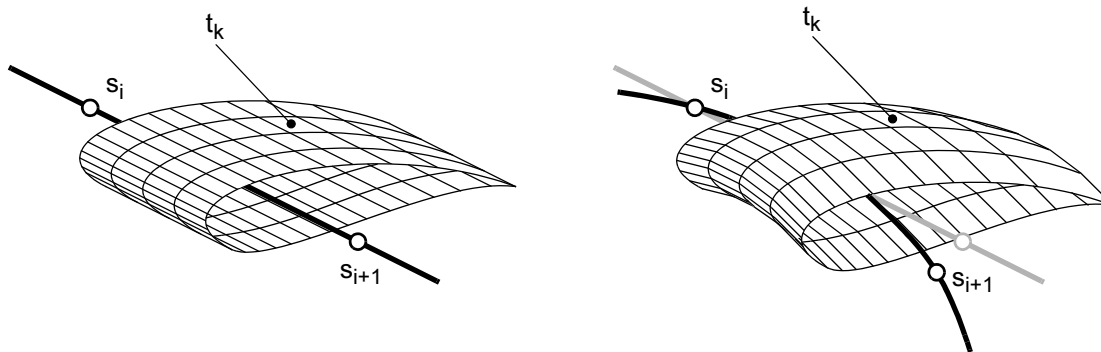


Figure 6.3 Illustration of Mapping of Modal Deformation onto a Detailed Aerodynamic Grid With Source Points s_i and Surface Element Reference Points as Target Points t_k

respectively the related approach of stiff cross sections, and coupling with finite interpolation elements. Both approaches allow bi-directional interpolation, i.e. the non-conservative structure-fluid coupling and the conservative fluid-structure coupling.

6.3.1 Coupling With Rigid Connexions

The elements of the aerodynamic surface mesh, and their related aerodynamic grid points, do not belong to the structural model, but they represent a part of the actual airframe structure. The grid points assigned to the elements, i.e. element corner points or surface element reference points, do not only define the shape of the aerodynamic grid (element corner points) and the local boundary conditions to the airflow (reference points), but are additionally the application points of the aerodynamic loads. Connecting the aerodynamic grid points with the nodes of the structural model by rigid elements (constraints) delivers a combined model which transfers structural deformations onto the aerodynamic surface grid and, in return, applies airloads onto the discretised aircraft structure.

The classical approach is to perpendicularly extend massless, undeformable arms (rigid connexions) from the linear spline connecting the source values of the structural model. Interpolation base functions may be global (for the entire model or the specific partition), e.g. beam spline interpolation, or local, e.g. cubic spline interpolation. This approach is not only straightforward from the theoretical point of view, but in most cases also represents the internal load-bearing rib-spar-structure of the wing of medium-to-high aspect ratio wings.⁴³ The disadvantage is that in general each element has to be evaluated separately. For wings with moderate sweep, however, it can be more efficient to use a variant of this method, the approach of rigid chord sections. Aerodynamic grids of quadrangular elements, e.g. for surface panel methods, often align the longitudinal edges of the element with the freestream direction. This results in a mesh where a row of elements form a chordwise section of the wing. Assuming rigid chord sections has two computational advantages which speed up the MBS aeroelastic preprocessing significantly: modifications of the CFD grid due to structural

43. This remark is given in respect to large transport aircraft. The construction of other aircraft categories, for example delta-wing fighter aircraft, may differ significantly.

deformations can be applied uniformly to all panel elements of the section, and most CFD codes deliver sectional summaries of forces and moments, respectively the sectional derivatives, which can be directly mapped onto the structural model. Both methods are illustrated in Figure 6.4. A closer look at one of the most common interpolation approaches, the cubic spline, may underline the differences.

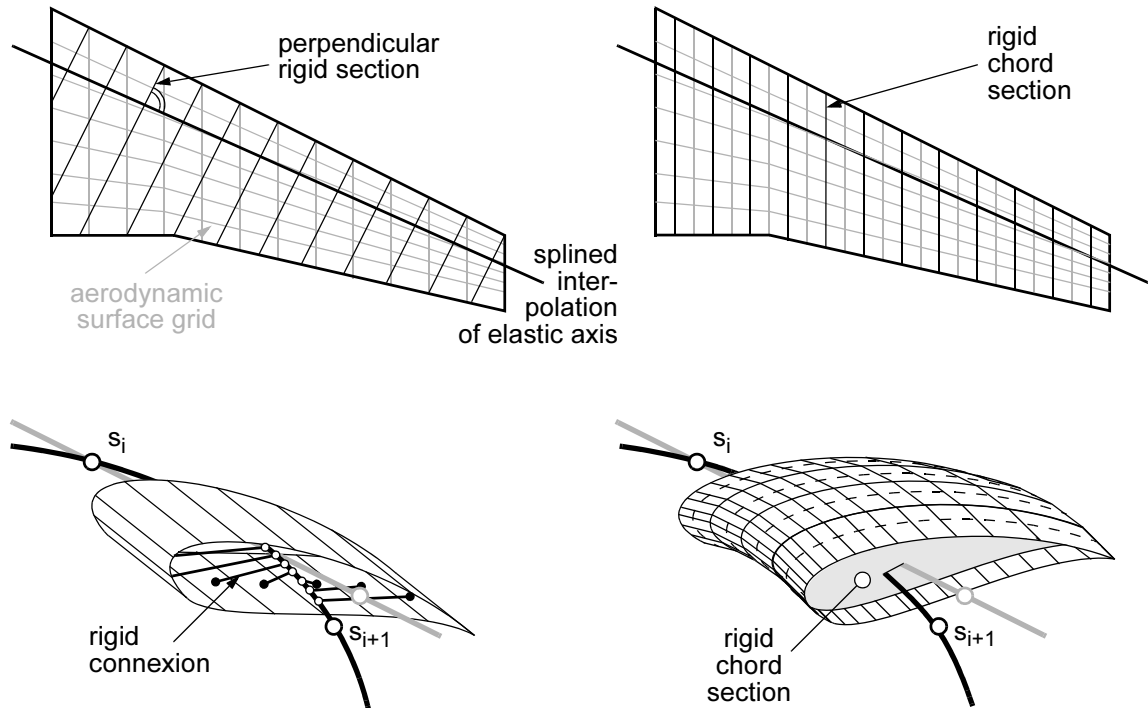


Figure 6.4 Approach of Rigid Connexions (left) and Approach of Rigid Chord Sections (right)

6.3.2 Cubic Spline Interpolation

A cubic spline is a three-dimensional curve $\mathbf{p}(s)$ constructed of m piecewise third-order polynomials $\mathbf{p}_j(s)$ which pass through a set of control points (structural nodes) $N_j, N_{j+1}, j \in [1, 2, \dots, m + 1]$. The second derivative of each polynomial is commonly set to zero at the endpoints, since this provides a boundary condition that completes the system of equations, leading to a simple tridiagonal system which can be solved easily to give the coefficients of the polynomials.

If the position vector at a curve point at the location $s = s_0$ of $\mathbf{p}(s)$ is given in cartesian coordinates,

$$\mathbf{p}(s) = \begin{bmatrix} p_x(s) \\ p_y(s) \\ p_z(s) \end{bmatrix}, \quad (86)$$

the normal plane of $\mathbf{p}(s)$ at s_0 is given by

$$(\mathbf{r}_P - \mathbf{p}(s_0)) \frac{d\mathbf{p}(s_0)}{ds} = 0. \quad (87)$$

To calculate the base point on $\mathbf{p}(s)$ for a rigid connexion to an aerodynamic grid point P with the position vector \mathbf{r}_P , Eq. (87) has to be solved for s_0 . The roots of the resulting polynomial of degree 5 can be found by iteration approaches, e.g. Newton- or Laguerre-methods. Theoretically, each aerodynamic grid point may have up to 5m normals on \mathbf{p} . Although the number of calculations can be restrained by neighbourhood search algorithms or other approaches, it still takes some computational effort to establish a coupling between detailed models. Strategies to select a physically reasonable connexion in a multiple assignment situation as well as to attach grid points located in blind spots, i.e. zones from which no perpendicular connexion to the spline is possible, have to be added to receive a precise, robust interpolation.

Assuming rigid chord sections simplifies the task: assignment of grid points to a rigid section is definite, and attachment of cross sections to the structural spline is straightforward. For interpolation of fuselage sections (where stiff cross sections are considered rather than chord sections) and unswept wings, the method leads to similar results. Whether it can be applied for swept wings depends on a multitude of factors; among them: configuration and construction of the actual aircraft, modelling and meshing strategies of the virtual model, and precision requirements of the application.

6.3.3 Finite Interpolation Elements

Interpolation elements are local (piecewise) elements defined by a simple shape function in a local coordinate system which are mapped onto the structure given in the global Cartesian coordinate system. In FEA, they are commonly used to couple the mechanical degrees of freedom of incompatible structural discretisations or to transmit forces and moments from a reference point to several averaged points. But finite interpolation elements may also be used for conservative and non-conservative interpolation between source and target points. One advantage of this method is that it does not introduce additional geometric constraints or stiffnesses to the model, as rigid connexions do. For interpolation of a beam-like partition of the structural model, one-dimensional linear or quadratic interpolation elements may be used. Especially the approach of linear interpolation elements, [92], offers a straightforward, robust algorithm which can be performed (semi-)automatically with only minimal user input. Beckert, [88], demonstrated efficiency and precision of one-dimensional interpolation elements for conservative interpolation in cases which bear close resemblance to the characteristics of a CFD-mCSM coupling.

In general, a local coordinate system is defined for a unidirectional element which is aligned with the element main axis, using the free coordinate r . The polynomial expansion for a global (structural) coordinate x may be written as

$$x = a_0 + a_1 r + a_2 r^2 + a_3 r^3 + \dots \quad (88)$$

For unidirectional (one-dimensional) linear ($d=2$) or quadratic ($d=3$) interpolation elements, it may nevertheless be advantageous to define r over the range of $-1 \leq r \leq 1$. The shape functions h_i , $i \in [1, 2, \dots, d]$, then couple the local free coordinate r of an interpolation element to the global (structural) coordinates x_i of the nodes N_i , yielding the global coordinate x as

$$x = \sum_{i=1}^d h_i(r)x_i. \quad (89)$$

The shape functions h_i have the unit value 1 at x_i and the value 0 at the other node(s), as shown for the quadratic variation in Figure 6.5.

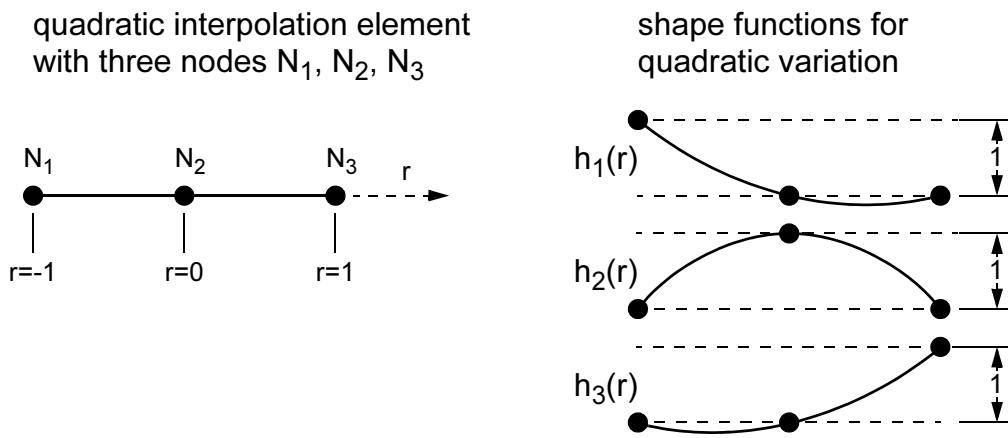


Figure 6.5 Unidirectional Interpolation Element (Origin of Local Coordinate System at Centre Node) for Quadratic Variation

Table 6.1 gives the shape functions and their partial derivatives in respect to the local coordinate r .

Conservative interpolation of a force F_r acting at point r is easily obtained by

$$F_i = h_i F_r \quad (90)$$

for the assigned coupling nodes N_i . Converting a torque moment M_r into equivalent nodal forces F_{Mi} uses the gradient of the local coordinate at point r , writing

$$F_{Mi} = \frac{\partial h_i}{\partial r} M_r. \quad (91)$$

For non-conservative interpolation, for example of coordinates or elastokinematic properties like displacements, a source value x , is interpolated according to Eq. (89).

Unidirectional linear or quadratic interpolation has proved to be an efficient interpolation method for CFD - mCSM coupling. It is nevertheless possible to use higher-order approaches. For higher-order unidirectional interpolation using n -order variation, Lagrange or Hermite polynomials may be used, [92], and n -dimensional interpolation approaches can be found in [93].

	linear interpolation element		quadratic interpolation element	
	shape function	partial derivative	shape function	partial derivative
Node 1 (i=1)	$h_1 = \frac{1}{2}(1-r)$	$\frac{\partial h_1}{\partial r} = -\frac{1}{2}$	$h_1 = \frac{1}{2}(1-r) - \frac{1}{2}(1-r^2)$	$\frac{\partial h_1}{\partial r} = -\frac{1}{2} + r$
Node 2 (i=2)	$h_2 = \frac{1}{2}(1+r)$	$\frac{\partial h_2}{\partial r} = \frac{1}{2}$	$h_2 = 1-r^2$	$\frac{\partial h_2}{\partial r} = -2r$
Node 3 (i=3)	n/a	n/a	$h_3 = \frac{1}{2}(1+r) - \frac{1}{2}(1-r^2)$	$\frac{\partial h_3}{\partial r} = \frac{1}{2} + r$

Table 6.1 Shape Functions and Respective Partial Derivatives of Unidirectional Interpolation Elements

6.3.4 Scattered Data Interpolation

The findings of Beckert reveal, however, that for applying structural deformations on an aerodynamic grid, better results are obtained for scattered data interpolation methods, using compactly supported radial functions such as the Gaussian function, [94], Euclid’s Hat, [95], or Wu’s function, [96]. As already indicated by the name, radial functions are given in respect to the Euclidian distance between interpolation point and source point. As an example for compactly supported radial functions, the normalised Euclid’s Hat (for the two-dimensional case) and the Gaussian function are depicted in Figure 6.6.

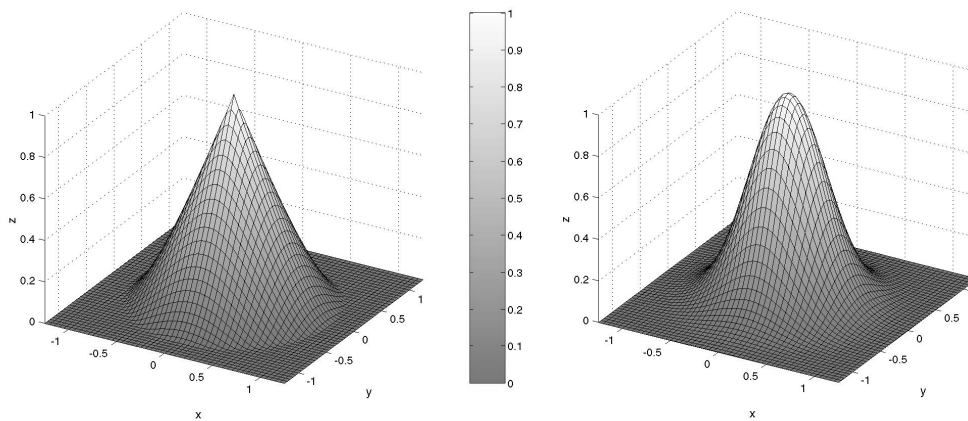


Figure 6.6 Normalised Euclid’s Hat (left) and Gaussian Function (right) as Examples for Compactly Supported Radial Functions

6.3.5 Automated CFD - mCSM Interpolation

The relatively simple composition of modally reduced CSM meshes mapped onto comparatively detailed CFD meshes proves to be good-natured in respect to automated execution of this interpolation. Several aspects, however, remain which may be critical for a reasonable solution:

- The algorithm for perpendicular projection onto interpolation elements, as it is necessary for the approach of rigid connexions, has to ensure that all target points (CFD grid points) are connected. If multiple projections are possible, selection is easy and unambiguous by establishing the shortest possible connexion. More problems arise when no orthogonal projection is possible, e.g. for grid points in blind spots or at the tips of wings and stabilisers, Figure 6.7. A robust solution which is often applied is to directly attach the target point to the closest source point instead of perpendicular connexion to an interpolation element, but special features of the application might demand other approaches, [97].

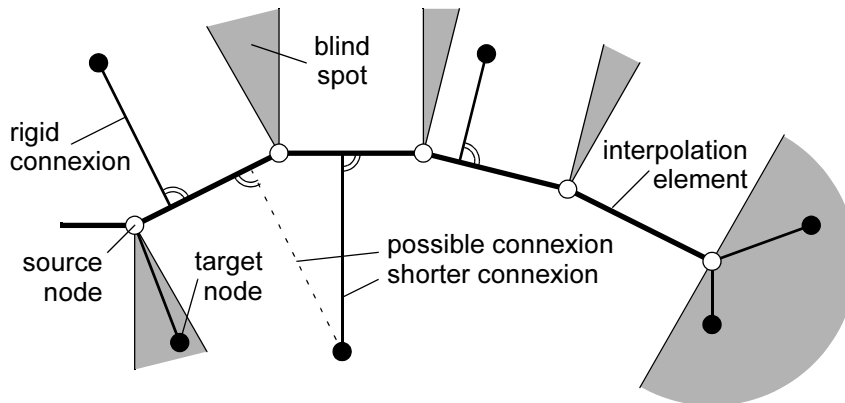


Figure 6.7 Example of Coupling With Perpendicular Rigid Connexions

- The modally reduced structural model should be divided into parts which can be assigned to corresponding components of the aerodynamic model to enforce a physically correct coupling between mCSM nodes and CFD grid points. This assignment ensures that, for example, a CFD grid point of the horizontal stabiliser can only be connected with a node of the horizontal tail structure, although a node of the vertical tail happens to be located nearer to the CFD grid point. For most tasks performed so far, a convenient separation was to assign nodes of the mCSM model to patches of the CFD model. Patches are usually a good choice because
 - most CFD models for modal preprocessing are subdivided in patches, whereas other subdivisions such as bodies or components may not exist in many models;
 - patching is usually performed under consideration of the natural components of an aircraft, which accommodates user input and improves clarity of the modelling;
 - additional patches are defined at critical locations such as intersections to improve convergence and precision of the CFD solution, so these areas which are also sensitive in respect of automated interpolation can be treated separately and in detail by the user in the pre-assignment process.

The principle of pre-assignment is shown in Figure 6.8 on the example of a sketched fuselage-wing intersection.

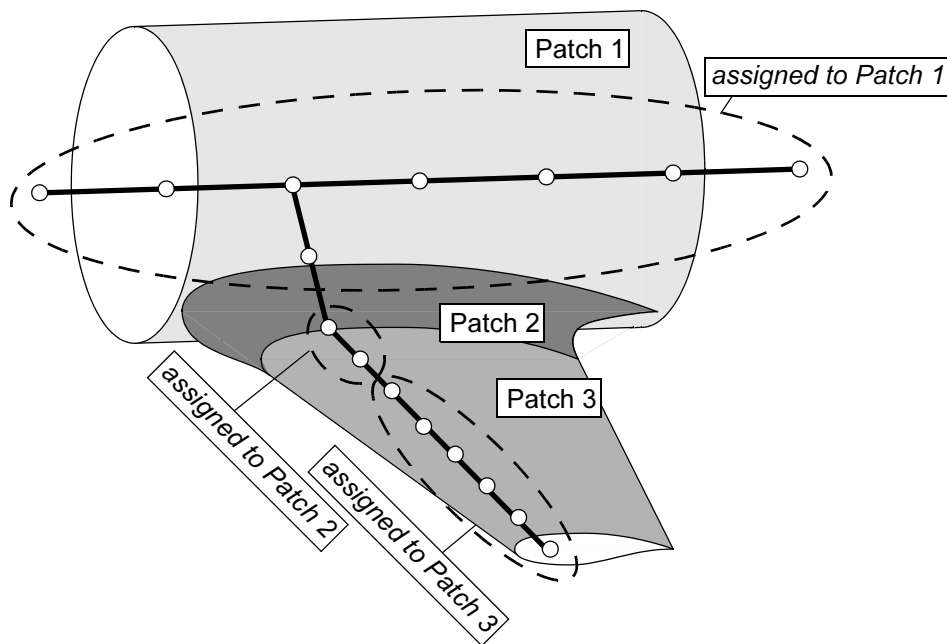


Figure 6.8 Pre-assignment Between Interpolation Points Using Patches of the CFD Model

- Besides pre-assignment, the user must have the possibility to exclude selected points or nodes from the interpolation points for the CFD-to-mCSM coupling, as nodes of the mCSM model may have been selected as reference nodes of the modally reduced structural model because of various reasons:
 - to serve as an application point for a load or as a connexion point of a joint in the MBS model;
 - to support the graphical representation of the deformable body in the simulation;
 - to be connected to a sensor in the multibody analysis.

The last two types of reference nodes are not necessarily located on or within the load-bearing primary structure of the aircraft. It may be necessary to consider these nodes for mapping geometric parameters such as modal deformations or deformation velocities onto the CFD mesh (mCSM-to-CFD coupling), but it could cause unrealistic deformations of the airframe in the dynamic analysis if aerodynamic loads were applied on these nodes. In case a node lacks a sufficiently stiff connexion to the primary structure, or other reasons require that this node should not be exposed to airloads, it has to be excluded from interpolation.

- Although interpolation routines like those described above are well-documented, e.g. in the literature quoted as references, and their basic implementation is rather simple and straightforward or routines may even be downloaded from various math libraries, it may be added that a lot of additional work is required to adjust the algorithm and its implementation, and to cover particularities, special cases and other oddities. It is therefore recommended to use the special interpolation libraries and tools which are provided by packages like MpCCI / COCOLIB. Additionally, it has proven to be advantageous to crosscheck the quality of the interpolation, e.g. by a comparison between different interpolation methods.

7 Applications

7.1 Reference Aircraft Models

7.1.1 Reference Model 1: Aerobatic Glider

Reference model 1 was generated in an exemplary multidisciplinary approach, as indicated by Figure 7.1. The model was set up basing on design and certification data of the Mü 28, designed and built by Akaflieg München, but it should be noted that the model has not been adjusted or calibrated to represent the actual aircraft. Evaluation of the reference scenarios was performed by multibody simulation using the MBS-tool SIMPACK. Elastic properties of the airframe originate from an FEA beam model for MSC.NASTRAN which was set up using data from the Mü 28 mass distribution table, design loads and stress analysis of the certification documentation and the design document of the fuselage, [98]. The CFD mesh was generated by processing a CAD model of the aircraft, which was set up in Pro-ENGINEER from Mü 28 drawings and airfoil data, [99].

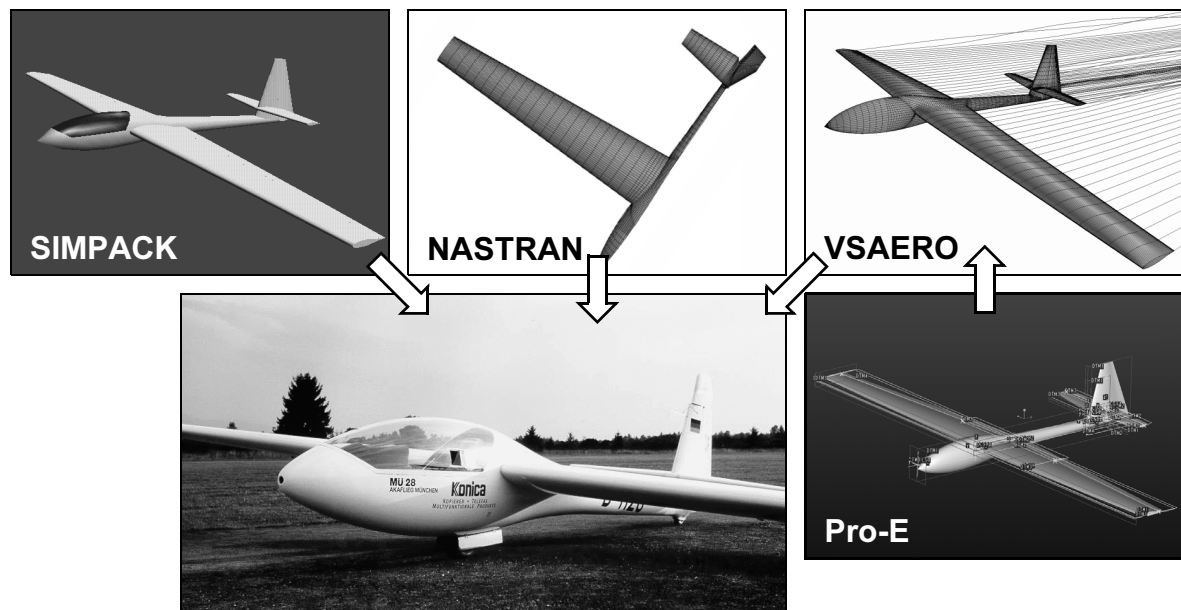


Figure 7.1 Set-Up of Reference Model 1 Basing on Data of Mü 28 (Akaflieg München)

Control inputs for the reference scenarios base on flight test data of the Mü 28, Figure 7.2, but have been smoothed and slightly reworked to deliver the desired manoeuvres.⁴⁴

44. Although the model set-up has not been adjusted or calibrated, the initial performance of the control input functions for the SIMPACK model from flight test data was astonishingly good, e.g. an aileron roll could be performed from scratch, resulting only in a roll overshoot of approx. 20°.

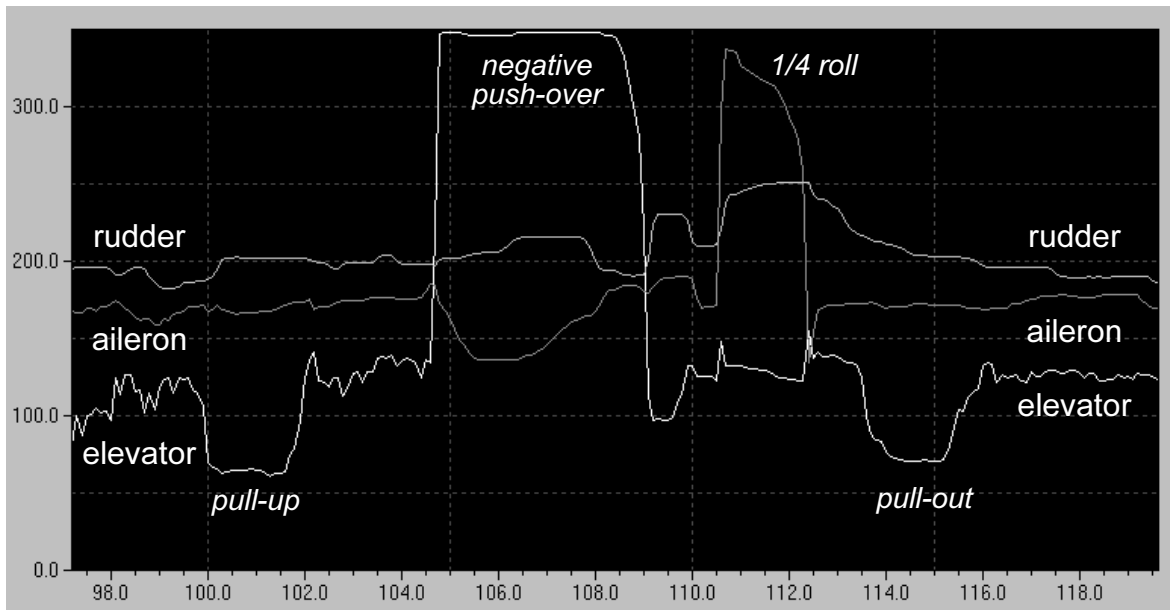


Figure 7.2 Control Inputs for an Aerobatic Manoeuvre (Humpty-Bump with $1/4$ -Vertical Roll)

7.1.2 Reference Scenarios and Simulation Models

Selected Reference Scenarios

Two aerobatic manoeuvres serve as reference scenarios for the performance evaluation (see also Table 7.1):

- Scenario 1 is a barrel roll, which is a combination between a loop and a roll. The flight path during a barrel roll has the shape of a horizontal helix, see Figure 7.3.
- Scenario 2 is a sequence of a $3/4$ -loop with a $1/4$ -vertical roll and subsequent pull-out to level flight.

Reference Model 1: Aerobatic Glider			
Scenario	Manoeuvre	Duration	Steps
1	barrel roll	10 sec.	241
2	$3/4$ -loop with $1/4$ -roll in vertical dive and pull-out	16 sec.	301

Table 7.1 Reference Scenarios for Computational Performance Evaluation

Simulation Models

Simulation models either possess aerodynamic force elements (FEL type) or modal aerodynamics (MA type). They can be rigid, account for the three most important deformation modes, i.e. first symmetric wing bending and first symmetric and anti-metric wing torsion, or contain the first 20 eigenmodes of the structural model. To give an impression of the influence of the number of aerodynamic force elements on the

performance, FEL2-models have twice, and FEL5-models five times the number of force elements of the FEL-models, Table 7.2.

Reference Model 1: Aerobatic Glider				
Model Name	Elastic Properties			Aerodynamic Force Elements
	Marker Nodes	Modes	Frequency	
FEL-rigid	48	-	-	37
FEL-03M	48	3	4.7 - 13.4 Hz	37
FEL-20M	48	20	4.7 - 41.4 Hz	37
FEL2-rigid	48	-	-	74
FEL2-03M	48	3	4.7 - 13.4 Hz	74
FEL2-20M	48	20	4.7 - 41.4 Hz	74
FEL5-rigid	48	-	-	185
FEL5-03M	48	3	4.7 - 13.4 Hz	185
FEL5-20M	48	20	4.7 - 41.4 Hz	185
MA-03M	48	3	4.7 - 13.4 Hz	1
MA-20M	48	20	4.7 - 41.4 Hz	1

Table 7.2 Variations of the Reference Aircraft Model 2

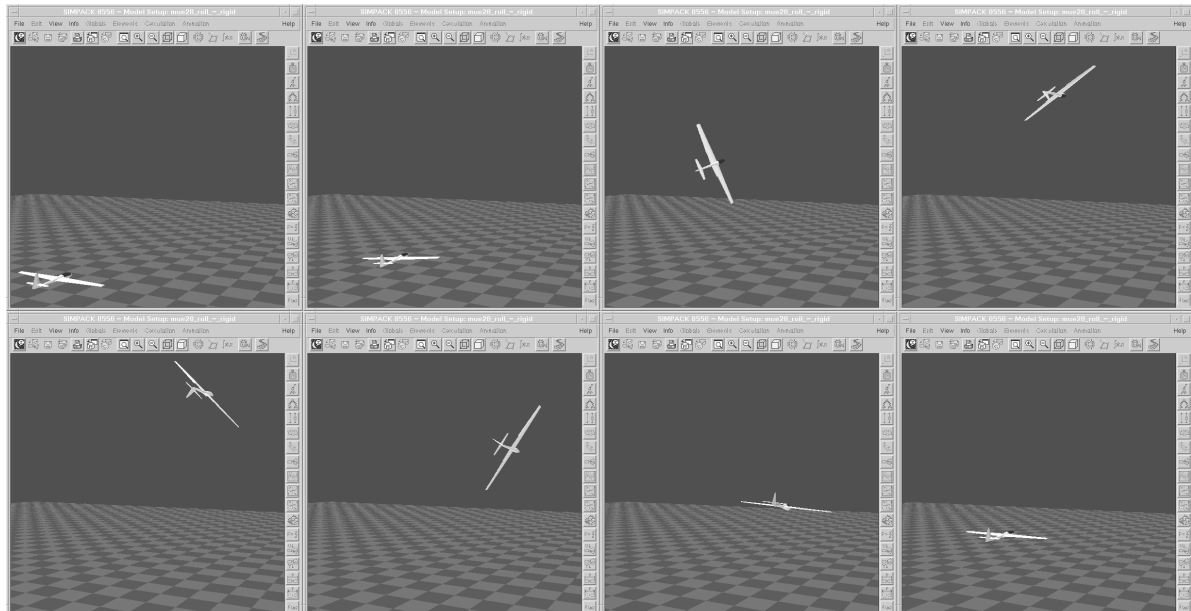


Figure 7.3 Reference Scenario 1: Aerobatic Manoeuvre "Barrel Roll"

7.1.3 Reference Model 2: Large Transport Aircraft

Large transport aircraft are among those types which are affected most by resonance phenomena and vibrational problems. Accordingly, a reference aircraft has been modelled to serve as a generic model. It is a wide-bodied, four engine long-haul transport in the 300 seats class which loosely bases on the design and lay-out of the Airbus A340-300. Like this aircraft, it possesses a conventional tricycle landing gear with additional centre landing gear. The main landing gear is a four-wheel bogey configuration. The aircraft has an overall length of 63.6 m and a span of 60.6 m. With a total landing weight of 190.0 metric tonnes, touch-down speed according to certifications (FAR 25, [52]) is 70 m/s , with a maximum descent velocity of 3.048 m/s (10 ft/s).

The SIMPACK model consists of the flexible airframe, condensed from an FEA shell model, and the landing gear legs as rigid MBS substructures, Figure 7.4. The modally reduced MSC.NASTRAN model is composed of 11 selected eigenmodes and has 534 elastic degrees of freedom. The aerodynamic data derives from a VSAERO test case model and has been significantly modified to represent A340-alike high-lift aerodynamics. Basic modelling data can be found in Table 7.3. The graphical representation derives from a Pro-ENGINEER model, but no CAD data has been used for modelling purposes.

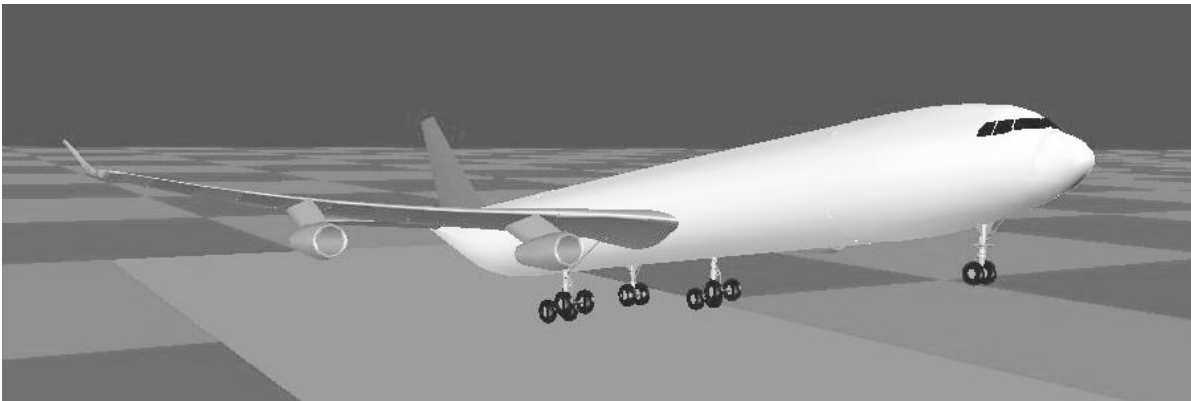


Figure 7.4 SIMPACK Model of Reference Aircraft 2

7.1.4 Reference Scenarios and Simulation Models

The reference simulations have been selected with the idea to cover representative examples from a wide range of possible touch-down scenarios. Two of them are certification cases from FAR 25, the third is a wing-low landing to seize the current trend to additionally analyse realistic, asymmetric landing sequences, and the last simulates a landing in which lift dumping devices (spoilers) are deployed after touch-down.

The first three scenarios, A to C, were simulated with three model variants: the classic approach of a rigid aircraft touching down at zero or reduced gravity (FAR 25.473 c(3)), the more advanced scaled gravity vector model with elastic airframe (FAR 25.473 c(4)), and a model with an elastic airframe exposed to aerody-

dynamic and aeroelastic effects. Scenario A was additionally simulated with aerodynamics, but rigid airframe. Reference scenario D, on the other hand, is only meaningful with elastic airframe modelling and realistic aerodynamics, so no simulation with zero / reduced gravity was performed.

Scenario A: Tail-Down Landing

The sequence modelled in scenario A is a tail-down landing according to FAR 25.481 at a high angle of attack of $\alpha = 11.5^\circ$. The airspeed is 70 m/s and the aircraft descends at the maximum design rate of 3.048 m/s . For the cases which actually model the aerodynamic and aeroelastic effects, the aircraft approaches in steady, trimmed flight. In accordance to FAR, derotation of the aircraft is not controlled in any of the cases, which leads to a heavy impact of the nose gear.

Scenario B: Level Landing (Three-Point Touch-Down)

The scenario bases on FAR 25.479, part c(2), where main landing gear and nose landing gear tyres touch the runway at the same instant. The landing is also performed at the maximum descent velocity of 3.048 m/s . This case is a theoretical scenario and almost impossible to realise in a test flight: at the specified approach speed, no stable level flight can be maintained in the required nose-down attitude. Flying this manoeuvre would mean to derotate the aircraft to -2.5° immediately before touch-down, stop the derotation and have the aircraft impacting the runway at the specified descent velocity. Simulation of this sequence is easier to perform (and less dangerous), but for models with applied aerodynamics, it can also only be achieved in a dynamic setting similar to that described for flight tests.

Scenario C: Landing With Bank Angle (Wing-Low Landing)

An asymmetric landing case is added which simulates a hard landing with a low wing, for example to compensate for sidewind. Touch-down is at a bank angle of 5.73° in tail-down configuration at a sinking speed of 2.85 m/s .

Scenario D: Lift Dumper Deployment

The last scenario simulates a firm tail-down landing at 2.7 m/s , where lift dumping devices (here: ground spoilers) are deployed in the moment of rebound, approximately 1.2 seconds after initial contact. The evaluation compares dynamics and loads of this case with a landing at similar conditions, but without spoiler deployment.

Scenarios C and D are not documented sequences like the certification cases A and B, but shall serve as examples that in modern aircraft design, additional scenarios have to be considered to generate a safe, reliable, competitive and high-performing lay-out of both, airframe and landing gear. Asymmetric cases as in scenario C are already state-of-the-art with aircraft and landing gear manufacturers, but the author is not aware of more than sporadic simulations which include realistic aerodynamics.

Simulation Models

Simulations with aerodynamics were performed with both methods, force elements and modal aerodynamics. Table 7.3 outlines the basic modelling data of the two models. As simulation results on aircraft behaviour, performance and loads show only marginal, if any, difference, no differentiation has been made in Section 7.2. Comparison, however, is necessary when it comes to computational performance of the respective methods; this evaluation can be found in Section 7.3.

Reference Model 2	Elastic Properties			Aerodynamic Force Elements
	Marker Nodes	Modes	Frequency	
Aerodynamic Modelling	90	11	1.09 - 9.51 Hz	48
Force Elements	90	11	1.09 - 9.51 Hz	1
Modal Aerodynamics	90	11	1.09 - 9.51 Hz	1

Table 7.3 Modelling Data of Reference Model 1

Names and characteristics of the model variants used in the reference simulations are listed in Table 7.4. In the model names, the first letter stands for the scenario, subsequent letters denote the type of airframe modelling (R - rigid, E - elastic) and the method of lift modelling (G - gravity vector scaling, A - modal aerodynamics), respectively if the landing is performed with lift dumpers (LD) or without (WO).

Model Name	Description of Landing Case	Structure Model	Aerodyn. Model	Descent Velocity	Angle of Attack	Bank Angle
A-RG	Tail-down landing	rigid	grav.vector	-3.05 m/s	11.5°	0°
A-EG	Tail-down landing	flexible	grav.vector	-3.05 m/s	11.5°	0°
A-RA	Tail-down landing	rigid	aerodyn.	-3.05 m/s	11.5°	0°
A-EA	Tail-down landing	flexible	aerodyn.	-3.05 m/s	11.5°	0°
B-RG	Level landing	rigid	grav.vector	-3.05 m/s	-2.4°	0°
B-EG	Level landing	flexible	grav.vector	-3.05 m/s	-2.4°	0°
B-EA	Level landing	flexible	aerodyn.	-3.05 m/s	-2.4°	0°
C-RG	Low-wing landing	rigid	grav.vector	-2.85 m/s	11.5°	5.7°
C-EG	Low-wing landing	flexible	grav.vector	-2.85 m/s	11.5°	5.7°
C-EA	Low-wing landing	flexible	aerodyn.	-2.85 m/s	11.5°	5.7°
D-WO	Landing w/o spoilers	flexible	aerodyn.	-2.70 m/s	11.5°	0°

Table 7.4 Reference Model Variants of Landing Simulations

Model Name	Description of Landing Case	Structure Model	Aerodyn. Model	Descent Velocity	Angle of Attack	Bank Angle
D-LD	Landing with spoilers	flexible	aerodyn.	-2.70 m/s	11.5°	0°

Table 7.4 Reference Model Variants of Landing Simulations

7.2 Aerodynamics in Aircraft Ground Dynamics Simulation

In Section 3.1, shortcomings of the conventional approach and the importance to include aerodynamic and aeroelastic effects in ground dynamic analysis have been addressed. But what is the actual impact of aerodynamics on the dynamical behaviour of a flexible aircraft? A closer look at the simulation of a large transport aircraft touching down in the four reference scenarios shall give some answers to this question.

7.2.1 Dynamic Behaviour of the Aircraft

Simulation of the reference scenarios reveals that the dynamic behaviour of the aircraft at a landing, i.e. touch-down, derotation and landing run, depends strongly on the prevailing aerodynamic forces: for all scenarios, aerodynamics prove to have far more impact on the actual behaviour and performance of the aircraft than the elastic response of the airframe. For illustration, Figure 7.5 shows plots of the vertical position and descent velocity of the reference frame in scenario A. A significant difference exists between the models with gravity vector scaling and those with modal aerodynamics, but rather similar results are obtained for rigid and elastic airframe modelling.

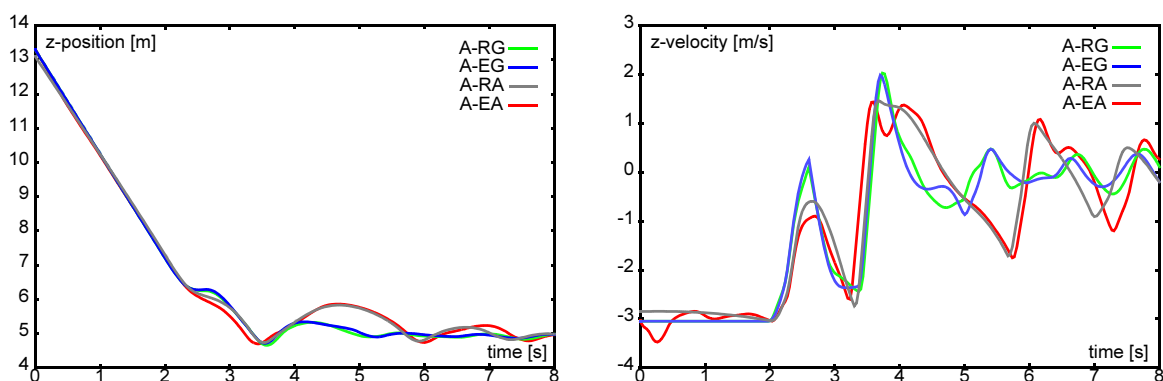


Figure 7.5 Scenario A: Vertical Position (left) and Descent Velocity (right) of Aircraft Reference Frame Over Time

In the certification scenarios A and B as well as in the asymmetric scenario C, the presence of realistically simulated aerodynamic effects, the touch-down impact resulted in a slower but more violent response of the aircraft, Figures 7.6 - 7.8.⁴⁵ Looking on the impact of aerodynamic effects by comparing the cases with elastic air-

45. Scenario D cannot be simulated at all without a model for realistic aerodynamic conditions.

frame representation, the acceleration caused by the initial landing impact is slightly lower for the model with aerodynamic effects than for the model using conventional gravity vector scaling in scenario A and C. Main cause is the aerodynamic damping, caused by the downwards motion of the flexing wings.

In scenario B, the realistic representation of aerodynamic forces raises a problem: at the attitude defined by FAR 25.479, the aircraft is subject to “negative lift”, i.e. the aerodynamic forces push the aircraft towards the ground. With increasing descent velocity, the resulting angle of attack is increased and the negative lift almost disappears, but we are still far from the assumed “lift equals weight”-condition of FAR 25.479. With the aircraft rapidly increasing its descent rate, it is difficult to adequately model the scenario: setting up the model to have the required rate of descent at the very moment of initial ground contact of a tyre, the aircraft still increases its vertical velocity

until tyre and oleo are sufficiently compressed to build up a strong counterpoise. Thus, the amount of energy which has to be dissipated at touch-down is significantly higher.

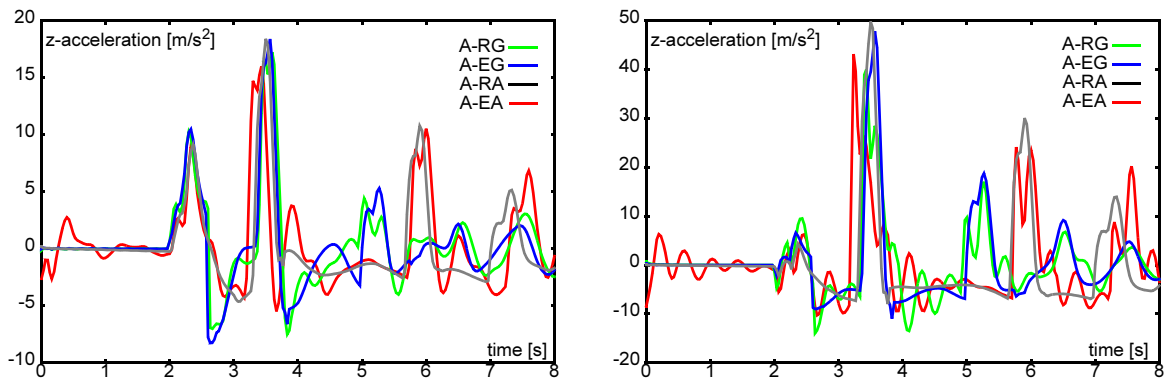


Figure 7.6 Scenario A: Vertical Acceleration of Aircraft Reference Point (left) and of Cockpit (right) Over Time

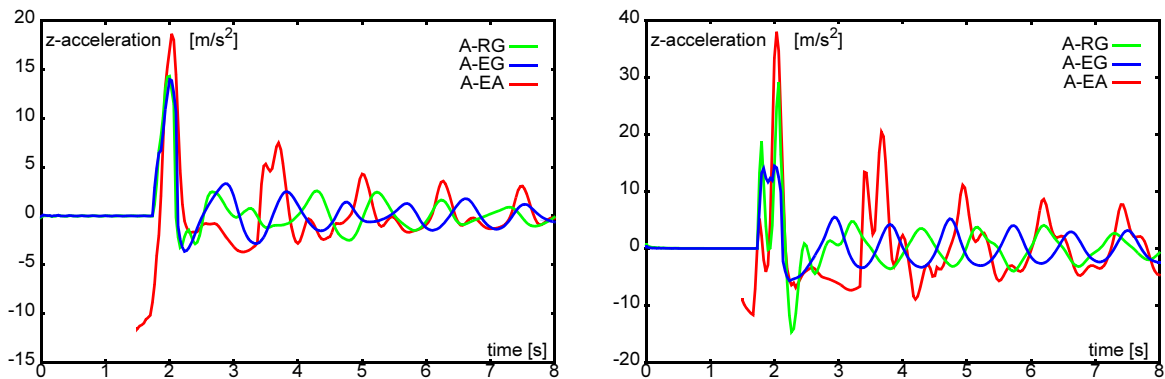


Figure 7.7 Scenario B: Vertical Acceleration of Aircraft Reference Point (left) and of Cockpit (right) Over Time

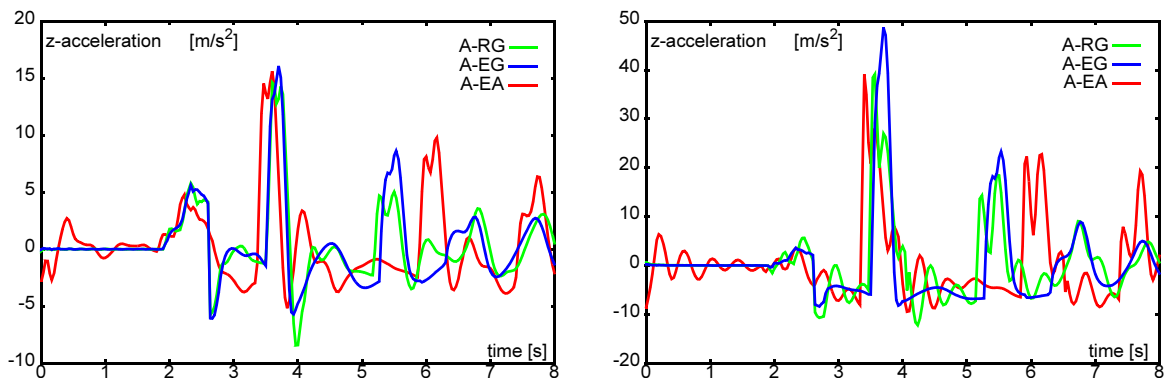


Figure 7.8 Scenario C: Vertical Acceleration of Aircraft Reference Point (left) and of Cockpit (right) Over Time

For the simulations performed here, a different approach was applied in order to come closer to the scenario which is defined in FAR 25.479: initial conditions were chosen such that the maximum descent rate of the aircraft in the scenario (at about 0.35 s after initial contact) is equal to the specified rate of 3.048 m/s . Because of the “missing”

lift, accelerations are nevertheless still higher than those for models using gravity vector scaling, Figure 7.7.

7.2.2 Impact of Aeroelastic Effects on Dynamic Landing Gear Loads

In Figure 7.9, the order magnitude of maximum vertical loads of scenario A at the main and nose landing gear mainfittings does not depend on the type of modelling. The maximum load at the nose gear during that sequence is even slightly reduced due to the influence of the horizontal stabiliser.

Figure 7.10, which gives the same measurements for scenario B, appears to tell a different story: here, the load level at the main landing gear is more than 40% higher, and at the nose gear, the level of dynamic loads even more than doubles. But as it has already been stated above (Section 7.2.1), the physical conditions of a FAR-conform model and a model accounting for aerodynamic effects do not match: a direct comparison of values is not possible. But it also reveals that for the modelled configuration, if actually performed in a flight test, this certification case could overload landing gear and structure. One cannot but accept the obvious, empirically established fact that this case, for conventional aircraft designs, leads to a safe landing gear design for nose-down landings.

In scenario C, again the initial contact shows little difference, see left graph in Figure 7.11, but for the main gear which touches second (right graph), a striking difference appears: in the conventionally modelled simulation, the second gear is subject to loads which are about 14% higher than those for gear number one, but with aerodynamics, aerodynamic damping leads to loads which are 12% lower. Thus, we receive a difference of almost 30% between both solutions.

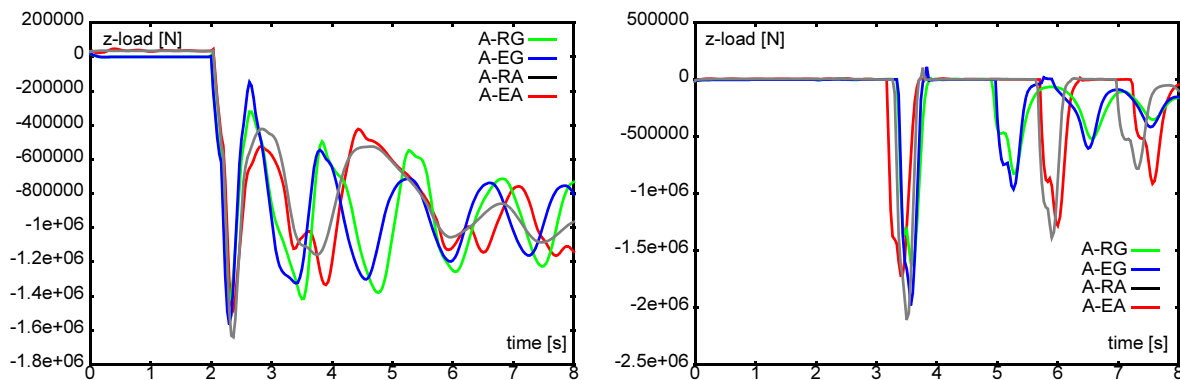


Figure 7.9 Scenario A: Vertical Load on Left Main Landing Gear Mainfitting (left) and Nose Landing Gear Mainfitting (right) Over Time

Scenario D, the case of lift dumper deployment in the moment of rebound, demonstrates that there may be conditions where the highest loads are not necessarily experienced at a hard landing impact, Figure 7.12. The simulation reveals that in this

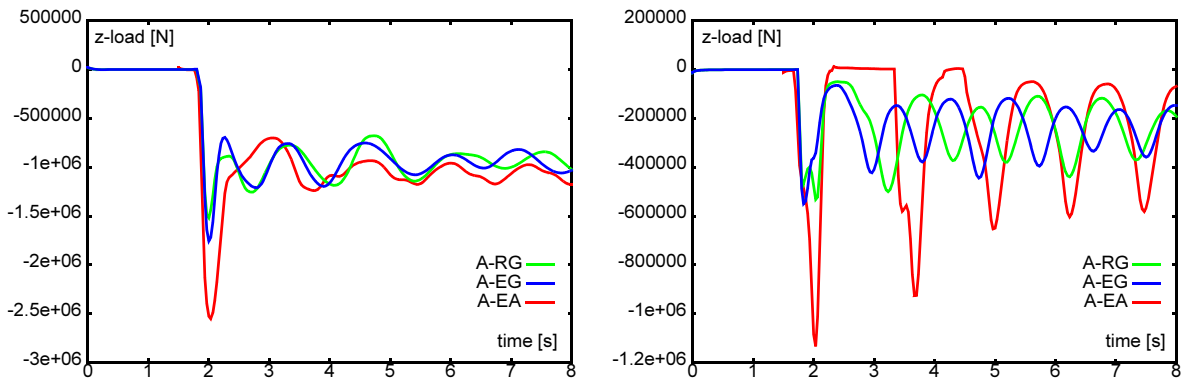


Figure 7.10 Scenario B: Vertical Load on Left Main Landing Gear Mainfitting (left) and Nose Landing Gear Mainfitting (right) Over Time

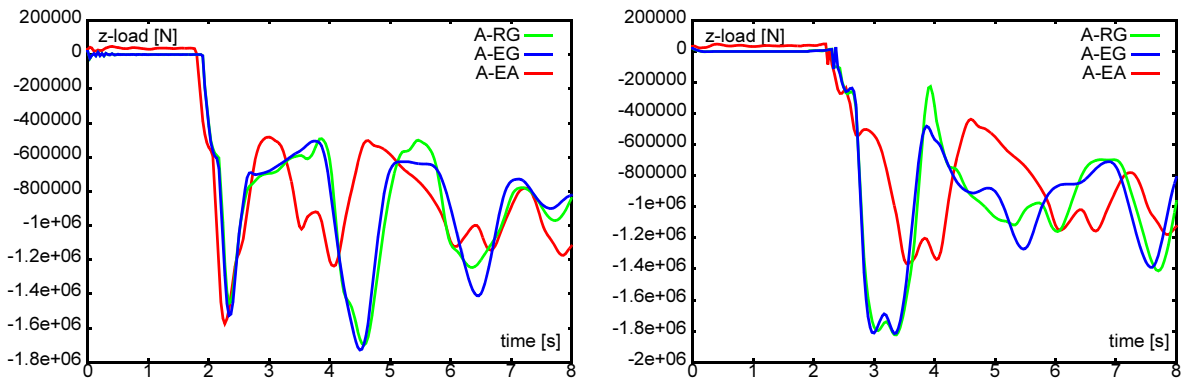


Figure 7.11 Scenario C: Vertical Load on Right (left) and Left (right) Main Landing Gear Mainfitting Over Time

scenario, the hard shock comes when the aircraft drops back into still compressed oleos because of the sudden loss of lift.

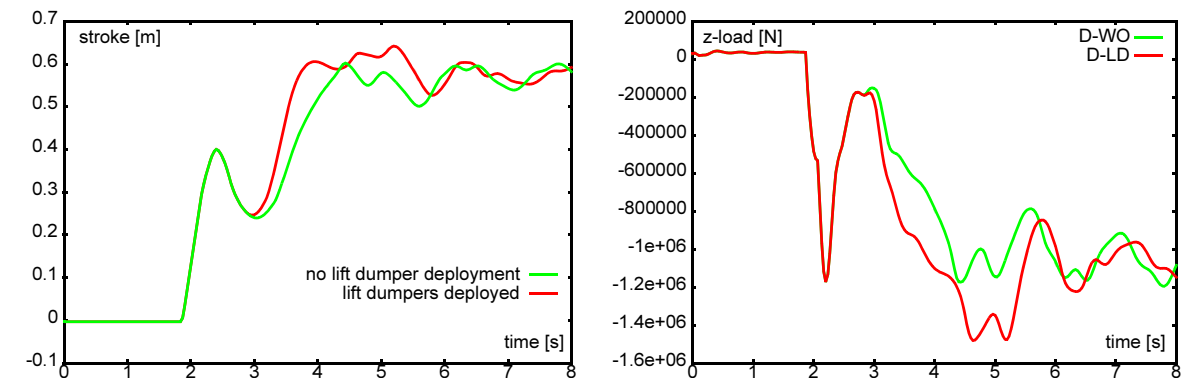


Figure 7.12 Scenario D: Stroke of Left Main Landing Gear Oleo (left) and Vertical Load on Left Main Landing Gear Mainfitting (right) Over Time

An additional analysis has been performed to demonstrate the influence of aeroelastic effects. For scenario C, the effect is obvious: aerodynamic damping is responsible for a significant reduction of ground loads on the landing gear touching down second in a low-wing landing. But it has also some effects in a symmetrical scenario. Figure 7.13

shows the difference between a sequence where only steady aerodynamic forces are applied, to a simulation which accounts for transient effects by kinematic velocities.

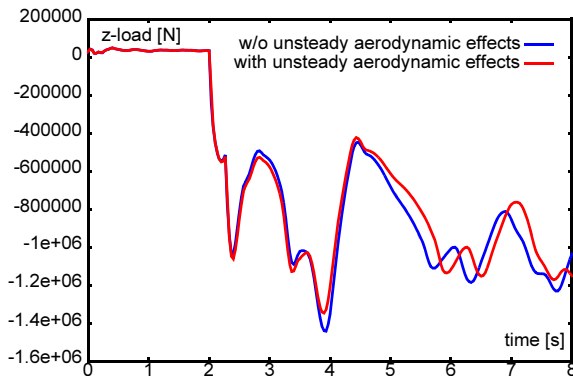


Figure 7.13 Scenario A: Difference Between Simulation With and Without Unsteady Aerodynamic Effects (Aerodynamic Excitation / Damping)

7.2.3 Relevance of Aeroelastic Effects in Aircraft Ground Dynamics

From a loads point of view, there are very few cases where the landing gear of a modern transport aircraft fails in a hard landing simply because of overstress due to initial impact. This demonstrates that the certification requirements for landing gears lead to a reasonably safe design in this respect. This is also in line with the finding of this work: presence of aerodynamic and aeroelastic effects did not lead to an increase of ground loads at initial impact (with exception of scenario B - but the cause for discrepancies in this simulation case have already been discussed). But there are other reasons to have a closer look at the load conditions: landing impact is the critical load case for only about one-fifth of the parts of a landing gear, load peaks do not load stringently occur at landing impact only, load history and its impact on fatigue performance is ignored - all good reasons to go for a deeper and more comprehensive understanding of the loading conditions of the evolving design.

Concerning the aircraft's dynamic behaviour in complex manoeuvres or sequences, little analysis or simulation is required for certification. Knowledge about the system's dynamics in ground operations, especially in a landing, is nevertheless important: layout of landing gear and supporting airframe structure, design of control systems architecture, prevention of rigid body oscillations (e.g. heave-pitch modes) or resonance vibrations, comfort issues, design conditions for subsystems are but a few examples where realistic predictions may save a lot of time and money, or even be essential for a successful design altogether.

To subsume the results in a nutshell: aerodynamic forces and aeroelastic effects have a significant impact on the results of aircraft landing simulations and should not be disregarded.

7.3 Computational Performance of Aeroelastic Preprocessing

Multibody simulations of free-flying, or landing, aircraft generally are good-natured problems. Unlike with other applications such as numerically very stiff problems, jobs can usually be computed within several minutes, and rarely take over a half-hour for state-of-the-art desktops or workstations. Nevertheless, computational performance is an issue for MBS as well, e.g. for the acceptance of regular cross-checks for overall system performance and interdisciplinary interactions during the design process, or for multidisciplinary optimisation problems where the sheer number of re-runs in the optimisation process calls for fast computation.

For an evaluation of the computational performance of aeroelastic preprocessing, the approach of modal aerodynamics has been compared to conventional modelling with aerodynamic force elements. The aerodynamic matrices of the modal representation fell back on the same linearised aerodynamic data set which was also used for the definition of the force elements. Thus, both approaches fundamentally base on the same equations of motion; they differ only in the way they are represented in the MBS algorithm. Not astonishingly, the results of the simulation for both reference aircraft are almost identical.

With the approach of aeroelastic preprocessing targeting the MBS representation of a free-flying, controllable elastic aircraft,⁴⁶ reference model 1 serves for the general evaluation of computational effort. Complexity level and scope of modelling of reference model 2 represent the current state-of-the-art in practical applications; comparison between different modelling strategies gives an impression of the actual computational performance the new approach may be able to provide.

7.3.1 Computational Performance of Reference Aircraft Model 1

Computation of these models was performed on a Hewlett-Packard C360 workstation. The most relevant results of this evaluation are the overall CPU times of the jobs. For information, the numbers of integration steps, right handside (RHS) calls and computations of the Jacobian matrix are also listed. For scenario 1 the results are listed in Table 7.5, Table 7.6 gives the computational performance data for scenario 2.

For complex MBS models, a multitude of factors influence the overall computation time of a simulation. An inherent advantage of modal aerodynamics is that it avoids most of the time-consuming measurement evaluations which are performed every time a force element is called. Additional advantages may contribute to the performance gain, but depend strongly on the actual conditioning of the system.

46. This statement should not lead to the assumption that the principle of aeroelastic preprocessing represents a general approach for the flight mechanics of elastic aircraft. As described in Chapter 3, it has been designed to simulate the behaviour of a manoeuvring, elastic aircraft with focus on take-off, landing approach and ground run.

Reference Model 1: Scenario 1				
MBS Model	CPU Time	Integration Steps	RHS-Calls	Jacobians
FEL-rigid	2.43 s	336	729	1
FEL-03M	10.57 s	628	1578	11
FEL-20M	140.23 s	877	2321	8
MA-03M	6.93 s	814	1981	16
MA-20M	76.79 s	966	2474	8

Table 7.5 Performance Data for Integration of Respective Model in Scenario 1

Reference Model 1: Scenario 2				
MBS Model	CPU Time	Integration Steps	RHS-Calls	Jacobians
FEL-rigid	2.11 s	258	633	5
FEL-03M	18.78 s	1031	2817	30
FEL-20M	190.92 s	858	3181	24
FEL2-rigid	4.92 s	363	930	9
FEL2-03M	31.91 s	1224	3462	39
FEL2-20M	198.00 s	841	2943	20
FEL5-rigid	17.45 s	628	1595	14
FEL5-03M	59.59 s	1260	3570	38
FEL5-20M	268.48 s	843	3025	22
MA-03M	5.07 s	715	1592	5
MA-20M	97.76 s	1004	3174	20

Table 7.6 Performance Data for Integration of Respective Model in Scenario 2

Adding aeroelastic matrices to the equation of motion influences the right handside of the equations of motion and may have a moderate impact on the number of RHS calls. New evaluation of the Jacobian matrix is an expensive job, too. The main difference in terms of these numbers is that for modal aerodynamics, only one force routine has to be evaluated during an integration loop, instead to the multiple routines of FEL-type models. If this leads to some computational advantage, as in scenario 2, or results in a minor time penalty as in scenario 1, depends on the specific particularities of the simulation. Tuning of integrator settings such as integration method, tolerances and scaling factors may compensate for some disadvantage. As an example, in the simulations performed so far, modal aerodynamics was more robust in respect to larger integration steps. But as the computational performance can be influenced, but hardly controlled by the user, modifications of integrator properties were not included in this evaluation.

To give an impression of the dependency on the actual, time-dependent conditions of an integration, the stepsize of scenario 2 is depicted in Figure 7.14 for the models with 20 elastic modes, FEL-20M and MA-20M, with standard integrator settings. Higher stepsize values are usually advantageous (scale is logarithmic), so the larger stepsize of the MA model between 3-6.5 sec results in a minor overall computational gain.

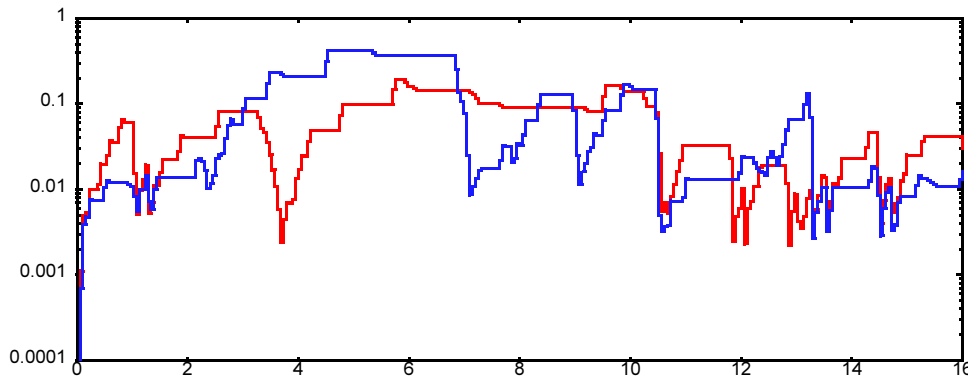


Figure 7.14 Integrator Stepsize for Models FEL-20M and MA-20M in Scenario 2

The main impact on computation times, however, is related to the number of force elements used in the simulation, and here lies the effective advantage of the approach of modal aerodynamics.

To resume the actual benefit in CPU time, the percentile gain of modal aerodynamics versus the corresponding model with force elements is given in Table 7.7.

Reference Model 1: Aerobatic Glider						
Scenario	Model MA-03M			Model MA-20M		
	FEL-03M	FEL2-03M	FEL5-03M	FEL-20M	FEL2-20M	FEL5-20M
1	34%			45%		
2	73%	84%	91%	49%	51%	64%

Table 7.7 Reference Model 1: Reduction of CPU Time by Modal Aerodynamics

7.3.2 Computational Performance of Reference Aircraft Model 2

A similar comparison was performed for the more complex simulation of the landing transport aircraft, Section 7.2. All three referred methods of aircraft ground dynamics analysis, gravity vector scaling, force elements and modal aerodynamics, have been used in scenarios A - C; scenario D could only be analysed with the latter two, as only those account for distributed aerodynamics and aeroelastic effects. The CPU times required to compute the respective jobs are given in Table 7.8. With the reference simulations having revealed that distributed aerodynamics and aeroelastic effects have a decisive influence on the results, Table 7.8 also contains the percentile time penalty for realistic aerodynamic modelling, either by force elements or modal aerodynamics, in respect to the performance of the conservative approach of gravity vector scaling.

Reference Model 2: Landing Transport Aircraft						
Scenario	CPU Time			Percentile CPU Time Penalty		
	Grav. Vector Scaling	Force Elements	Modal Aerodyn.	Grav. Vector Scaling	Force Elements	Modal Aerodyn.
A	111.77 s	524.36 s	141.23 s	100%	+369%	+26%
B	81.83 s	447.04 s	116.04 s	100%	+446%	+42%
C	117.29 s	625.83 s	175.38 s	100%	+434%	+49%
D		599.48 s	213.99 s			

Table 7.8 Performance Data for Integration of Reference Model 2 in Scenarios A - D

Comparing the results of scenarios A - C, the analysis with modal aerodynamics takes about 40% longer to compute than a simulation with gravity vector scaling - a moderate penalty for including aerodynamics and, to some extent, fluid-structure interaction.

Using aerodynamic force elements may provide almost similar functionality, but at the expense of sharply increased computation times. Table 7.9 gives the percentile performance gain achieved by modal aerodynamics for each scenario.

Reference Model 2: Landing Transport Aircraft				
Comparison Between Force Elements and Modal Aerodynamics	Scenario			
	A	B	C	D
Reduction of CPU Time	73%	74%	72%	64%

Table 7.9 Reference Model 2: Reduction of CPU Time by Modal Aerodynamics

Averaged over all four scenarios, modal aerodynamics reduces CPU time by more than 70% in respect to a comparable simulation with conventional force elements. This is a considerable advantage, especially when many simulations have to be performed, for example for a multitude of aircraft configurations (alterations of weight, centre of gravity position, distribution of payload, ...) or in an optimisation sequence.

It may be added that the connected functionality of aeroelastic preprocessing significantly simplifies model set-up. Positive as a significant reduction in CPU time may be, the author considers this convenience in modelling and interdisciplinary integration as the decisive advantage of aeroelastic preprocessing. The benefit of semi-automated modelling, however, is hard to quantify at the current state, and even when established in actual design processes, dependable numbers cannot be easily obtained but have to be derived from a rather elaborate examination.

8 Conclusion

8.1 Summary

Reliable predictions of the dynamic behaviour and performance of commercial passenger transport aircraft on or near the ground are playing an increasingly important rôle in modern aircraft design. Nonlinear multibody simulation of the aircraft in characteristic scenarios is a frequently used tool to analyse the design during take-off, landing and ground run. Research activities and practical realisation in recent years have mainly focused on questions of structural flexibility, airframe-landing gear interaction and advanced scenario modelling. Software tools and design processes have been developed or modified to enable fast and efficient modelling, analysis and evaluation of the aircraft, under consideration of dynamic structural deformation and in realistic scenarios. With these capabilities, aircraft ground dynamics analysis has been established as a valuable tool in virtual design processes.

Less effort, however, was spent so far to adequately include aspects of aerodynamic lift and drag on the ground dynamics of the deformable, manoeuvring aircraft. This motivated research for an advanced approach to adequately account for aerodynamic and aeroelastic effects in hybrid multibody simulation. Three main objectives had to be met:

- The approach had to fulfil the specific needs of aircraft ground dynamics analysis. This imposed certain demands, such as robust representation of the aircraft in high-lift configuration, but also allowed for a number of simplifications, e.g. in respect of compressibility.
- The consideration of aerodynamic and aeroelastic effects had to have as less impact on computational performance of the multibody simulation as possible. Other widely applied approaches for fluid-structure interaction, such as co-simulation, were no option in this respect.
- Even more important than the computational performance of the single simulation, the manual effort for setting up a multidisciplinary simulation of the aircraft had to be minimised. This included factors like establishment of an effective interdisciplinary workflow, efficiency in creating and updating the aeroelastic functionality, degree of user-knowledge required to execute an application, and practical handling issues.

The proposed approach, referred to as aeroelastic preprocessing, is to pre-compute the aerodynamic and aeroelastic properties of the aircraft in a form which allows to include them into the MBS model by an aeroelastic input file. A wide range of aerodynamic models may provide the initial data for the MBS-preceding computation of the input file. The preprocessing sequence can be automated, requiring user input only to set the general conditions. The method has been evaluated on two application examples: one to demonstrate the impact of detailed aerodynamic and aeroelastic modelling on the simulation of a large transport aircraft during landing, and one to estimate the computational advantage.

The reference simulations reveal that aerodynamic and aeroelastic effects have a determining influence on the aircraft's dynamic behaviour during ground operations. The proposed approach allows to represent them very efficiently in multibody simulation: while delivering similar results, the computation times of different landing sequences of a transport aircraft were reduced by more than 70%, compared to a conventional modelling approach. The benefit of aeroelastic preprocessing on design process level, e.g. by streamlined modelling, optimised handling or updating of interdisciplinary data and process oriented interconnectivity, can be expected to be significant; at the current stage, however, no quantitative estimation is possible.

8.2 Contributions

Starting from the representation of deformable bodies in multibody simulation algorithms, a method was developed to link aeroelastic effects (deformation and deformation velocity dependent airloads) to the modal representation of the elastic body. Thus, the impact of airloads on the deformation state of the aircraft could be accounted for by inexpensive matrix addition in the modal representation of the elastic body, which barely affects the computational effort. The overall motion of the aircraft due to aerodynamic forces on the flexing structure is determined by simple, rigid body-alike aerodynamics which, in MBS, can be covered by a simple force routine.

Additionally, this approach allows to pre-compute an aeroelastic input file to MBS. This file can be used for all simulations of a given aircraft configuration. Only changes of basic aircraft parameters, such as a modified structure, altered aerodynamic design or a different setting of aerodynamic devices such as flaps, which have not been accounted for in the generation of the input file, enforce a new preprocessing step. Setting up an MBS input file requires little aerodynamic knowledge - in the sense of efficient interdisciplinary design, engineers from other disciplines such as system dynamics, structure dynamics or loads may create or modify it for their purposes.⁴⁷

The approach clearly focuses on aircraft ground dynamics. Here, it exerts its specific strengths, and here, its restrictions do not take effect. Other fields of application can be imagined, e.g. from aeroservoelasticity, flight mechanics of large aircraft and alike. Before translating this approach, it has nevertheless to be accessed thoroughly if aeroelastic preprocessing, and with it the method of modal aerodynamics, may be used for the application in question, and if so, where the limits will be.

47. The author is aware that automation has its limits. The more detailed the application is going to be, the more proper modelling and achieved results have to be checked by professionals. In actual design processes, however, the initial modelling approach is usually defined or accompanied by aerodynamic experts; the subsequent adaptations to moderate model modifications may then be performed by a "non-professional", which means that streamlined modelling and analysis still adds up to a significant advantage.

8.3 Future Work

Aeroelastic preprocessing is a fast and stable approach for the simulation of the free-flying, manoeuvring elastic aircraft in interdisciplinary aircraft ground analysis. That said, it proposes but one possible approach of a number of possibilities. Besides competitive methods for fluid-structure coupling in multibody simulation, new opportunities open up for future work. Three interesting topics may be highlighted in the following.

- Plausibility of results in general, and simulations of reference examples in particular, permit some confidence in the accuracy of results. Thorough comparison of MBS simulations with modal aerodynamics to actual flight data of large commercial passenger transport aircraft is nevertheless required to establish the proposed approach as a proven and reliable tool of aircraft ground dynamics analysis.⁴⁸
- Although a method has been established on how to generate an aerodynamic / aeroelastic input file for MBS, a robust, universal implementation has yet to be realised. This may appear as a mere programming job, but the demands go far beyond. For example, the preprocessing routine has to contain a decent amount of expert knowledge to be able to automatically modify the aerodynamic model(s), user inputs have to be checked for plausibility faulty information has to be detected, and different CFD tools have to be served.
- The possibilities of the underlying methodology reaches far beyond the regime of aircraft ground dynamics, or aerospace applications in general. Various questions of multiphysical phenomena distributed over an deformable MBS body may be treated by this approach - in fact, most interdisciplinary effects which can, at least section-wise, be linearised in its impact on the multibody system, may be modelled by the same strategy.

Multibody simulation is a tool which offers far-reaching possibilities in the field of computer aided engineering by representing a “virtual testbed” for new concepts and designs, and continuous progress in the field of interdisciplinary design is a key element of the future success of this CAE application. Hopefully, the contribution presented in this work will have some share in further promoting this very interesting and exciting technology.

48. A dependable verification of any method in this regime requires a validated model (including MBS set-up, elastic modelling and aerodynamics), accurate and detailed reproduction of an actual landing sequence, and, last but not least, access to comprehensive flight test data on that very landing. The author may add, from his own experience, that the last point may prove to be the most difficult.



Appendix A Aircraft Coordinate Systems

For the representation of the aeroplane motion due to the presence of aerodynamic forces, a set of four coordinate systems is used in this work,⁴⁹ Figure 5.4. These are

- the inertial coordinate system ${}_I\mathbf{e}$ (index I): a geodetic, earth centred-earth fixed (ECEF) reference frame;
- the body-fixed coordinate system ${}_B\mathbf{e}$ (index B): attached to the body reference frame (or identical with it), with its x- and z-axis placed in the aircraft's symmetry plane and, if not stated otherwise, positioned at the centre of gravity (CG) - this system serves as the aircraft's reference system;
- the aerodynamic coordinate system ${}_A\mathbf{e}$ (index A): a reference frame located at the origin of the body-fixed coordinate system, with its x-axis in line but opposed to the free-stream velocity \mathbf{u}_∞ and its z-axis in the aircraft symmetry plane;
- the experimental coordinate system ${}_X\mathbf{e}$ (index X)⁵⁰ as an "intermediate system" between the body-fixed and the aerodynamic system: similar to ${}_B\mathbf{e}$, but rotated about the ${}_B y$ -axis by the angle of attack α so its x-axis runs parallel to the projection of the free-stream velocity vector \mathbf{u}_∞ onto the symmetry plane (a further rotation about the ${}_X z$ -axis by the yaw angle β delivers the aerodynamic system).

All coordinate frames are right-handed Cartesian systems. The components of these systems are defined in Table 8.1, they are distinguished by their respective indices i.

Component of Aircraft Coordinate Systems			
Axes	${}_i x$	${}_i y$	${}_i z$
Angular displacements about axes	${}_i \phi$	${}_i \theta$	${}_i \psi$
Linear velocities along axes	${}_i u$	${}_i v$	${}_i w$
Angular velocities about axes	${}_i \dot{\phi}$	${}_i \dot{\theta}$	${}_i \dot{\psi}$
Resultant aerodynamic forces along axes	${}_i X$	${}_i Y$	${}_i Z$
Resultant aerodynamic moments about axes	${}_i L$	${}_i M$	${}_i N$

Table 8.1 Definition of Components the Aircraft Coordinate Systems (Example Shown in Figure: Body-Fixed Reference System B)

49. The definition of coordinate systems and their respective components corresponds to ISO 1151 (DIN 9300), [82]-[85].

50. This coordinate frame is not explicitly used here, but has proved to be helpful in some cases to generate the MBS measurements of the aerodynamic properties.

Appendix B

Acronyms and Abbreviations

1D	One-dimensional
2D	Two-dimensional
3D	Three-dimensional
ACE	Airbus Concurrent Engineering
AoA	Angle of Attack
BGLM	Boltzmann Gas Lattice Method
CACE	Computer Aided Control Engineering
CAD	Computer Aided Design
CAE	Computer Aided Engineering
CAM	Computer Aided Manufacturing
CAX	Computer Aided x ⁵¹
CE	Concurrent Engineering
CFD	Computational Fluid Dynamics
CG	Centre of Gravity
COCOLIB	Coupling Communication Library
CPU	Central Processing Unit
CSM	Computational Structural Mechanics
DAE	Differential-Algebraic Equation
DNS	Direct Numerical Simulation
DoD	Department of Defense (of the United States of America)
DOF	Degree of Freedom
EA	Elastic Axis
ECEF	Earth Centred Earth Fixed
EqM	Equations of Motion
FCS	Flight Control System
FEA	Finite Element Analysis
FEL	Force Element(s)

51. Arbitrary single discipline of CAE which is represented by wildcard x

GUI	Graphical User Interface
HIL	Hardware-in-the-Loop
IPC	Inter-Process Communication
IPD	Integrated Product Development
LES	Large-Eddy Simulation
LLM	Lifting Line Method
LSM	Lifting Surface Method
MA	Modal Aerodynamics
MBS	Multibody Simulation
mCSM	Modally Reduced Computational Structural Mechanics
MDICE	Multi-Disciplinary Computing Environment
MDO	Multidisciplinary Design Optimisation
MOPO	Multi-Objective Parameter Optimisation
MOPS	Multi-Objective Parameter Synthesis
MpCCI	Mesh-based parallel Code Coupling Interface
MTOW	Maximum Take-Off Weight
NSE	Navier-Stokes Equations
NTSB	National Transport Safety Board
ODE	Ordinary Differential Equation
OWE	Operational Weight Empty
PDE	Partial Differential Equations
PDM	Product Data Management
PFM	Potential Flow Method
RANS	Reynolds Averaged Navier-Stokes Equations
RHS	Right Hand-Side
SID	Standard Input Data
SPM	Surface Panel Method
VLM	Vortex Lattice Method

Appendix C

List of Symbols

Variables

Latin Symbols

Lower Case Letters

a	acceleration
c	aerodynamic derivative (local, two-dimensional)
c	reference chord
d	local displacement velocity
d	damping factor
dV	infinite volume element
f	force
h	shape function
i	integer number
l	moment (torque)
m	mass
m	integer number
n	integer number
p	polynomial
q	generalised coordinates
q	dynamic pressure
r	position vector
t	time
u	displacement vector
u	(freestream) velocity
v	translational velocity
x	coordinate
y	coordinate
z	coordinate
z	state vector

Upper Case Letters

C	coefficient matrix
C	aerodynamic derivative
D	damping matrix
E	unity matrix
G	Lagrangian multipliers
J	inertia tensor
K	stiffness matrix
M	mass matrix

Q	aerodynamic matrix
S	reference area

Greek Symbols

Lower Case Letters

α	rotational acceleration
α	angle of attack
β	yaw angle
γ	roll angle
δ	control surface deflection
λ	lagrangian multipliers
ρ	density
ϕ	base function
ω	rotational velocity
ω	eigenfrequency

Upper Case Letters

Π	potential of internal elastic deformation forces
Φ	mode matrix
Ψ	Jacobian matrix of elastic states

Indices

Latin Symbols

Lower Case Letters

a	aerodynamic (short form)
aero	aerodynamic
app	applied (force)
cstr	constrained (force)
def	deformation
dV	infinite volume element
e	external (undermentioned)
e	elastic body
elast	elastic
f	force related
grav	gravity
gyro	gyroscopic
i	internal (undermentioned)
k	stiffness related
kin	kinematic
l	moment related

pitch	pitch rate related
plunge	plunge rate related
q	related to generalised coordinates
r	rotational
ref	reference
s	coordinate of a curve
s	steady
t	translational
v	unsteady (velocity dependent)

Upper Case Letters

A	aerodynamic system
B	body-fixed frame
C	control
E	elastic coordinates
F	linearised (discretised results by FEA)
I	inertia frame
J	aerodynamic moment (L, M, N)
L	lift
L	aerodynamic moment about x-axis
M	aerodynamic moment about y-axis
N	aerodynamic moment about z-axis
R	rigid (body) coordinates
V	volume element
X	experimental system
X	aerodynamic force in x-direction
Y	aerodynamic force in y-direction
Z	aerodynamic force in z-direction

Greek Symbols

Lower Case Letters

α	angle of attack
β	yaw angle
γ	roll angle
ζ	Lehr's damping factor
ρ	density related
σ	stress related

Other Symbols

0	initial (reference) data
0, 1, ...	numbering (where appropriate: order)
∞	in infinity (e.g. for freestream velocity)

Denotation of Variables

a	scalar	regular
\mathbf{a}	vector	bold lower case letter (latin or greek)
\mathbf{A}	matrix	bold upper case letters (latin or greek)
$\underline{\mathbf{a}}$	underlined	vector basis
\mathbf{a}_b	subscript right	label b to variable \mathbf{a}
${}_B\mathbf{a}$	subscript left	variable \mathbf{a} in reference to coordinate frame B
$\hat{\mathbf{a}}$	hatted	variable \mathbf{a} in modal coordinates

Appendix D

List of Figures

Figure 2.1	The Concept of Concurrent Engineering	14
Figure 2.2	Multibody Simulation in a Concurrent Engineering Environment	19
Figure 2.3	Elements of MBS Models	22
Figure 2.4	Typical MBS Applications: Automotive, Wheel / Rail, Aerospace	26
Figure 2.5	Main Characteristics of an Aircraft Design Process	27
Figure 2.6	Distributed Aerodynamic MBS Force Elements on MBS Model	28
Figure 2.7	Inter-Process Communication (IPC) Between MBS and CFD	30
Figure 3.1	Deflection of an A340-300 Wing at a Hard Touch-Down	39
Figure 3.2	Flow Scheme of Aeroelastic Preprocessing	41
Figure 4.1	Deformation of a Deformable Body	46
Figure 5.1	Superposition of Aerodynamic Effects	57
Figure 5.2	AMP Wing - Unloaded, with Linearised and Nonlinear Aerodynamics	58
Figure 5.3	Superposition of Basic Deformation Modes of a Deformable Body	59
Figure 5.4	Flight Attitude Measurements for the Vector of Rigid Body States	63
Figure 5.5	Example of Control Efficiency Function	67
Figure 5.6	Lift and Drag of a Wing Section Under Consideration of Wing Torsion	69
Figure 5.7	Aerodynamic Analysis of Flexible Body Deformed by Base Function	70
Figure 5.8	Kinematic Velocities at a Wing Section: Dynamic Wing Bending	71
Figure 5.9	Kinematic Velocities at a Wing Section: Dynamic Wing Torsion	72
Figure 5.10	Analysis of Aerodynamic Damping/Excitation by Base Function	72
Figure 5.11	1st Bending Mode of a Cantilever Beam	73
Figure 6.1	Overview of Workflow of Aeroelastic Preprocessing	79
Figure 6.2	Interpolation of Four Source Points to a Target Point	85
Figure 6.3	Mapping of Modal Deformation onto an Aerodynamic Grid	86
Figure 6.4	Approach of Rigid Connexions and Approach of Rigid Chord Sections	87
Figure 6.5	Unidirectional Interpolation Element for Quadratic Variation	89
Figure 6.6	Normalised Euclid's Hat and Gaussian Function	90
Figure 6.7	Example of Coupling With Perpendicular Rigid Connexions	91
Figure 6.8	Pre-assignment Between Interpolation Points Using Patches	92
Figure 7.1	Set-Up of Reference Model 1 Basing on Data of Mü 28	93
Figure 7.2	Control Inputs for an Aerobatic Manoeuvre	94
Figure 7.3	Reference Scenario 1: Aerobatic Manoeuvre "Barrel Roll"	95
Figure 7.4	SIMPACT Model of Reference Aircraft 2	96
Figure 7.5	Scenario A: Vertical Position and Descent Velocity of Aircraft	99
Figure 7.6	Scenario A: Vertical Acceleration of Aircraft Ref. Point and Cockpit	100

Figure 7.7	Scenario B: Vertical Acceleration of Aircraft Ref. Point and Cockpit	100
Figure 7.8	Scenario C: Vertical Acceleration of Aircraft Ref. Point and Cockpit	100
Figure 7.9	Scenario A: Vertical Load on Main and Nose Gear Mainfitting	101
Figure 7.10	Scenario B: Vertical Load on Main and Nose Gear Mainfitting	102
Figure 7.11	Scenario C: Vertical Load on Main and Nose Gear Mainfitting	102
Figure 7.12	Scenario D: Stroke and Vertical Load on Left Main Landing Gear	102
Figure 7.13	Scenario A: Simulation With and Without Unsteady Aerodynamics	103
Figure 7.14	Integrator Stepsize for Models FEL-20M and MA-20M	106

Appendix E

List of Tables

Table 2.1	Numerical Integration Methods for MBS Equations of Motion	25
Table 6.1	Shape Functions and Partial Derivatives of Interpolation Elements	90
Table 7.1	Reference Scenarios for Computational Performance Evaluation	94
Table 7.2	Variations of the Reference Aircraft Model 2	95
Table 7.3	Modelling Data of Reference Model 1	98
Table 7.4	Reference Model Variants of Landing Simulations	98
Table 7.5	Performance Data for Integration of Respective Model in Scenario 1	105
Table 7.6	Performance Data for Integration of Respective Model in Scenario 2	105
Table 7.7	Reference Model 1: Reduction of CPU Time by Modal Aerodynamics	106
Table 7.8	Performance Data for Integration of Reference Model 2	107
Table 7.9	Reference Model 2: Reduction of CPU Time by Modal Aerodynamics	107
Table 9.1	Definition of Components the Aircraft Coordinate Systems	113

References

- [1] Bisplinghoff, R. L.; Ashley, A.; Halfman, R. L.: *Aeroelasticity*
Dover Publications, Inc; Mineola, NY, USA; 1996.
- [2] Winner, R. I.; Pennell, J. P.; Bertrand, H. E.; Slusarezuk, M. M. G.: *The Role of Concurrent Engineering in Weapons System Acquisition*
IDA-Report R-338, Institute for Defense Analyses; Alexandria, VA, USA; 1988.
- [3] Stalk, G. Jr.; Webber, A. M.: *Japan's Dark Side of Time*
in: *Harvard Business Review*; Vol. 71(4); Harvard Business School Publishing;
Boston, MA, USA; 1993.
- [4] Kortüm, W.; Goodall, R. M.; Hedrick, J. K.: *Mechatronics in ground transportation - Current trends and future possibilities*
in: *Annual Review in Control*; Vol. 22; Elsevier Science; Amsterdam, The Netherlands; 1998.
- [5] Schelke, E.; Witte, L.; Mutter, C.: *Strategische Entwicklungselemente bei der Boxter-Entwicklung*
in: *Automobiltechnische Zeitschrift / Motortechnische Zeitschrift*; Sonderausgabe ATZ/MTZ; Porsche Boxter; GWV Fachverlage GmbH; Wiesbaden, Germany; 1996.
- [6] Trautenberg, W.: *Bidirektionale Kopplung zwischen CAD- und Mehrkörpersimulationssystemen*
Dissertation an der Technischen Universität München, Lehrstuhl für Feingerätebau und Mikrotechnik; München, Germany; 2000.
- [7] Wu, J.K.; Choong, F. N.: *Data and Process Models for Concurrent Engineering of Mechanical Systems*
in: E. D. Haug (editor): *Concurrent Engineering: Tools and Technologies for Mechatronic Systems Design*; Springer-Verlag Berlin Heidelberg; Berlin, Germany; 1993.
- [8] Young, J. A.; Anderson, R. D.; Yurkovich, R. N.: *A Description of the F/A-18 E/F Design and Design Process*
in: *Proceedings of 7th AIAA/USAF/NASA/ISSMO Symposium on Multidisciplinary Analysis and Optimization*; Part 1, Report AIAA-98-4701; St. Louis, MO, USA; 1998.
- [9] Glende, W. L.: *The Boeing 777: A Look Back*
NASA Technical Report ID 1999 000 8079; NASA Center of Aerospace Information (CASI); Hanover, MD, USA; 1999.
- [10] Shokralla, S. H.: *The 21st Century Jet*
Master Thesis, University of California at Berkley; Berkley Expert Systems Technology Laboratory; Berkley, CA, USA; 1995.

- [11] Moses, R. W.; Shah, G. H.: *Spatial Characteristics of F/A-18 Vertical Tail Buffet Pressures Measured in Flight*
in: *Proceedings of 39th AIAA/ASME/ASCE/AHS/ASC Structures, Structural Dynamics, and Materials Conference*; Report AIAA-98-1956; Long Beach, CA, USA; 1998
- [12] Breuhaus, M.; Fowler, K.; Zanetta, J.: *Innovative Aspects of the Boeing 777 Development Programme*
in: *Proceedings of the 20th Congress of the International Council of the Aeronautic Sciences*; Sorrento/Napoli, Italy; 1996.
- [13] Mecham, M.: *Getting Software Right Is Part of the New Airbus*
in: *Aviation Week & Space Technology*; Vol. 149, No. 20; The McGraw-Hill Companies; New York, NY, USA; 1998.
- [14] Mechler, H.; Schmitt, D.: *Parameterised Geometric Modelling - The New Aircraft (Pre-)Design Process*
in: Hönlinger, H. (editor): *CEAS Conference on Multidisciplinary Aircraft Design and Optimization*; DGLR Deutsche Gesellschaft für Luft- und Raumfahrt Lilienthal-Oberth e.V.; Bonn, Germany; 2001.
- [15] Pink, J.: *Structural Integrity of Landing Gears*
in: Tanner, J. A.; Ulrich, P. C.; Medzorian, J. P.; Morris, D. L. (editors): *Emerging Technologies in Aircraft Landing Gear*; SAE Society of Automotive Engineers, Inc.; SAE Publications Group, Progress in Technology Series No. PT-66; Warrendale, PA, USA; 1997.
- [16] Young, D.W.S.: *Aircraft Landing Gears: the Past, Present and Future*
in: Tanner, J.A. (editor): *Aircraft Landing Gear Systems*; SAE Society of Automotive Engineers, Inc.; SAE Publications Group, Progress in Technology Series No. PT-37; Warrendale, PA, USA; 1990.
- [17] Jenkins, S. F. N.: *Landing Gear Design and Development*
in: *Proceedings*; Part G1, Journal of Aerospace Engineering; Vol. 203; IMechE Institution of Mechanical Engineers; Professional Engineering Publishing, Ltd.; Bury St. Edmunds and London, UK; 1989.
- [18] Conway, H. G.: *Landing Gear Design*
Chapman & Hall; London, U.K.; 1958.
- [19] Krüger, W.; Besselink, I.; Cowling, D.; Doan, D. B.; Kortüm, W.; Krabacher, W.: *Aircraft Landing Gear Dynamics: Simulation and Control*
in: *Vehicle System Dynamics*; Vol. 28; Swets & Zeitlinger Publishers; Lisse, The Netherlands; 1997.
- [20] Shepherd, A.; Catt, T.; Cowling, D.: *The Simulation of Aircraft Landing Gear Dynamics*
in: *Proceedings of 18th Congress of the International Council of the Aeronautic Sciences*; Beijing, China; 1992.

-
- [21] Shepherd, A.; Catt, T.; Cowling, D.: *An aircraft landing gear parametric leg model* in: *UK Simulation Society Conference of Computer Simulation 1993*; Keswick, U.K.; 1993.
- [22] Ogata, K.: *Modern Control Engineering*
Prentice Hall, Inc.; Upper Saddle River, NJ, USA; 1996.
- [23] Bishop, R. H.: *Modern Control Systems Analysis and Design Using Matlab and Simulink*
Addison-Wesley Publishing Co.; Boston, MA, USA; 1998.
- [24] Hassul, M.; Shahian, B.: *Control System Design Using MATRIXx*
Prentice Hall, Inc.; Upper Saddle River, NJ, USA; 1992.
- [25] Rulka, W.: *SIMPACK - a Computer Program for Simulation of Large-Motion Multibody Systems*
in: Schiehlen, W. (editor): *Multibody Systems Handbook*
Springer-Verlag Berlin Heidelberg; Berlin, Germany; 1990.
- [26] Smith, R. C.; Haug, E. J.: *DADS - Dynamic Analysis and Design System*
in: Schiehlen, W. (editor): *Multibody Systems Handbook*
Springer-Verlag Berlin Heidelberg; Berlin, Germany; 1990.
- [27] Orlandea, N.: *ADAMS - Theory and Applications*
in: DePater, A. D.; Pacejka, H. B. (editors): *Proceedings of the 3rd Seminar on Advanced Vehicle Systems Dynamics*; Swets and Zeitlinger Publishers; Lisse, The Netherlands; 1987.
- [28] Etzkorn, J.: *ELGAR: European Landing Gear Advanced Research - Final Report Subtask 1.1.2*
DLR Bericht IB 532-00-2; Oberpfaffenhofen, Germany; 2000.
- [29] Wentscher, H.: *Design and Analysis of Semi-Active Landing Gears for Transport Aircraft*
DLR Forschungsbericht; Report Nr. 96-11; Köln, Germany; 1996.
- [30] Krüger, W. R.: *Integrated Design Process for the Development of Semi-Active Landing Gears for Transport Aircraft*
DLR Forschungsbericht; Report Nr. 2001-27; Köln, Germany; 2001.
- [31] Trubshaw, B.; Lowe, J.: *Concorde: The Inside Story*
Sutton Publishing, Ltd.; Stroud, UK; 2000.
- [32] Hitch, H. P.: *Aircraft Ground Dynamics*
in: *Vehicle System Dynamics*; Vol. 10; Swets & Zeitlinger Publishers; Lisse, The Netherlands; 1981.
- [33] Krüger, W. R.; Spieck, M.: *Abschlußbericht "Flexible Aircraft"*
Sachbericht des DLR zum nationalen Luftfahrtforschungsprogramm "Flexible Aircraft", AP6 "Integrierter Entwurf Fahrwerk / Flugzeug"; DLR - Institut für Aeroelastik; Oberpfaffenhofen, Germany; 1999.

- [34] CEC: *Aeronautics related research: Synopses of current projects selected under the 1995 calls for proposal*
European Commission report, EUR-OP reference number CG-NA-16972-EN-C; Bruxelles, Belgium; 1996.
- [35] Kortüm, W.; Schiehlen, W. O.; Arnold, M.: *Software Tools: From Multibody System Analysis to Vehicle System Dynamics*
in: Aref, H.; Phillips, J. W. (editors): *Mechanics for a New Millennium*
Kluwer Academic Publishers; Dordrecht, The Netherlands; 2001.
- [36] Roberson, R. E.; Schwertassek, R.: *Dynamics of Multibody Systems*
Springer-Verlag Berlin Heidelberg; Berlin, Germany; 1988.
- [37] Roberson, R. E.; Wittenburg, J.: *A Dynamical Formalism for an Arbitrary Number of Interconnected Rigid Bodies with Reference to the Problem of Satellite Attitude Control*
in: *Proceedings of the 3rd IFAC Congress*; London, United Kingdom; International Federation of Automatic Control, IFAC Publications Office; Oxford, United Kingdom; 1966.
- [38] Kane, T. R.; Levinson, D.; Likins, P.: *Spacecraft Dynamics*
The McGraw-Hill Companies; New York, NY, USA; 1983.
- [39] Brandl, H.; Johanni, R.; Otter, M.: *A Very Efficient Algorithm for the Simulation of Robots and Similar Multibody Systems without Inversion of the MassMatrix*
in: *Proceedings of IFAC/IFIP International Symposium on Theory of Robots*; Wien, Austria; 1986.
- [40] Brandl, H.; Johanni, R.; Otter, M.: *An Algorithm for the Simulation of Multibody Systems with Kinematic Loops*
in: *Proceedings of the 7th World Congress on the Theory of Machines and Mechanisms*; Sevilla, Spain; 1987.
- [41] Eichberger, A.: *Simulation von Mehrkörpersystemen auf parallelen Rechnerstrukturen*
Fortschritt-Berichte VDI, Reihe 8, No. 332; VDI Verlag GmbH; Düsseldorf, Germany; 1993.
- [42] Eich, E.; Führer, C.: *Numerische Methoden in der Mehrkörperdynamik*
in: Bachem, A., Juenger, M., Schrader, J. (editors): *Mathematik in der Praxis - Fallstudien aus Industrie, Wirtschaft, Naturwissenschaften und Medizin*; Springer-Verlag Berlin Heidelberg; Berlin, Germany; 1995.
- [43] Kortüm, W.; Sharp, R. S.: *A Report on the State-of-Affairs on "Application of Multibody Computer Codes to Vehicle System Dynamics"*
in: *Vehicle System Dynamics*, Vol. 20, Nr. 3-4; Swets & Zeitlinger Publishers; Lisse, The Netherlands; 1991.
- [44] Schiehlen, W. (editor): *Multibody Systems Handbook*
Springer-Verlag Berlin Heidelberg; Berlin, Germany; 1990.

-
- [45] IMechE: *Multibody Dynamics - New Techniques and Applications*
Automobile and Railway Divisions of the Institution of Mechanical Engineers (IMechE); Professional Engineering Publishing, Ltd.; Bury St. Edmunds and London, UK; 1998.
- [46] Rulka, W.; Eichberger, A.: *SIMPACK - An Analysis and Design Tool for Mechanical Systems*
in: Kortüm, W.; Sharp, R. S. (editors): *Multibody Computer Codes in Vehicle System Dynamics*; Swets & Zeitlinger Publishers; Lisse, The Netherlands; 1993.
- [47] Shabana, A. A.: *Dynamics of Multibody Systems*
Cambridge University Press; Cambridge, U.K.; 1998.
- [48] Rulka, W.: *Effiziente Simulation der Dynamik mechatronischer Systeme für industrielle Anwendungen*
Dissertation at the Technical University of Wien (Vienna); resp. DLR Bericht IB 532-01-06; Oberpaffenhofen, Germany; 2001.
- [49] Kortüm, W.; Rulka, W.; Spieck, M.: *Simulation of Mechatronic Vehicles with SIMPACK*
in: Proceedings of MOSIS 97; 31st International Conference on Modelling and Simulation of Systems; Ostrava, Czech Republik; 1997.
- [50] Kortüm, W.; Lugner, P.: *Systemdynamik und Regelung von Fahrzeugen*
Springer-Verlag Berlin Heidelberg; Berlin, Germany; 1994.
- [51] Raymer, D. P.: *Aircraft Design: A Conceptual Approach*
AIAA Education Series #1: Airplanes - Design and Construction; AIAA American Institute of Aeronautics and Astronautics, Inc; Reston, VA, USA; 1999.
- [52] U.S. Department of Transportation, Federal Aviation Administration (FAA): *Advisory Circular "Taxi, Take-Off and Landing Roll Design Loads"*
Advisory Circular Nr. AC 25-491-1 (10/30/00); Transport Airplane Directorate, Aircraft Certification Service (ANM-100); Washington, DC, USA; 2000.
- [53] Hablowitz, T.: *Advanced Helicopter Flight and Aeroelastic Simulation Based on General Purpose Multibody Code*
in: *Proceedings of AIAA Modeling and Simulation Technologies Conference*; Report AIAA 2000-4299; Denver, CO, USA; 2000.
- [54] W. Krüger, R. Heinrich, M. Spieck: *Fluid-Structure Coupling using CFD and Multibody Simulation Methods*
in: *Proceedings of ICAS 2002 - 23rd Congress of the Aeronautical Sciences*; International Council of the Aeronautical Sciences (ICAS); Stockholm, Sweden; 2002.
- [55] Veitl, A.: *Integrierter Entwurf innovativer Stromabnehmer*
Fortschritt-Berichte VDI, Reihe 12, No. 449; VDI Verlag GmbH; Düsseldorf, Germany; 2001.

- [56] Anderson, J. D.: *A History of Aerodynamics*
Cambridge Aerospace Series 8; Cambridge University Press; Cambridge, UK; 1998.
- [57] Anderson, J. D.: *Computational Fluid Dynamics*
McGraw-Hill Series in Mechanical Engineering; The McGraw-Hill Companies; New York, NY, USA; 1995.
- [58] Lock, R. C.; Williams, B. R.: *Viscous-Inviscid Interaction in External Aerodynamics*
in: *Progress in Aerospace Sciences*; Vol. 24, Nr. 2; Elsevier Science; Amsterdam, The Netherlands; 1987.
- [59] Le Balleur, J. C.: *Couplage Visqueux-Non Visqueux : Méthode Numérique et Applications aux Écoulements Bidimensionnels Transsoniques et Supersoniques*
in: *La Recherche Aéronautique*; ONERA Report Nr. TP 1978-55; Office National d'Études et de Recherches Aéronautiques (ONERA); Châtillon, France; 1978.
- [60] Veldman, A. E. P.: *New, Quasi-Simultaneous Method to Calculate Interacting Boundary Layers*
in: *AIAA Aircraft*; Vol. 19 (79-85); American Institute of Aeronautics and Astronautics, Inc; Reston, VA, USA; 1981.
- [61] Drela, M.; Giles, M. B.: *A Two-Dimensional Viscous Aerodynamic Design and Analysis Code*
in: *Proceedings of the AIAA 25th Aerospace Sciences Meeting 1987*; Report AIAA-86-0424; St. Louis, MO, USA; 1987
- [62] Le Balleur, J. C.: *Numerical Viscid-Inviscid Interaction in Steady and Unsteady Flows*
ONERA Report Nr. TP 1983-8; Office National d'Études et de Recherches Aéronautiques (ONERA); Châtillon, France; 1983.
- [63] Spieck, M.; Krüger, W. R.: *Interdisciplinary Landing Gear Layout for Large Transport Aircraft*
in: *Proceedings of 7th AIAA/USAF/NASA/ISSMO Symposium on Multidisciplinary Analysis and Optimization*; St. Louis, MO, USA; 1998.
- [64] *Aeronautical Technologies for the Twenty-First Century*
Committee on Aeronautical Technologies of the Aeronautics and Space Engineering Board; National Research Council; National Academy Press; Washington, DC, USA; 1992.
- [65] Dowell, E. H.: *A Modern Course in Aeroelasticity*
Kluwer Academic Publishers; Dordrecht, The Netherlands; 1995.
- [66] Karpel, M.: *Time-Domain Aeroservoelastic Modeling Using Weighted Unsteady Aerodynamic Forces*
in: *Journal of Guidance, Control and Dynamics*; Vol. 13, Nr. 1; American Institute of Aeronautics and Astronautics, Inc; Reston, VA, USA; 1990.

-
- [67] Wallrapp, O.: *Linearized Flexible Multibody Dynamics Including Geometric Stiffening Effects*
in: *Mechanics of Structures and Machines*; Vol. 19 Issue 3; Marcel Dekker, Inc.; New York, NY, USA; 1991.
- [68] Wallrapp, O.: *Standardization of Flexible Body Modelling in Multibody System Codes - Part I: Definition of Standard Input Data*
in: *Mechanics of Structures and Machines*; Vol. 22 Issue 3; Marcel Dekker, Inc.; New York, NY, USA; 1994.
- [69] Schwertassek, R.; Wallrapp, O.: *Dynamik flexibler Mehrkörpersysteme*
Vieweg & Sohn Verlagsgesellschaft mbH; Braunschweig, Germany; 1999.
- [70] Rulka, W.: *Bewegungsgleichungen für hybride mechanische Systeme mit freiheitsgradproportionalem Aufwand*
DLR Bericht IB 515-86/12; Oberpfaffenhofen, Germany; 1986.
- [71] Bremer, H.; Pfeiffer, F.: *Elastische Mehrkörpersysteme*
Teubner Studienbücher: Mechanik; B. G. Teubner Verlag Stuttgart; Stuttgart, Germany; 1992.
- [72] Riemer, M.; Wauer, J.; Wedig, W.: *Mathematische Methoden der Technischen Mechanik*
Springer-Verlag Berlin Heidelberg; Berlin, Germany; 1993.
- [73] Sachau, D.: *Berücksichtigung von flexiblen Körpern und Fügestellen in Mehrkörpersystemen zur Simulation aktiver Raumfahrtstrukturen*
Dissertation at the University of Stuttgart; Bericht aus dem Institut A für Mechanik 1/1996; Stuttgart, Germany; 1996.
- [74] Wallrapp, O.: *Standard Input Data of Flexible Members in Multibody Systems*
in: Schiehlen, W. (editor): *Advanced Multibody System Dynamics*; Kluwer Academic Publishers; Dordrecht, The Netherlands; 1993.
- [75] Bürger, E.; Becker, W.: *Kontinuumsmechanik: Eine Einführung in die Grundlagen und einfache Anwendungen*
Teubner Studienbücher: Mechanik; B. G. Teubner Verlag Stuttgart; Stuttgart, Germany; 1975.
- [76] Wallrapp, O.; Sachau, D.: *Space Flight Dynamics Simulations Using Finite Element Analysis Results in Multibody Systems*
in: *Proceedings of the 2nd International Conference on Computational Structures Technology*; Athens, Greece; 1994.
- [77] Wallrapp, O.: *Entwicklung rechnergestützter Methoden der Mehrkörperdynamik in der Fahrzeugdynamik*
DLR Forschungsbericht; Report Nr. DFVLR/FB-89/17; Oberpfaffenhofen, Germany; 1989.
- [78] Hafner, X.; Sachs, G.: *Flugmechanik*
Springer-Verlag Berlin Heidelberg; Berlin, Germany; 1993.

- [79] Pamadi, B.: Performance, Stability, Dynamics, and Control of Airplanes
AIAA Education Series; AIAA American Institute of Aeronautics and Astronautics, Inc; Reston, VA, USA; 1998.
- [80] W. Krüger, R. Heinrich, M. Spieck: *Fluid-Structure Coupling using CFD and Multibody Simulation Methods*
in: *Proceedings of ICAS 2002 - 23rd Congress of the Aeronautical Sciences*;
International Council of the Aeronautical Sciences; Stockholm, Sweden; 2002.
- [81] Katz, J.; Plotkin, A.: *Low-Speed Aerodynamics*
Cambridge University Press; New York, NY, USA; 2001.
- [82] *ISO 1151-1: Flight Dynamics - Concepts, Quantities, and Symbols, Part 1: Aircraft Motion Relative to the Air*
International Organization for Standardisation (ISO); Geneva, Switzerland; 1988
- [83] *ISO 1151-2: Flight Dynamics - Concepts, Quantities, and Symbols, Part 2: Motions of the Aircraft and the Atmosphere Relative to the Earth*
International Organization for Standardisation (ISO); Geneva, Switzerland; 1985
- [84] *ISO 1151-3: Flight Dynamics - Concepts, Quantities, and Symbols, Part 3: Derivatives of Forces, Moments and their Coefficients*
International Organization for Standardisation (ISO); Geneva, Switzerland; 1989
- [85] *ISO 1151-4: Flight Dynamics - Concepts, Quantities, and Symbols, Part 4: Concepts and Quantities Used in the Study of Aircraft Stability and Control*
International Organization for Standardisation (ISO); Geneva, Switzerland; 1994
- [86] Schlichting, H.; Truckenbrodt, E.: *Aerodynamik des Flugzeuges - Erster Band*
Springer-Verlag Berlin Heidelberg; Berlin, Germany; 1967.
- [87] Strganac, T. W.: *Principles of Aeroelasticity*
Proceedings to KSU Short Course "Aeroelasticity"; University of Kansas; Kansas, KS, USA; 1998.
- [88] Beckert, A.: *Ein Beitrag zur Strömung-Struktur-Kopplung für die Berechnung des aeroelastischen Gleichgewichtszustandes*
DLR Forschungsbericht; Report Nr. 97-42; Köln, Germany; 1997.
- [89] Carmichael, R. L.; Erickson, L. L.: *PAN AIR - A Higher Order Panel Method for Predicting Subsonic or Supersonic Linear Potential Flows About Arbitrary Configurations*
in: *AIAA Meeting Papers 1981*; Report AIAA-81-1255; AIAA American Institute of Aeronautics and Astronautics, Inc; Reston, VA, USA; 1982.
- [90] Fornasier, L.: *HISSS - A Higher-Order Subsonic-Supersonic Singularity Method for Calculating Linearized Potential Flow*
in: *AIAA Meeting Papers 1984*; Report AIAA-84-1646; AIAA American Institute of Aeronautics and Astronautics, Inc; Reston, VA, USA; 1985.
- [91] Maskew, B.: *Program VSAERO Theory Document: A Computer Program for Calculating Nonlinear Aerodynamic Characteristics of Arbitrary Configurations*

-
- NASA Technical Report NASA-CR-4023 (ID 19900004884 N); NASA Center of Aerospace Information (CASI); Hanover, MD, USA; 1987.
- [92] Chung, T. J.: *Computational Fluid Dynamics*
Cambridge University Press; Cambridge, UK; 2002.
- [93] Gallager, R.-H.: *Finite Element Analysis*
Springer-Verlag Berlin Heidelberg New-York; New York, USA; 1976.
- [94] Schaback, R.: *Creating Surfaces from Scattered Data Using Radial Basis Functions*
in: Dæhlen, M.; Lyche, T.; Schumaker, L. L.: *Mathematical Methods for Curves and Surfaces*; Vanderbilt University Press; Nashville, TN, USA; 1995.
- [95] Wendland, H.: *Konstruktion und Untersuchung radialer Basisfunktionen mit kompaktem Träger*
Dissertation an der Universität Göttingen; Institut für numerische und angewandte Mathematik (NAM); Göttingen, Germany; 1996.
- [96] Buhmann, M. D.: *Radial Basis Functions*
in: Iserles, A. (editor): *Acta Numerica 2000*; Vol. 9; Cambridge University Press; Cambridge, U.K.; 2000.
- [97] Chung, T. J.: *Computational Fluid Dynamics*
Cambridge University Press; Cambridge, U.K.; 2002.
- [98] Raeder, Klaus: *Umkonstruktion des Rumpfes eines in Serie gefertigten Segelflugzeuges der Lufttüchtigkeitsgruppe "U" zur Erfüllung der Kunstflugauforderungen nach LFSM*
Konstruktive Semesterarbeit TUM-MW14/8111-SA; Lehrstuhl für Leichtbau, Technische Universität München; München, Germany; 1981.
- [99] Althaus, D.; Wortmann, F. X.: *Stuttgarter Profilkatalog I*
Vieweg Friedr. + Sohn Verlag; Braunschweig Wiesbaden, Germany; 1981.